National Library of Canada
Acquisitions and Bibliographic Services Branch
395 Wellington Street
Ottawa, Ontario
K1A 0N4

Bibliothèque nationale du Canada
Direction des acquisitions et des services bibliographiques
395, rue Wellington
Ottawa (Ontario)
K1A 0N4

Your file *Votre référence*

Our file *Notre référence*

NOTICE

The quality of this microform is heavily dependent upon the quality of the original thesis submitted for microfilming. Every effort has been made to ensure the highest quality of reproduction possible.

If pages are missing, contact the university which granted the degree.

Some pages may have indistinct print especially if the original pages were typed with a poor typewriter ribbon or if the university sent us an inferior photocopy.

Reproduction in full or in part of this microform is governed by the Canadian Copyright Act, R.S.C. 1970, c. C-30, and subsequent amendments.

AVIS

La qualité de cette microforme dépend grandement de la qualité de la thèse soumise au microfilmage. Nous avons tout fait pour assurer une qualité supérieure de reproduction.

S'il manque des pages, veuillez communiquer avec l'université qui a conféré le grade.

La qualité d'impression de certaines pages peut laisser à désirer, surtout si les pages originales ont été dactylographiées à l'aide d'un ruban usé ou si l'université nous a fait parvenir une photocopie de qualité inférieure.

La reproduction, même partielle, de cette microforme est soumise à la Loi canadienne sur le droit d'auteur, SRC 1970, c. C-30, et ses amendements subséquents.

Canada

UNIVERSITY OF ALBERTA

Tunable Erbium Fiber Lasers

BY

Terrance Rosadiuk ©

A thesis submitted to the Faculty of Graduate Studies and Research in partial fulfillment of the requirements for the degree of **Master of Science**.

DEPARTMENT OF ELECTRICAL ENGINEERING

Edmonton, Alberta

Fall, 1994

National Library
of Canada

Acquisitions and
Bibliographic Services Branch

395 Wellington Street
Ottawa, Ontario
K1A 0N4

Bibliothèque nationale
du Canada

Direction des acquisitions et
des services bibliographiques

395, rue Wellington
Ottawa (Ontario)
K1A 0N4

Your file Votre référence

Our file Notre référence

The author has granted an irrevocable non-exclusive licence allowing the National Library of Canada to reproduce, loan, distribute or sell copies of his/her thesis by any means and in any form or format, making this thesis available to interested persons.

L'auteur a accordé une licence irrévocable et non exclusive permettant à la Bibliothèque nationale du Canada de reproduire, prêter, distribuer ou vendre des copies de sa thèse de quelque manière et sous quelque forme que ce soit pour mettre des exemplaires de cette thèse à la disposition des personnes intéressées.

The author retains ownership of the copyright in his/her thesis. Neither the thesis nor substantial extracts from it may be printed or otherwise reproduced without his/her permission.

L'auteur conserve la propriété du droit d'auteur qui protège sa thèse. Ni la thèse ni des extraits substantiels de celle-ci ne doivent être imprimés ou autrement reproduits sans son autorisation.

ISBN 0-315-95105-2

Canada

Name TERRANCE ROSADIUK

Dissertation Abstracts International is arranged by broad, general subject categories. Please select the one subject which most nearly describes the content of your dissertation. Enter the corresponding four-digit code in the spaces provided.

ELECTRONICS & ELECTRICAL

SUBJECT TERM

0544

SUBJECT CODE

U·M·I

Subject Categories

THE HUMANITIES AND SOCIAL SCIENCES

COMMUNICATIONS AND THE ARTS

Architecture 0729
Art History 0377
Cinema 0900
Dance 0378
Fine Arts 0357
Information Science 0723
Journalism 0391
Library Science 0399
Mass Communications 0708
Music 0413
Speech Communication 0459
Theater 0465

EDUCATION

General 0515
Administration 0514
Adult and Continuing 0516
Agricultural 0517
Art 0273
Bilingual and Multicultural 0282
Business 0688
Community College 0275
Curriculum and Instruction 0727
Early Childhood 0518
Elementary 0524
Finance 0277
Guidance and Counseling 0519
Health 0680
Higher 0745
History of 0520
Home Economics 0278
Industrial 0521
Language and Literature 0279
Mathematics 0280
Music 0522
Philosophy of 0998
Physical 0523

Psychology 0525
Reading 0535
Religious 0527
Sciences 0714
Secondary 0533
Social Sciences 0534
Sociology of 0340
Special 0529
Teacher Training 0530
Technology 0710
Tests and Measurements 0288
Vocational 0747

LANGUAGE, LITERATURE AND LINGUISTICS

Language
- General 0679
- Ancient 0289
- Linguistics 0290
- Modern 0291

Literature
- General 0401
- Classical 0294
- Comparative 0295
- Medieval 0297
- Modern 0298
- African 0316
- American 0591
- Asian 0305
- Canadian (English) 0352
- Canadian (French) 0355
- English 0593
- Germanic 0311
- Latin American 0312
- Middle Eastern 0315
- Romance 0313
- Slavic and East European 0314

PHILOSOPHY, RELIGION AND THEOLOGY

Philosophy 0422
Religion
- General 0318
- Biblical Studies 0321
- Clergy 0319
- History of 0320
- Philosophy of 0322

Theology 0469

SOCIAL SCIENCES

American Studies 0323
Anthropology
- Archaeology 0324
- Cultural 0326
- Physical 0327

Business Administration
- General 0310
- Accounting 0272
- Banking 0770
- Management 0454
- Marketing 0338

Canadian Studies 0385
Economics
- General 0501
- Agricultural 0503
- Commerce-Business 0505
- Finance 0508
- History 0509
- Labor 0510
- Theory 0511

Folklore 0358
Geography 0366
Gerontology 0351
History
- General 0578
- Ancient 0579
- Medieval 0581
- Modern 0582
- Black 0328
- African 0331
- Asia, Australia and Oceania 0332
- Canadian 0334
- European 0335
- Latin American 0336
- Middle Eastern 0333
- United States 0337

History of Science 0585
Law 0398
Political Science
- General 0615
- International Law and Relations 0616
- Public Administration 0617

Recreation 0814
Social Work 0452
Sociology
- General 0626
- Criminology and Penology 0627
- Demography 0938
- Ethnic and Racial Studies 0631
- Individual and Family Studies 0628
- Industrial and Labor Relations 0629
- Public and Social Welfare 0630
- Social Structure and Development 0700
- Theory and Methods 0344

Transportation 0709
Urban and Regional Planning 0999
Women's Studies 0453

THE SCIENCES AND ENGINEERING

BIOLOGICAL SCIENCES

Agriculture
- General 0473
- Agronomy 0285
- Animal Culture and Nutrition 0475
- Animal Pathology 0476
- Food Science and Technology 0359
- Forestry and Wildlife 0478
- Plant Culture 0479
- Plant Pathology 0480
- Plant Physiology 0817
- Range Management 0777
- Wood Technology 0746

Biology
- General 0306
- Anatomy 0287
- Biostatistics 0308
- Botany 0309
- Cell 0379
- Ecology 0329
- Entomology 0353
- Genetics 0369
- Limnology 0793
- Microbiology 0410
- Molecular 0307
- Neuroscience 0317
- Oceanography 0416
- Physiology 0433
- Radiation 0821
- Veterinary Science 0778
- Zoology 0472

Biophysics
- General 0786
- Medical 0760

EARTH SCIENCES

Biogeochemistry 0425
Geochemistry 0996

Geodesy 0370
Geology 0372
Geophysics 0373
Hydrology 0388
Mineralogy 0411
Paleobotany 0345
Paleoecology 0426
Paleontology 0418
Paleozoology 0985
Palynology 0427
Physical Geography 0368
Physical Oceanography 0415

HEALTH AND ENVIRONMENTAL SCIENCES

Environmental Sciences 0768
Health Sciences
- General 0566
- Audiology 0300
- Chemotherapy 0992
- Dentistry 0567
- Education 0350
- Hospital Management 0769
- Human Development 0758
- Immunology 0982
- Medicine and Surgery 0564
- Mental Health 0347
- Nursing 0569
- Nutrition 0570
- Obstetrics and Gynecology 0380
- Occupational Health and Therapy 0354
- Ophthalmology 0381
- Pathology 0571
- Pharmacology 0419
- Pharmacy 0572
- Physical Therapy 0382
- Public Health 0573
- Radiology 0574
- Recreation 0575
- Speech Pathology 0460
- Toxicology 0383

Home Economics 0386

PHYSICAL SCIENCES

Pure Sciences

Chemistry
- General 0485
- Agricultural 0749
- Analytical 0486
- Biochemistry 0487
- Inorganic 0488
- Nuclear 0738
- Organic 0490
- Pharmaceutical 0491
- Physical 0494
- Polymer 0495
- Radiation 0754

Mathematics 0405
Physics
- General 0605
- Acoustics 0986
- Astronomy and Astrophysics 0606
- Atmospheric Science 0608
- Atomic 0748
- Electronics and Electricity 0607
- Elementary Particles and High Energy 0798
- Fluid and Plasma 0759
- Molecular 0609
- Nuclear 0610
- Optics 0752
- Radiation 0756
- Solid State 0611

Statistics 0463

Applied Sciences

Applied Mechanics 0346
Computer Science 0984

Engineering
- General 0537
- Aerospace 0538
- Agricultural 0539
- Automotive 0540
- Biomedical 0541
- Chemical 0542
- Civil 0543
- Electronics and Electrical 0544
- Heat and Thermodynamics 0348
- Hydraulic 0545
- Industrial 0546
- Marine 0547
- Materials Science 0794
- Mechanical 0548
- Metallurgy 0743
- Mining 0551
- Nuclear 0552
- Packaging 0549
- Petroleum 0765
- Sanitary and Municipal 0554
- System Science 0790

Geotechnology 0428
Operations Research 0796
Plastics Technology 0795
Textile Technology 0994

PSYCHOLOGY

General 0621
Behavioral 0384
Clinical 0622
Developmental 0620
Experimental 0623
Industrial 0624
Personality 0625
Physiological 0989
Psychobiology 0349
Psychometrics 0632
Social 0451

UNIVERSITY OF ALBERTA

RELEASE FORM

NAME OF AUTHOR: Terrance Rosadiuk

TITLE OF THESIS: Tunable Erbium Fiber Lasers

DEGREE: Master of Science

YEAR THIS DEGREE GRANTED: 1994

Permission is hereby granted to the University of Alberta Library to reproduce single copies of this thesis and to lend or sell such copies for private, scholarly or scientific research purposes only.

The author reserves all other publication and other rights in association with the copyright in the thesis, and except as hereinbefore provided neither the thesis nor any substantial portion thereof may be printed or otherwise reproduced in any material form whatever without the author's prior written permission.

T. Rosadiuk

800 Park Plaza
10611-98 Avenue
Edmonton, Alberta, Canada
T5K 2P7

October 3, 1994

UNIVERSITY OF ALBERTA

FACULTY OF GRADUATE STUDIES AND RESEARCH

The undersigned certify that they have read, and recommend to the Faculty of Graduate Studies and Research for acceptance, a thesis entitled TUNABLE ERBIUM FIBER LASERS submitted by TERRANCE ROSADIUK in partial fulfillment of the requirements for the degree of MASTER OF SCIENCE.

Dr. J. Conradi, Supervisor

Dr. J. McMullin, Internal

Dr. G. Horlick, External

September 23, 1994

Abstract

This thesis discusses theoretical and experimental investigations of tunable erbium fiber lasers that are pertinent to the development of a 1550 nm light source for the optical fiber communications industry. Three aspects are investigated: wavelength tuning due to changes in the output coupling, relative intensity noise in the laser, and digital optical fiber communications using the laser as a source. A novel laser resonator layout is also presented. The experimental results obtained were found to be in reasonable agreement with simplified theoretical models.

Based on the work done, significant insight was gained, and recommendations regarding future research in the area of erbium fiber lasers are discussed.

Acknowledgments

This work was supported by the Natural Sciences and Engineering Research Council of Canada, Bell Northern Research Limited, and TRLabs through the NSERC/BNR/TRLabs Industrial Research Chair in Fiber Optic Communications at the University of Alberta. The Chair is directed by Dr. J. Conradi, without whom this project would not have been attempted or completed.

J. Haugen and J. Freeman were helpful in providing insight into some of the lab equipment used and many erbium fiber amplifier related subjects.

The well organized laboratory layout, and suggestions on equipment use by 7th floor manager D. Clegg, made for a more productive research environment.

Laboratory equipment borrowed from Dr. G. Cormack, specifically the variable fiber optic coupler used in preliminary laser wavelength tuning tests and in a final mode reduction filter resonator, was very useful.

The lightwave signal analyzer on loan from Hewlett Packard through representative D. Vincent was used in measuring laser RIN values.

Digital transmission experimental results were obtained using modulation equipment set up by K. Benterud.

Table of Contents

1.0 Introduction 1

1.1 Project Background 1

1.2 The State of the Art 1

1.3 Industrial Communication Requirements 2

1.4 Project Objective 3

1.5 Thesis Layout 3

2.0 Erbium Fiber Laser Design 5

2.1 Background Theory 5

2.2 Erbium Doped Fiber Construction 7

2.3 Light Amplification and Absorption 9

2.4 Basic Laser Resonator Configurations 11

2.5 Gain Conditions For Laser Operation 13

2.6 Phase Requirements For Lasing 13

2.7 Laser Wavelength Operation 15

2.8 Laser Linewidth 17

2.9 Laser Output Power 18

2.10 Pump Power Efficiency 19

2.11 Resonator Power Extraction Efficiency 20

2.12 Power Extraction Efficiency Versus Losses 22

2.13 Laser Efficiency Versus Reflectivity 23

2.14 Power Extraction Efficiency Versus Gain 24

2.15 Light Output Power Versus Pump Power 26

2.16 Laser Steady State Time 26

2.17 Relaxation Oscillations 27

2.18 Relative Intensity Noise 29

2.19 Lab Equipment 31

3.0 Output Coupling Induced Wavelength Shifts in Erbium Doped Fiber Lasers 33

3.1 Introduction 33

3.2 Tuning Theory 34

3.3 Tuning Results 36

4.0 Laser Spectral Width and Noise Properties 45

4.1 Mode Measurement Theory 45

4.2 Measurement Equipment 48

4.3 Laser Noise Results for Basic Loop Configuration 48

4.4 Reduction of Modes 50

4.4.1 Band Pass Filtering 50

4.4.2 Fiber Filtering 53

4.4.2.1 Passive Loop Filter Theory- Equating of Fields 54

4.4.2.2 Passive Loop Filter Theory- Matrix Approach 55

4.4.2.3 Simulation Results 59

4.4.2.4 Experimental Results 63

4.5 Relative Intensity Noise Measurement 70

4.6 Low Frequency Observations 71

4.7 Linewidth Measurements 72

5.0 Transmission Using An Erbium Doped Fiber Laser Light Source 75

5.1 Introduction 75

5.2 Results 76

5.3 Time Domain Analysis 79

6.0 Conclusions 82

6.1 Summary 82

6.2 Future Research 82

References 84

Appendix A **Relative Intensity Noise Calculations Using LabVIEW** 88

A.1 Introduction 88

A.2 RIN VI 91

Appendix B **Spectrum Analyzer Data Capture VI** 104

B.1 Introduction 104

B.2 Screen Capture VI for HP 7000 Series Spectrum Analyzers 105

Appendix C **Polarization Rotator Design** 112

C.1 Overview 112

C.2 Operating Notes 112

C.3 Mechanical Drawings 114

Appendix D **Directional Coupler Operation** 119

D.1 Coupler Theory 119

D.2 Fiber Mirror Theory 119

List of Figures

Figure 2.1 Ideal energy level diagram for a three level laser.....5

Figure 2.2 Cross section of the dopant distribution within the glass fiber core shown as compared to the normalized mode shapes for the pump (980 nm) and signal (1550 nm) wavelengths considered 8

Figure 2.3 Conceptual view of the amplification and absorption process through sections of pumped and un-pumped erbium doped fiber.....9

Figure 2.4 Traveling wave ring resonator 12

Figure 2.5 Standing wave Fabry-Perot resonator 12

Figure 2.6 Conceptual view of resonating modes that satisfy the phase requirement for laser resonator operation in a Fabry-Perot type resonator.....14

Figure 2.7 Graph depicting the many resonant longitudinal modes that could satisfy the gain and phase requirements for lasing 15

Figure 2.8 Depiction of mode reduction through homogeneous gain suppression 16

Figure 2.9 Close up view of a single homogeneously broadened laser mode.....17

Figure 2.10 Typical output power versus pump power for a laser.....18

Figure 2.11 Ring resonator with losses 20

Figure 2.12 Fabry-Perot resonator with losses.....21

Figure 2.13 Power extraction efficiency vs. device insertion loss for the ring configuration 22

Figure 2.14 Power extraction efficiency vs. device insertion loss for fiber mirror configuration.....22

Figure 2.15 Extraction efficiency vs. reflectivity for ring configuration. G_o = 15 dB.....23

Figure 2.16 Extraction efficiency vs. reflectivity for Fabry-Perot configuration. G_o = 15 dB.....24

Figure 2.17 Extraction efficiency vs. reflectivity for ring resonator. L_1 = L_2 = 2 dB 25

Figure 2.18 Extraction efficiency vs. reflectivity for Fabry-Perot resonator. $L_1 = L_2 = 2$ dB.....25

Figure 2.19 Output power characteristic expected for the fiber mirror laser.....26

Figure 2.20 Conceptual view of laser response to initial pump power switching.....27

Figure 2.21 Depiction of disturbance in a lasers average output power.....28

Figure 2.22 Laser average output power over time.....29

Figure 3.1 Excited ion fraction that satisfies the lasing condition vs. wavelength (sample calculation for two different output mirror reflectivities).....36

Figure 3.2 Experimental laser configurations: (a) fiber ring laser (b) fiber mirror laser.....37

Figure 3.3 Wavelengths of Observed lasing peaks vs. reflectivity (a) ring configuration (b) fiber mirror configuration.....39

Figure 3.4 Typical spectral shape of observed laser oscillations.....41

Figure 3.5 Observed laser output power and pump residual power vs. reflectivity (a) ring configuration (b) fiber mirror configuration.....42

Figure 3.6 Measured output power vs. injected pump power for fiber mirror laser set at $R = 20\%$.....44

Figure 4.1 Experimental layout for measurement of laser modes.....45

Figure 4.2 Expected observed spectral beating effect of laser lines in the detection process as a function of the number of operating longitudinal modes: (a) one line (b) two lines (c) three lines (4) four lines.....47

Figure 4.3 Spectral output vs. frequency for ring laser (10 to 100 MHz).....49

Figure 4.4 Spectral output vs. frequency for ring laser (1 to 20 GHz scan).....50

Figure 4.5a Experimental layout for filtered fiber mirror configuration with intra-cavity tunable band pass filter.....51

Figure 4.5b Observed peak power vs. wavelength and various reflectivities for the fiber mirror laser with intra-cavity tunable bandpass filter.....51

Figure 4.6a Experimental layout for fiber mirror configuration using an intra-cavity optical attenuator....52

Figure 4.6b Peak output power vs. intra-cavity attenuation for the fiber mirror laser with intra-cavity tunable bandpass filter set at 1535 nm....52

Figure 4.7 Various ring resonator designs: (a) single loop (b) double loop (c) triple loop....53

Figure 4.8 Triple loop filter layout....54

Figure 4.9 Diagram showing the coupling of electric fields across a coupler....55

Figure 4.10 Input-output view of coupler for matrix approach....55

Figure 4.11 Input and output notation for sections of optical fiber when using the matrix formalism....56

Figure 4.12 Triple ring filter layout for matrix formalism....57

Figure 4.13 Input and output notation for filter transfer function....58

Figure 4.14 Theoretical response for a single 50 m loop filter....60

Figure 4.15 Theoretical response for a 50m/10m double loop filter....61

Figure 4.16 Theoretical response for a 50m/10m/1.4 m triple loop filter....62

Figure 4.17 Experimental triple ring resonator configuration....64

Figure 4.18 Output power versus injected pump power for the triple ring resonator configuration....65

Figure 4.19 Theoretical output power versus injected pump power for the triple ring resonator configuration....66

Figure 4.20 Measured laser output power versus operating wavelength for the triple ring resonator....66

Figure 4.21 Laser spectral output vs. frequency for triple ring resonator (10 to 100 MHz)....67

Figure 4.22 Laser spectral output vs. frequency for triple ring resonator (0.1 to 1 GHz)....68

Figure 4.23 Laser spectral output vs. frequency for triple ring resonator (1 to 20 GHz)....68

Figure 4.24 Laser spectral output vs. frequency for triple ring resonator (10 to 100 MHz) after various resonator modifications....69

Figure 4.25 Relative intensity noise (RIN) vs. frequency for triple ring resonator configuration 70

Figure 4.26 Spectral output vs. frequency for triple ring resonator at various injected pump power levels 71

Figure 4.27 Experimentally observed oscillation center frequency for triple ring resonator vs. pump power. Theoretical calculations shown for a single ring resonator of various cavity lengths 72

Figure 4.28 Experimental layout for measuring laser linewidth 73

Figure 4.29 Delayed self homodyne spectral output vs. frequency 73

Figure 5.1 Transmission experiment layout using the erbium fiber laser 76

Figure 5.2 Eye Diagram 78

Figure 5.3 Experimental setup for time domain measurement 79

Figure 5.4 Time domain plot of laser output. (1 s/Div scale) 79

Figure 5.5 Time domain plot of laser output. (1 ms/Div scale) 80

Figure 5.6 Time domain plot of laser output. (200 μs/Div scale) 80

Figure A.1 Block diagram illustrating technique used for calculating relative intensity noise (RIN) 90

Figure A.2 Experimental setup used for calculating relative intensity noise (RIN) 90

Figure D.1 Diagram showing the mixing of electric fields across a coupler 119

Figure D.2 Coupler configured in a fiber mirror configuration with power reflectivity R and power transmission T 120

1
Introduction

1.1 Project Background

Since its early development, the field of optical fiber communications has seen many improvements making it a practical, reliable and cost effective alternative to many conventional communications systems. This has led to increased demand for communications services and hence competition between companies and countries to maintain market share in a fast growing field. As a result, through financial encouragement, industry has been looking to university for new ideas to push the state of the art of optical communications further in order to maintain its competitive edge. The NSERC/BNR/TRlabs Industrial Research Chair headed by Dr. J Conradi has been established to address such concerns and this MSc thesis project has been conceived and managed to be in support of the Chair's objectives.

Toward this end, this project dealt with a relatively new potential optical communications light source: the single mode erbium fiber laser operating in the 1550 nm wavelength range. Since other related projects depend on high quality 1550 nm light sources, work to investigate and characterize an erbium fiber laser has obvious advantages. Among these is that this work used many of the components normally purchased or designed for other projects and could thus be undertaken with essentially no budget for equipment and has proved very efficient research as compared to other projects in terms of capital costs.

1.2 State of the Art

Although bulk glass erbium lasers have existed since the mid sixties, only relatively recently has the technology to produce single mode erbium doped fiber and low cost/high power 980 nm pump lasers been developed to the point where the state of the art erbium

fiber laser is seen as a practical reality. A literature search at the start of this project has shown a number of promising aspects of the erbium fiber laser:

1) Single Mode Fiber- The inherent single mode fiber design of the fiber makes for good coupling efficiency into systems that use single mode fiber (now the industry standard for high speed communications).

2) High power - More than 250 mW of 1550 nm power is attainable [1].

3) High Efficiency- Better than 51% slope efficiency reported [2]

4) Low Threshold- Threshold values less than 10 mW have been attained [2]

5) Narrow Line Widths - 10 to 60 KHz line widths have been reported [3], [4].

6) Thermal Stability - Claimed to be stable [5].

7) Wide Tunability- Using intra-cavity filters, the fiber laser has been shown to be tunable over a wide range, 1522 nm to 1567 nm. [6].

Each of these reported properties were not necessarily attained simultaneously for a given laser design; however, they do show the potential that exists for this device.

1.3 Industrial Communication Requirements

For current high speed digital communication systems and future high speed communication rates, such as been investigated by other chair projects [7], a laser of narrow line width and low relative intensity noise is a necessity. For transmission of analog signals such as cable television trunking distribution [8,9], and in the future fiber optic cable television to the home [10]-[15], it is imperative that laser noise be even lower as the quality of analog signals in the distribution network is highly sensitive to light source signal quality [16]. A tunable source is also desirable as this can be useful in future applications of wavelength division multiplexing. As far as power is concerned, a light

source of only a few mW is necessary, today, but several tens of mW may be needed in the future.

1.4 Project Objective

The main objective of this project is to produce a tunable optical source with low noise and narrow line width characteristics, suitable for use in optical communications systems. Three aspects of erbium fiber lasers not reported in related research journals were chosen as sub-objectives in working towards the main objective:

1) The inherent tuning of the laser wavelength due to changes in laser cavity output coupling.
2) The Relative Intensity Noise (RIN) inherent to the laser.
3) The experimental use of the laser in a digital transmission system.

In essence the project was intended to do research into niches not yet investigated that are both in the interests of industry, and of scientific merit, rather than to simply beat previously reported performance records.

1.5 Thesis Layout

Although several interesting concepts were looked into and many experiments were done in the lab, it is the intent of the author to write as concisely as possible and discuss only issues directly related to the objectives of the project thereby limiting the writing to six brief chapters.

Chapter two provides a brief discussion of the laser theory that is relevant to the experimental part of the thesis. Chapters three, four and five discuss the results of the three thesis sub-objectives investigated as stated above. Chapter six has some brief concluding

remarks on the project followed by a list of references and appendices with project related support information.

2

Erbium Fiber Laser Design

2.1 Background Theory

The generation of light in erbium lasers centers around what is generally described as a three level lasing system [17] since the erbium ion Er^{3+} cycles through three energy levels E_1, E_2 and E_3 as shown in Fig. 2.1.

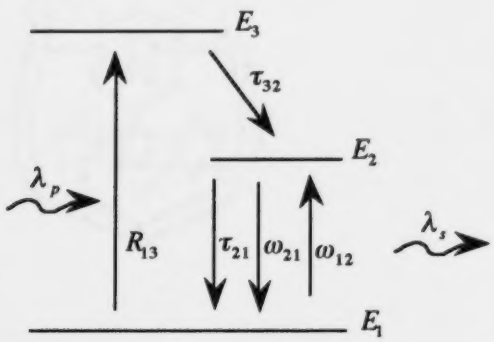

Figure 2.1 Ideal energy level diagram for a three level laser.

Normally, the erbium ion is primarily in level E_1, but under "pumping" it will rise to E_3. R_{13} is the rate at which ion are pumped up from E_1 to E_3 by absorbing photons at wavelength λ_p, $\frac{1}{\tau_{32}}$ is the rate at which ions relax from E_3 to E_2 and $\frac{1}{\tau_{21}}$ is the rate of spontaneous emission from E_2 to E_1. ω_{12} and ω_{21} are the absorption and stimulated emission rates of photons respectively at the infrared signal wavelength λ_s. All transition rates are in units of s^{-1}.

In mathematical terms, the total number of erbium ions N_T (ions/cm^3) will be distributed in an amount N_i in each energy level E_i and can be represented by the following set of rate equations [17],[30]:

$$\frac{\partial N_1}{\partial t} = -(R_{13} + \omega_{12})N_1 + (\omega_{21} + \frac{1}{\tau_{21}})N_2 \tag{2.1.1}$$

$$\frac{\partial N_2}{\partial t} = \omega_{12}N_1 - (\omega_{21} + \frac{1}{\tau_{21}})N_2 + \frac{N_3}{\tau_{32}} \tag{2.1.2}$$

$$\frac{\partial N_3}{\partial t} = R_{13}N_1 - \frac{N_3}{\tau_{32}} \tag{2.1.3}$$

The number of ions in the N_1 and N_2 states are critically important as their relative difference influences the expected level of absorption or amplification of 1550 nm light. Assuming the ion has a fast $\frac{1}{\tau_{32}}$ rate relative to the other transition rates and hence a low density of ions in the N_3 level, we can solve for the steady state case for N_1 and N_2 as:

$$N_1 = N_T\left[\frac{\omega_{21} + \frac{1}{\tau_{21}}}{\omega_{21} + \omega_{12} + R_{13} + \frac{1}{\tau_{21}}}\right] \tag{2.1.4}$$

$$N_2 = N_T\left[\frac{\omega_{12} + R_{13}}{\omega_{21} + \omega_{12} + R_{13} + \frac{1}{\tau_{21}}}\right] \tag{2.1.5}$$

where:

$$\omega_{12} = \frac{\sigma_a}{h\nu_s} I_s \tag{2.1.6}$$

$$\omega_{21} = \frac{\sigma_e}{h\nu_s} I_s \tag{2.1.7}$$

$$R_{13} = \frac{\sigma_p}{h\nu_p} I_p \tag{2.1.8}$$

and,

σ_a = the absorption cross-section (cm^2) at λ_s

σ_e = the emission cross-section (cm^2) at λ_s

σ_p = the absorption cross-section (cm^2) at λ_p

I_s = the signal light intensity (W/cm^2) at λ_s

I_p = the pump light intensity (W/cm^2) at λ_p

$h\nu_s$ = the energy (J) in a single photon at λ_s

$h\nu_p$ = the energy (J) in a single photon at λ_p

The stimulated emission or amplification property of the ion in the infrared wavelength range is what is behind the principle of the erbium laser. Careful incorporation of this ion into a glass optical fiber "host" creates characteristic cross-sections which allow the potential for a single mode erbium fiber amplifier operating in the 1550 nm range.

2.2 Erbium Doped Fiber Construction

Th optical fiber used for this type of laser work consists an erbium-doped glass center core surrounded by a cladding to confine light within the core. Due to the small core size and numerical aperture (NA), due to the difference between refractive indices between core and cladding, light photons can propagate in single transverse modes, with nearly Gaussian intensity profiles, and with very low loss through the fiber. Fig 2.2 shows the mode distribution with respect to the fiber core.

It is noted that the Er^{3+} ions are not distributed evenly throughout the core, but are confined within a region near the center of the core where the erbium ions can interact most strongly with the pump mode at its maximum intensity.

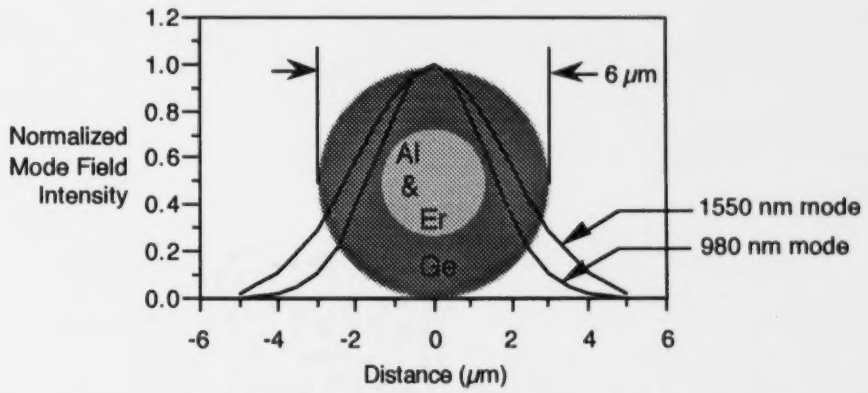

Figure 2.2 Cross section of the dopant distribution within the glass fiber core shown as compared to the normalized mode shapes for the pump (980 nm) and signal (1550 nm) wavelengths considered.

The erbium is the only active ion while the other dopants, aluminum and germanium, serve to enhance the Er^{3+} solubility and to increase the refractive index to achieve a desirable NA.

The glass host and dopants together produce unique σ_e , σ_a and σ_p values which vary depending upon wavelengths λ_s and λ_p . For the purposes of this thesis, λ_s will be considered a signal wavelength anywhere from 1530 nm to 1560 nm and λ_p to be fixed at 980 nm.

The doping level of the erbium is very low, typically a few hundred parts per million (ppm), and as a result, most erbium fiber amplifiers are several meters long in order to obtain usable gain levels.

2.3 Light Amplification and Absorption

Over a section of fiber there will be amplification or absorption of light as depicted in Fig. 2.3.

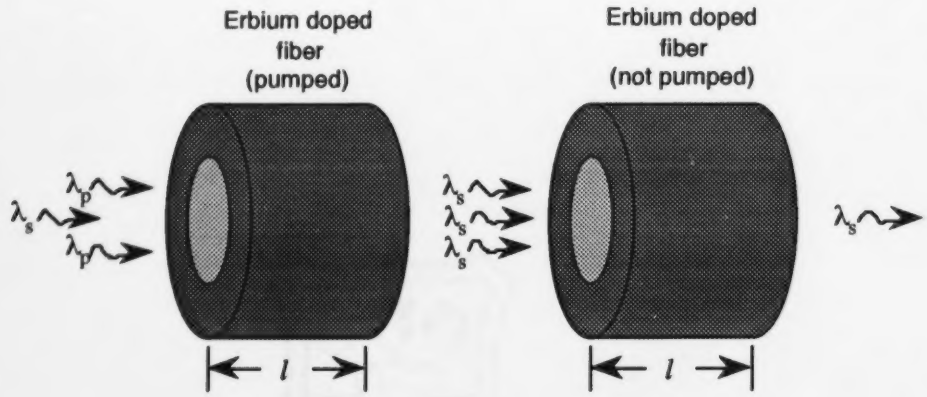

Figure 2.3 Conceptual view of the amplification and absorption process through sections of pumped and un-pumped erbium doped fiber.

Considering small input signals only, and ignoring the contributions of incoherent spontaneous emission, the input light will be amplified coherently, with phase, direction and polarization maintained, through the section of pumped fiber. Conversely, the signal will be attenuated through a section of fiber that is not pumped. The exact ratio of change or gain G in signal intensity from the input I_i to the output I_o over a section of fiber of length l is given by:

$$G = \frac{I_o}{I_i} = e^{\gamma l} \tag{2.3.1}$$

where the gain coefficient γ is given by:

$$\gamma = N_2\sigma_e - N_1\sigma_a \tag{2.3.2}$$

It must be noted that Fig. 2.3 is only a conceptual view, and that the output from a section of pumped fiber would contain some additional incoherent spontaneous emission, not necessarily at the exact wavelength of the input signal. Also, the values of N_2 and N_1 in general are not constant through the length of fiber for high input intensities resulting in a variation of the gain per unit length of fiber. For high light intensities equation (2.3.1) does not hold and a more involved analysis must be sought. The exact gain, the contributions of spontaneous emission amplified over a length of pumped fiber, and its dependency on input signal intensity are a whole study in themselves and have been dealt with in another chair project [18]. However, for leading to an understanding of the major mechanisms behind laser operation, the conceptual view is sufficiently accurate.

From (2.3.1) it can be readily inferred that to obtain amplification in the fiber, equation (2.3.2) must be positive otherwise absorption of light will occur, i.e. negative gain. Since the emission and absorption cross-sections are fixed, amplification can only be produced through pumping of the erbium doped fiber to ensure that $N_2\sigma_e$ is greater than $N_1\sigma_a$.

For very small input signals, the gain will be greatest and is termed the effective small signal gain. The gain G_o from input to output due to the small signal gain coefficient can be written as:

$$G_o = \frac{I_o}{I_i} = e^{\gamma_o l} \tag{2.3.3}$$

A small signal is loosely defined as a signal much less than the saturation intensity I_{sat}. The absorption I^a_{sat}, and emission I^e_{sat} saturation intensities can be written as [48]:

$$I^a_{sat} = \frac{h\nu_s}{\sigma_a \tau_{21}} \tag{2.3.4}$$

$$I_{sat}^{e} = \frac{h\nu_s}{\sigma_e \tau_{21}} \tag{2.3.5}$$

Rather than viewing the gain coefficient in terms of the levels of N_2 and N_1 as equation (2.3.2), the gain can be written in terms of the light intensity I_s within the fiber [49]:

$$\gamma = \frac{\gamma_o}{1 + \frac{I_s}{I_{sat}}} \tag{2.3.6}$$

For very low intensities the gain coefficient is relatively constant; however, at higher signal intensities the gain drops. Essentially an input signal that reduces the small signal gain coefficient by 50% is at the saturation intensity.

2.4 Basic Laser Resonator Configurations

After light is amplified in a section of pumped fiber, repeated amplification is produced by feeding the output back into the erbium amplifier and confining it there to form a light resonator, conventionally known as a laser resonator. Allowing some of the light within the resonator to escape as usable light results in a potential source of erbium doped fiber laser light.

Two basic resonator designs are possible: the traveling wave ring type, as shown in Fig. 2.4 and the standing wave Fabry-Perot type as depicted in Fig. 2.5.

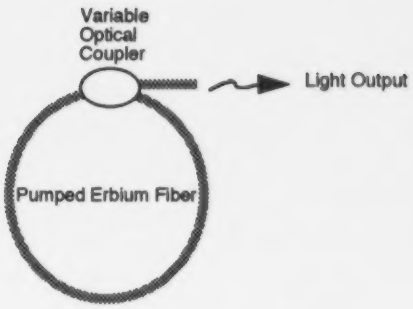

Figure 2.4 Traveling wave ring resonator.

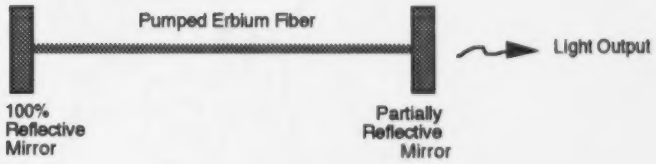

Figure 2.5 Standing wave Fabry-Perot resonator.

For convenience purposes however, the Fabry-Perot resonator mirrors can be simulated using variable couplers to create "fiber mirrors". As a result the configuration will sometimes be referred to as the fiber mirror configuration. See Appendix D for further information on fiber mirrors.

It is also noted that there is no external "input signal" applied to the cavity to act as source for repeated amplification. The input signal is essentially produced by a small amount of spontaneous emission created upon initial pumping. If laser gain and phase conditions are met, lasing within the cavity will then occur.

2.5 Gain Conditions For Laser Operation

For a traveling wave ring resonator, the round trip gain must equal the round trip losses. The minimum or threshold gain coefficient value γ_{th} required to start the laser lasing is given by [50]:

$$\gamma_{th} = -\frac{\ln(R(1-L))}{l} \tag{2.5.1}$$

where R is the effective fractional power reflectivity of the coupler or (1 - the fractional power coupling). L is the total lumped fractional intensity loss per round trip and l is the total round trip distance. One round trip equals the total ring circumference.

For the standing wave Fabry-Perot resonator, the minimum gain needed is:

$$\gamma_{th} = -\frac{\ln(R(1-L))}{2l} \tag{2.5.2}$$

where R is the fractional power reflectivity of the output mirror and $2l$ is the round trip distance. l is the distance between the mirrors according to Fig. 2.5.

2.6 Phase Requirements For Lasing

The phase requirement for laser operation is that an integer number of optical wavelengths resonating must fit within one round trip of the laser's resonator cavity as shown in Fig. 2.6.

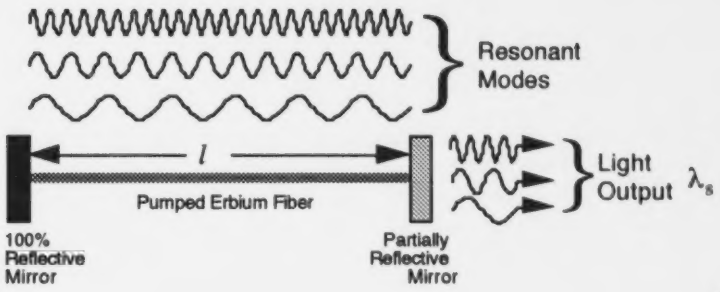

Figure 2.6: Conceptual view of resonating modes that satisfy the phase requirement for laser resonator operation in a Fabry-Perot type resonator.

Since the resonator length is very large relative to the resonant wavelengths, there are many wavelengths, commonly referred to as longitudinal modes, which could satisfy the phase condition. For a multi-longitudinal mode operating Fabry-Perot laser, the expected frequency spacing *df* between modes is given by [33]:

$$df = \frac{c}{2nl} \tag{2.6.1}$$

Where *c* is the speed of light in a vacuum, *n* is the optical fiber refractive index and *l* is the resonator cavity length as shown in Fig. 2.6. Similarly, for a ring resonator, the expected frequency spacing is estimated as:

$$df = \frac{c}{nl} \tag{2.6.2}$$

Where *l* is the total ring circumference. Given that *l* is typically several tens of meters, it would be expected that transverse modes should be separated by approximately 4 - 10 MHz. In terms of wavelength, this translates into a wavelength spacing $\Delta\lambda$, of about 0.00004 nm.

Knowing that the typical amplification range for erbium doped fiber spans more than 30 nm from about 1530 nm to 1560 nm as depicted in Fig. 2.7, many longitudinal operating modes can be expected to satisfy the phase and minimum gain requirements for lasing. In other words it is potentially a highly multi-mode laser.

It must also be noted that light generated will be coherent within each mode (intra-modally coherent) but incoherent between different modes (inter-modally incoherent).

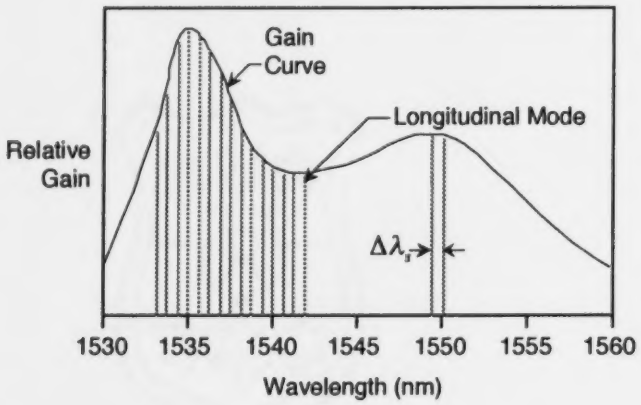

Figure 2.7 Graph depicting the many resonant longitudinal modes that could satisfy the gain and phase requirements for lasing.

2.7 Laser Wavelength Operation

Ideally, it is desirable to have the laser operating on only one of the many possible longitudinal modes. To some extent there will be some competition between modes as wavelengths that have stronger gain will draw energy from the weaker transitions due to the homogeneous broadening effect [51]. As light is repeatedly reflected back into the lasing cavity, the intra-cavity light intensity increases, and the gain is suppressed as predicted by equation (2.3.6). The resulting uniform or "homogeneously broadened" gain suppression is conceptually shown in Fig. 2.8. The end result is that fewer wavelengths can meet the gain requirement for lasing, fewer modes remain in the cavity, and the laser's spectral output narrows.

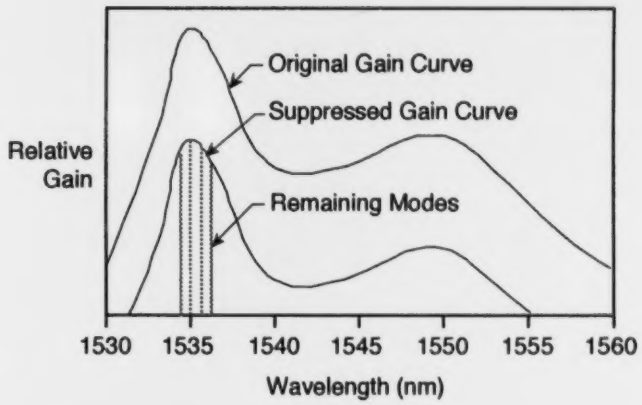

Figure 2.8 Depiction of mode reduction through homogeneous gain suppression.

However there are flat points on the gain vs. wavelength curve where there is little difference in gain over a limited wavelength range, so there may not necessarily be a clear mode competition "winner" and the output spectrum may be spread out somewhat due to "mode hopping" effects or to simultaneously operating modes.

Normally, to produce a single desired mode competition winner or single mode output, the resonator is set up to ensure that the other competing wavelengths lose. This has been typically accomplished using intra-cavity filters or modified resonator configurations [3],[4] that massively attenuate undesirable wavelengths. Of special interest is the use of tunable bandpass filters and multiple loop fiber filter resonators, since these can be readily implemented at TRLabs using existing equipment. A combination of both should ensure tunable single mode operation, and this method of mode selection and control is explored in section 4 of this thesis.

Without intra-cavity filtering, it is noted that equations (2.5.1) and (2.5.2) predict that the gain conditions for lasing can be changed through intra-cavity loss or reflectivity. Since the gain of the laser varies with wavelength, the laser should be somewhat tunable purely due to changes in the output mirror reflectivity. The extent of reflectivity induced

tuning, its practicality and mode behavior are solely dependent upon the emission and absorption cross-sections, and forms the subject of section 3.

2.8 Laser Linewidth

An erbium fiber laser operating in a single longitudinal mode is not infinitely narrow in spectral width. It has a homogeneously broadened Lorentzian line shape centered about the mode's center optical frequency ν_s as shown in Fig 2.9. The spectrum is spread out due to phonon interactions between the erbium ions which essentially "dephase" each other [52], forcing emission of wavelengths slightly off the center operating frequency.

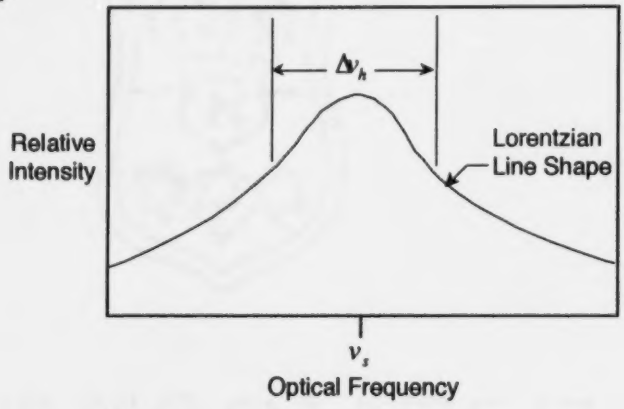

Figure 2.9 Close up view of a single homogeneously broadened laser mode.

The full width half maximum (FWHM) of the Lorentzian curve, or mode "linewidth" $\Delta\nu_h$ is commonly stated in frequency units (Hz) and can be approximated by [52]:

$$\Delta\nu_h \cong \frac{1}{\pi T_2} \tag{2.8.1}$$

where T_2 is the mean time between phase interruptions of the erbium ions and ranges quite widely depending upon laser type considered. T_2 is an inherent parameter not readily

measurable at TRLabs for erbium doped fiber; however, erbium fiber laser linewidths have been often reported to be less than 100 KHz [3],[4]. The exact linewidth is normally determined by experiment.

2.9 Laser Output Power

The output power varies reasonably linearly with respect to the pump power above a certain pump threshold level as shown in Fig 10.

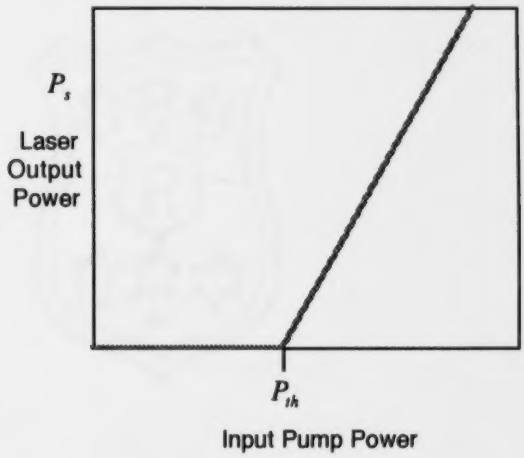

Figure 2.10 Typical output power versus pump power for a laser.

The amount of signal light power P_s emitted by the lasing cavity can be approximated by [42],[53]:

$$P_s = P_f(\frac{P_p}{P_{th}} - 1)\eta_c \qquad (2.9.1)$$

where P_p is the pump power at λ_p, and P_{th} is the pump power required to produce minimum threshold gain, the point where lasing starts. η_c is the power extraction

efficiency of the resonator and P_f is the spontaneous emission or fluorescence power emitted at threshold. For a three level laser P_f is given by [54]:

$$P_f = \frac{N_T}{2}\frac{h\nu_s}{\tau_{21}}V \tag{2.9.2}$$

where V is the total laser volume containing erbium ions of density N_T.

Assuming a 6 micron core fiber with an ion density of 750 ppm, 0.40 confinement factor, 15 meter length, and a spontaneous emission time of 14 ms, the fluorescence power would be about 5.3 mW.

For a three level laser, the minimum threshold pump power is approximately the power needed to produce the fluorescence power.

2.10 Pump Power Efficiency

Some insight into pump power efficiency can be obtained from the ideal three level laser model shown earlier in Fig 2.1. A single photon of pump light at wavelength λ_p will cause a single erbium ion to rise from E_1 to E_3, the ion will then decay non-radiatively to energy level E_2 then eventually fall to E_1 while simultaneously emitting a photon of light at λ_s. Essentially there is one to one relationship between photons absorbed and emitted; however, the energy ratio η_q between them is not the same. Considering energy $h\nu_s$ for a photon at the emitted wavelength compared to energy $h\nu_p$ in a photon at the pump wavelength results in an efficiency of:

$$\eta_q = \frac{h\nu_s}{h\nu_p} \tag{2.10.1}$$

which is defined as the maximum pump power conversion efficiency. Taking λ_p = 980 nm and λ_s = 1550 nm, gives an efficiency of about 63%.

In the case of a laser resonator that produces 5.3 mW of fluorescence power at threshold, we would have to inject at least 8.4 mW of pump power.

2.11 Resonator Power Extraction Efficiency

For a laser resonator, once the pump power exceeds the threshold level, laser light will be produced and dissipated amongst cavity losses and the output coupling. Both are essentially losses as far as laser dynamics are concerned; however, the cavity losses are true power losses while the output coupling loss is a productive loss.

The fraction of the total cavity power that is coupled out of the resonator as useful light is the power extraction efficiency η_c. For low loss, low output coupling lasers this is relatively simple; however, high gain, high loss resonators require a Rigrod analysis [55].

For a unidirectional operating ring resonator, the losses cannot be considered as one lumped value but must be separated into two losses, L_1 and L_2 on either end of the gain medium as shown in Fig. 2.11.

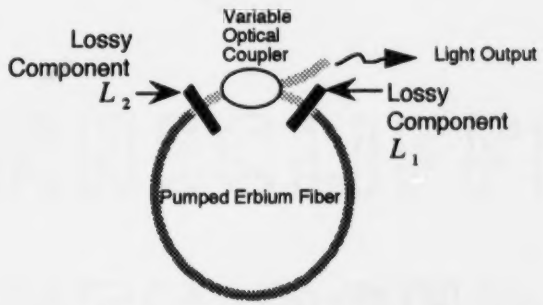

Figure 2.11 Ring resonator with losses.

The power extraction efficiency η_c for a unidirectional ring laser is derived as [55], [56]:

$$\eta_c = \frac{(1-R)(1-L_2)\ln\left[G_o R(1-L_1)(1-L_2)\right]}{\ln(G_o)\left[1-R(1-L_1)(1-L_2)\right]} \qquad (2.11.1)$$

where L_1 and L_2 are the fractional power loss through components L_1 and L_2. R is the effective fractional power reflectivity of the output coupler and G_o is the single pass small signal gain of the pumped erbium fiber. The losses of the coupler itself are considered lumped in with L_2.

Normally however fiber optic component losses are quoted in terms of "insertion loss" and therefore must be converted to the conventional laser term of fractional loss. For example, a 10 dB insertion loss would be equivalent to a 0.9 fractional loss.

Similarly, the Fabry-Perot configuration can be modeled as shown in Fig. 2.12.

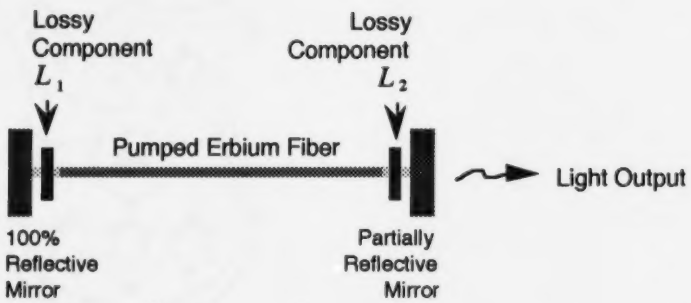

Figure 2.12 Fabry-Perot resonator with losses

The power extraction efficiency can be estimated as [55]:

$$\eta_c = \frac{(1-L_2)(1-R)\ln\left[G_o(1-L_1)(1-L_2)\sqrt{R}\right]}{\ln(G_o)\left[1+\frac{\sqrt{R}(1-L_2)}{(1-L_1)}\right]\left[1-\sqrt{R}(1-L_1)(1-L_2)\right]} \qquad (2.11.2)$$

The effects of each variable on the coupling efficiency can be best explained graphically.

2.12 Power Extraction Efficiency Versus Losses

For a fiber with a G_o = 15 dB and a resonator output coupling of R = 50%, the expected efficiency variation versus insertion loss for the ring configuration is shown in Fig. 2.13.

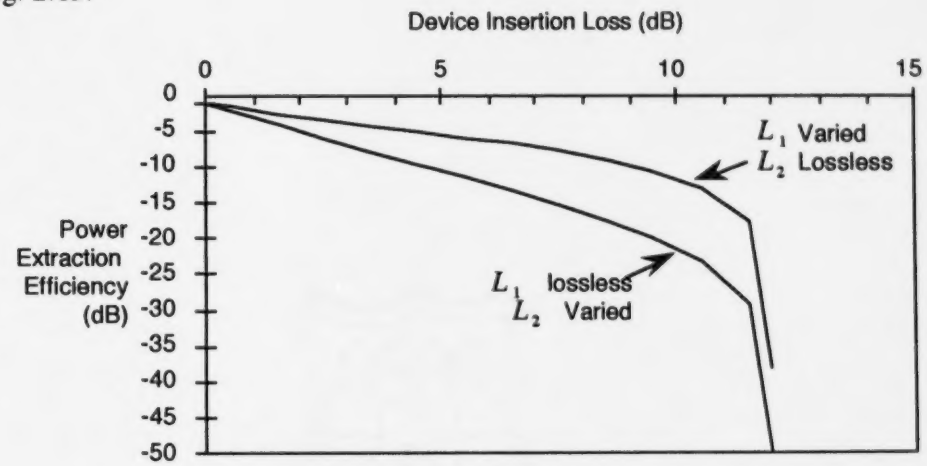

Figure 2.13 Power extraction efficiency vs. device insertion loss for the ring configuration.

The results for the Fabry-Perot resonator with the same variables is shown in Fig. 2.14

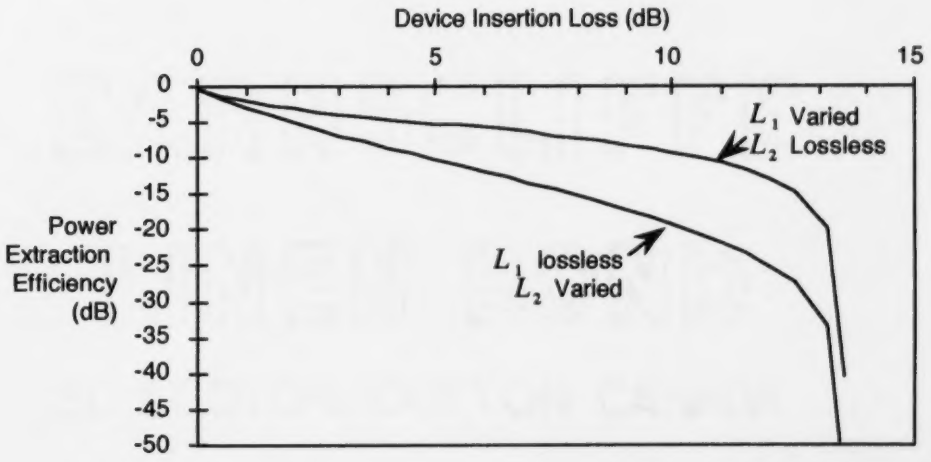

Figure 2.14 Power extraction efficiency vs. device insertion loss for fiber mirror configuration.

In both cases one component is considered lossless while the loss of the other is varied from 0 to 15 dB. It is seen that the output efficiency varies almost linearly for losses less than 10 dB and that losses at L_2 are twice as significant.

2.13 Laser Efficiency Versus Reflectivity

It is intuitive that the output power will depend on the output reflectivity. Some reflectivity is needed to meet the laser gain requirements; however, too much reflectivity will result in no output power. Too little reflectivity will impede lasing and result in a device producing incoherent amplified spontaneous emission: an erbium fiber flashlight. Between these two extremes, there will be an optimum coupling value which will depend on equations (2.11.1) and (2.11.2). Assuming a 15 dB small signal gain, the coupling efficiency has been calculated in Fig. 2.15 and Fig. 2.16 for the ring and Fabry-Perot configurations respectively for a variety of insertion losses.

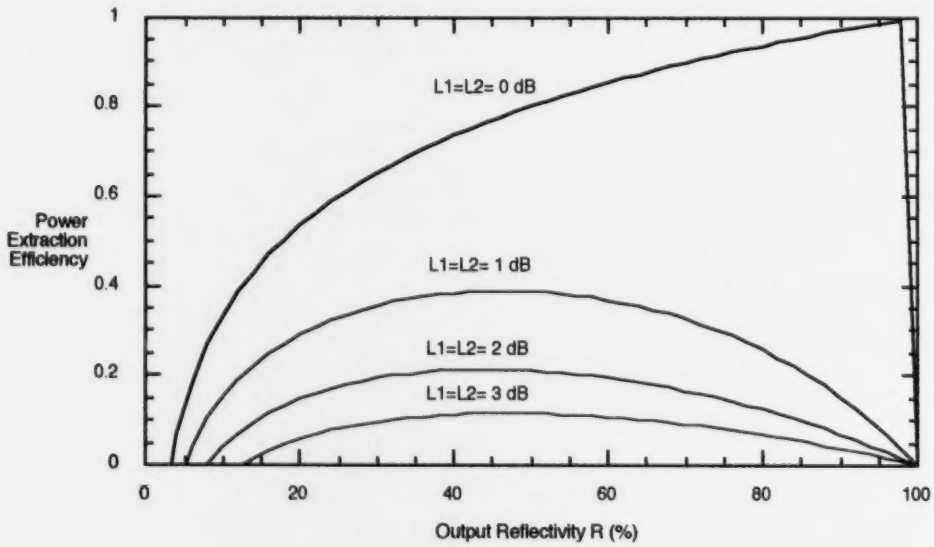

Figure 2.15 Extraction efficiency vs. reflectivity for ring configuration. G_o = 15 dB.

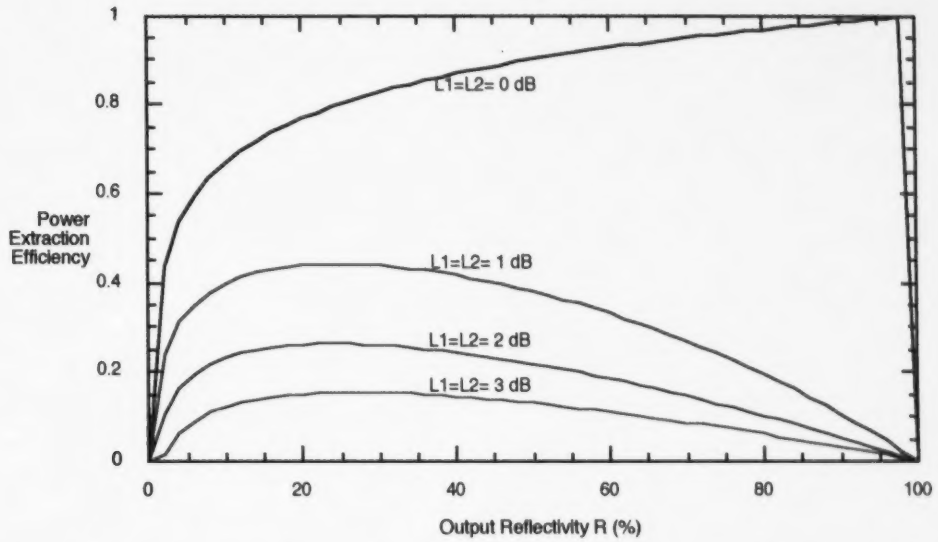

Figure 2.16 Extraction efficiency vs. reflectivity for Fabry-Perot configuration. G_o = 15 dB.

For insertion losses on the order of a few dB, it is apparent that the ring laser prefers reflectivities of about 45-50% and the Fabry-Perot laser is best suited to about 20-25%.

2.14 Power Extraction Efficiency Versus Gain

The small signal gain will influence the power extraction versus reflectivity characteristic. For $L_1 = L_2 = 2$ dB, some sample curves are shown plotted in Fig. 2.17 and Fig. 2.18 for the ring and Fabry-Perot laser configurations respectively.

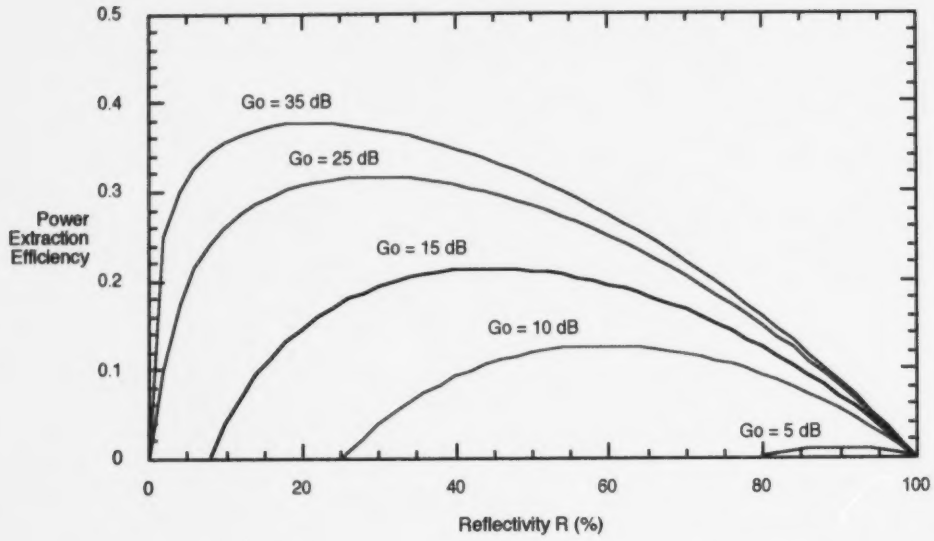

Figure 2.17 Extraction efficiency vs. reflectivity for ring resonator. $L_1 = L_2 = 2$ dB.

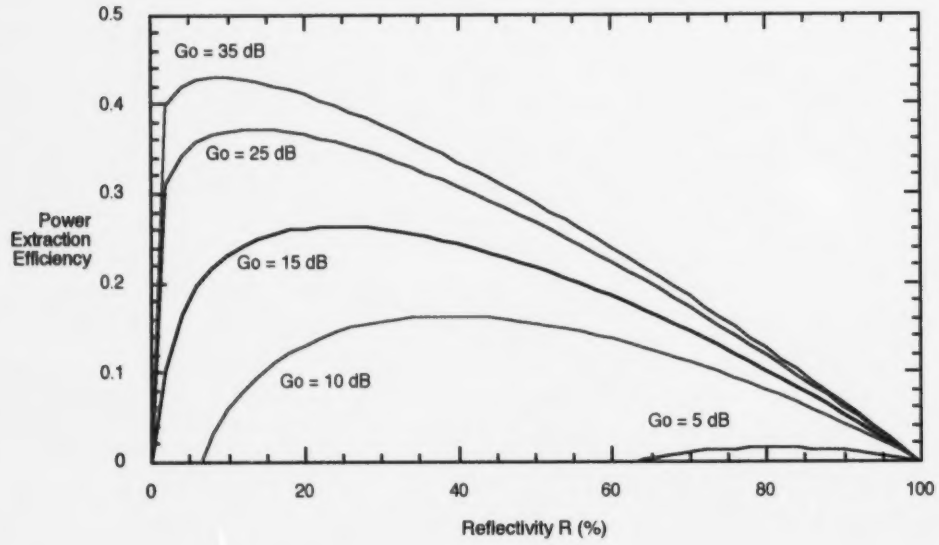

Figure 2.18 Extraction efficiency vs. reflectivity for Fabry-Perot resonator. $L_1 = L_2 = 2$ dB.

2.15 Light Output Power Versus Pump Power

Based on knowledge of coupling efficiency and equipment readily available in the lab it is possible to derive an expected power out versus power in characteristic based on equation (2.9.1). An expected power out versus pump power in graph is shown in Fig. 2.19 for a Fabry-Perot laser with G_o = 15 dB (pump power =18 mW), $L_1 = L_2$ = 2 dB, P_{th} = 8.4 mW and R = 20%.

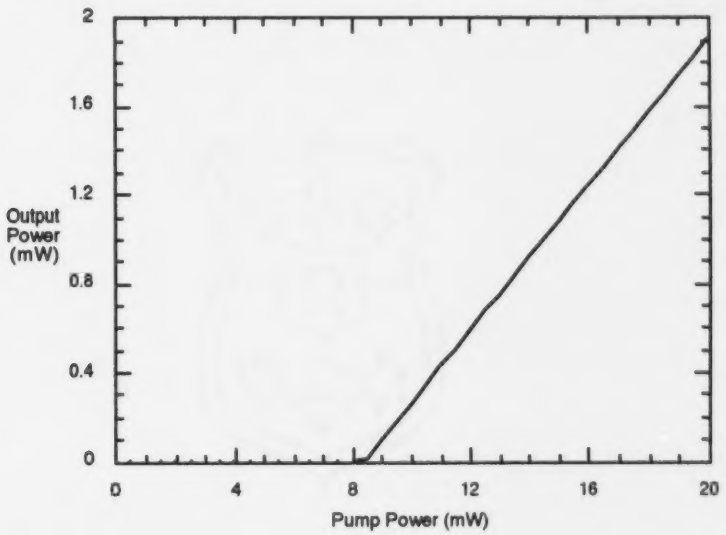

Figure 2.19 Output power characteristic expected for the fiber mirror laser.

2.16 Laser Steady State Time

From the instant of initial spontaneous emission within the laser cavity to the point where mode competition has completed, and the final steady state intensity value is reached, a portion of time has elapsed as depicted in Fig. 2.20. During this time the laser will peak and subside due to a combination of gain switched pulsing and mode hopping effects.

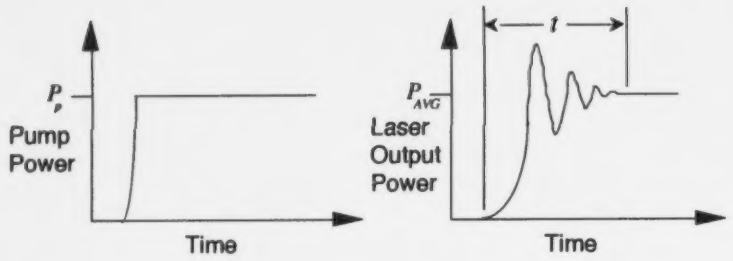

Figure 2.20 Conceptual view of laser response to initial pump power switching.

Assuming the pump power switching time is very fast, the time t to steady state can be estimated for a ring laser by [56]:

$$t = \frac{20nl}{\ln\left[G_o(1-R)(1-L)\right]c} \tag{2.16.1}$$

or for a Fabry-Perot laser:

$$t = \frac{40nl}{\ln\left[2G_o(1-R)(1-L)\right]c} \tag{2.16.2}$$

As a reasonable example, a laser with a small signal fiber gain on the order of 15 dB, reflectivity of 50%, losses at 4 dB, 20 m round trip length, the time to reach the steady state output power would be around 2.1 μs (Ring resonator) or 1.6 μs (Fabry-Perot resonator).

In terms of communications, if this laser were to be digitally modulated through switching the pump laser on and off, it would be limited to a bandwidth less than 700 KHz.

2.17 Relaxation Oscillations

A laser that is continuously producing a constant average output power may fluctuate occasionally due to small disturbances in the resonator conditions then settle back to its original level as shown conceptually in Fig. 2.21.

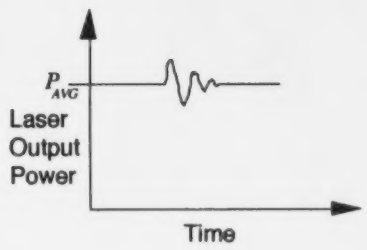

Figure 2.21 Depiction of disturbance in a lasers average output power.

The characteristic frequency at which the laser responds to the disturbance is termed the relaxation oscillation frequency f_{sp} . This value is inherently different for every laser type and can be reasonably estimated for three and four level laser systems by the following equation [57]:

$$f_{sp} = \frac{1}{2\pi}\sqrt{\left(\frac{P_p}{P_{th}} - 1\right)\frac{1}{\tau_{21}\tau_c}} \tag{2.17.1}$$

Where:

P_p is the pumping power,

P_{th} is threshold pump level,

τ_{21} is the upper state lifetime, and

τ_c is the lasers cavity photon lifetime.

For a ring laser of circumference l the photon lifetime is given by [58]:

$$\tau_c = \frac{nl}{c(1 - R(1 - L))} \tag{2.17.2}$$

For a Fabry-Perot laser with mirror separation l , the photon lifetime is given by :

$$\tau_c = \frac{2nl}{c(1 - R(1 - L))} \tag{2.17.3}$$

Where:

n = index of refraction

c = speed of light in vacuum

L = fractional round trip cavity intensity loss

R = effective cavity output mirror reflectivity

2.18 Relative Intensity Noise

The ideal single mode laser should produce a constant output power level, or continuous wave (CW), with no intensity fluctuations over time. In reality however, lasers do tend to *continually* fluctuate very slightly with respect to the average power they produce and this is termed relative intensity noise (RIN). This is shown greatly exaggerated in Fig. 2.22.

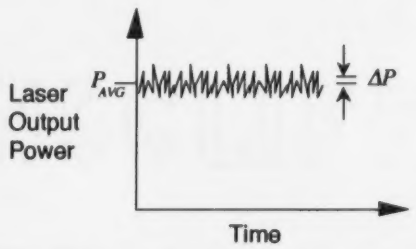

Figure 2.22 Laser average output power over time.

The RIN of a laser is given by [59]:

$$RIN = \frac{(\Delta P)^2}{(P_{AVG})^2} \tag{2.18.1}$$

where $(\Delta P)^2$ is the mean square noise power spectral density of the optical output and $(P_{AVG})^2$ is the average optical power squared. RIN does not occur at a single frequency

like relaxation oscillations but typically exists over a wide bandwidth and will vary with frequency. As a result, RIN is often referred to as a value measured at a particular frequency and within a 1 Hz bandwidth.

At the inception of the project a literature search indicated that no theoretical investigation or experimental measurements of the RIN expected for an erbium doped fiber laser had been reported; however, based on noise analysis done for other lasers, a number of inferences could reasonably be made regarding factors that influence the noise level.

The noise is not dominated by random spontaneous emission created within the amplifying medium as is the case with erbium doped fiber amplifiers. Although broad band spontaneous emission exists and increases with initial pumping, above laser threshold the contribution of spontaneous emission is clamped to the fluorescence level [60]. However, this power is randomly emitted in direction and is therefore relatively small compared to the coherent stimulated emission that is produced and coupled efficiently into the fiber.

There are generally two causes of RIN [47]: 1) quantum shot noise inherent to the laser and 2) random external fields disturbing the laser.

Quantum noise in the laser occurs due to the active laser medium absorbing pump power in discrete energy quanta or photons. The rate equations describing the laser dynamics naturally react to this by emitting discrete photons or quanta of energy at the signal wavelength. In other words, on the small scale, the pump power is not absorbed evenly, therefore light is not emitted evenly. This quantum noise is somewhat analogous to shot noise inherent to the optical detection process in optical detectors. It has been shown for gas, solid state, and diode lasers that this type of RIN generally dominates near threshold but decreases as the pump power is increased [47].

Random external fields disturbing the laser such as the method of pumping and environment of the laser dominate the RIN at higher pump powers. A pump laser that is unstable or pulsing will obviously cause instabilities in the rate equations and produce a

noisy output. Similarly, external forces on the laser resonator which causes changes in cavity loss also disrupts the steady state assumptions and undesirable modulation of the output occurs. External forces on the resonator cavity sounds similar to effects that cause relaxation oscillations; however, these interruptions are on a much smaller scale. In the case of laser diodes however RIN is known to peak or be at its worse right at the relaxation oscillation frequency.

For the development of a communications grade fiber laser incorporating a high quality pump source operating well above threshold, it would be expected that forces other than quantum noise and pump modulation noise would dominate the RIN. External forces are nearly impossible to model given all the variables involved; therefore, for this project a primarily experimental approach to investigating the RIN would have to be used.

2.19 Lab Equipment

Several erbium doped fiber designs are possible; however, this thesis study has limited itself to utilizing fiber that was designed previously [18] for use as an amplifier and that concentrated on designing erbium doped fiber for maximum amplification given the pump power available in the lab.

Given that the amplifier available had a small signal gain of 15 dB and that this gain was in excess of the total round trip losses expected for any resonator envisioned, an erbium laser was viewed as possible.

The fiber also had a wide range of amplified spontaneous emission from about 1530 nm to 1560 nm which would suggest a wide laser tuning range. However, the amplifier in the lab was also 15 meters long which in theory would allow for several thousand longitudinal modes to resonate within a resonator cavity. Some additional filtering equipment was available in the lab in the event that pure mode competition would not produce a single mode laser.

As a first step towards producing a low noise, tunable communications laser, the available erbium doped fiber was experimented with in the two basic un-filtered resonator configurations described earlier. Lasing was accomplished, and a noted tuning or shifting of the operating wavelength was observed as the output coupling was varied.

3

Output Coupling Induced Wavelength Shifts in Erbium Doped Fiber Lasers

3.1 Introduction

Several methods for obtaining tunable operation of erbium-doped fiber lasers have been reported, all of which require some form of wavelength selective element as part of the laser cavity. Typically, intra-cavity filters or gratings have been used to obtain broadband tuning and very narrow line operation of ring lasers as well as other laser configurations [20-23]. In [24] Scrivener et al. report tuning over certain wavelength bands and attribute the tuning to the optimization of the reflectivity of a variable fiber coupler, in which the coupling coefficient can be wavelength tuned enabling tuning of the laser output. Similarly, Chaoyu et al. [25] report a continuously tunable Nd^{3+} fiber ring laser in which the tuning is attributed to the wavelength dependent characteristics of a fiber coupler, using the same ring laser configuration as Scrivener et al. Millar et al. [26-27] also made use of a well characterized wavelength dependent variable coupler, configured in the form of a fiber mirror to produce a wavelength tunable fiber laser.

Recently, a simplified theory of fiber laser operation has been published [28] in which it is predicted that the wavelength of erbium doped fiber lasers can be tuned within and between wavelength bands simply by varying the wavelength *independent* reflectivity of the output coupling mirror. In this chapter experiments are presented in which an erbium doped fiber laser is wavelength tuned within and between three narrow wavelength bands using only the variable output coupling of one output mirror, taking extreme care to ensure that none of the components within the laser cavity has a significant wavelength

dependence that could cause the laser to be wavelength tuned, thus verifying the predicted reflectivity tuning operation of reference [28].

Most of this chapter has been published in reference [61].

3.2 Tuning Theory

For a standard two mirror, standing wave laser resonator, the round trip gain G = exp(g) at the signal or lasing wavelength λ_s can be written as [28];

$$g = 2\Gamma_s l\rho\left[\langle x_o\rangle\sigma_e(\lambda_s) - (1-\langle x_o\rangle)\sigma_a(\lambda_s)\right] + \ln(R_1) + \ln(R_2) + \ln(1-L) \qquad (3.1)$$

while for a laser in a traveling wave, ring resonator configuration, the corresponding equation is:

$$g = \Gamma_s l\rho\left[\langle x_o\rangle\sigma_e(\lambda_s) - (1-\langle x_o\rangle)\sigma_a(\lambda_s)\right] + \ln(R_1) + \ln(R_2) + \ln(1-L) \qquad (3.2)$$

σ_a and σ_e are the absorption and emission cross sections respectively at various wavelengths and L is the round trip fractional lumped component loss. l is the erbium fiber length, R_1 and R_2 are the effective mirror fractional power reflectivities of the lasing cavity and ρ is the erbium ion concentration. and $\langle x_o\rangle$ is the mean fraction of excited erbium ions along the fiber axis which is expressed as

$$\langle x_o\rangle = \frac{1}{l}\int_{z=0}^{l} x(r=0,z)dz \qquad (3.3)$$

Assuming that x is the fraction of erbium ions in an excited state at some point z along the fiber and some radius r in the fiber it is assumed

$$\int_0^l \int_0^a \rho x(r,z) I(r) 2\pi r \, dr dz \cong \Gamma \rho l \langle x_o \rangle \tag{3.4}$$

Γ, being the signal modal confinement factor which can be calculated using,

$$\Gamma = \int_0^a I(r) 2\pi r \, dr \tag{3.5}$$

The lasing condition $g = 0$ will be satisfied over a range of wavelengths for pump powers above threshold. However, because of the wavelength dependent emission and absorption cross sections, the value of $\langle x_o \rangle$, the mean fraction of excited erbium ions along the fiber axis, that satisfies this lasing condition will also be wavelength dependent. This can be calculated from equation (3.1) and is illustrated for example in Fig. 3.1 where, for our laser configurations, $R_1 = 1$ and $R_2 = R$ = (1 - output coupling). Thus the lasing wavelength for a particular set of parameters l, pump power, erbium concentration etc., will be that wavelength at which the choice of $\langle x_o \rangle$ results in a maximum gain cross-section $\sigma_g = \left[\langle x_o \rangle \sigma_e(\lambda_s) - (1 - \langle x_o \rangle)\sigma_a(\lambda_s)\right]$. For example in figure 3.1 this wavelength will be $\approx$ 1550 nm for R = -3 dB and $\approx$ 1536 for R = -10 dB. By varying the wavelength *independent* reflectivity of the cavity mirrors, a tunable laser can result. In the traditional methods of obtaining tunable lasers, strong wavelength dependence in the reflectivities R_1 and R_2 or in the internal cavity loss L is introduced.

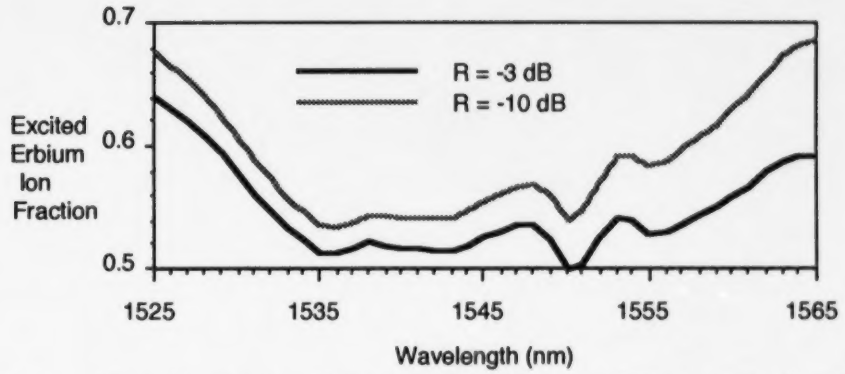

Figure 3.1 Excited ion fraction that satisfies the lasing condition vs. wavelength (sample calculation for two different output mirror reflectivities).

3.3 Tuning Results

Two fiber laser configurations were used in the experiments as shown in Fig. 3.2a and Fig. 3.2b. The directional coupler, 50/50 coupler, and optical isolator were tested to ensure that over the wavelength range of the amplified spontaneous emission there was insignificant wavelength dependence in the coupling coefficient and/or transmission loss. The erbium doped fiber was step index fiber, co-doped with aluminum and germanium, with a core diameter of 6.1 μm and NA = 0.16. The erbium concentration was $\approx$ 750 ppm, confined to the central $\approx$ 40% of the refractive index core radius, and the length of this fiber was 15 meters. Assumed emission and absorption cross-sections were based on reference [29]. The injected pump power was $\approx$ 18 mW as referenced to the input of the erbium doped fiber.

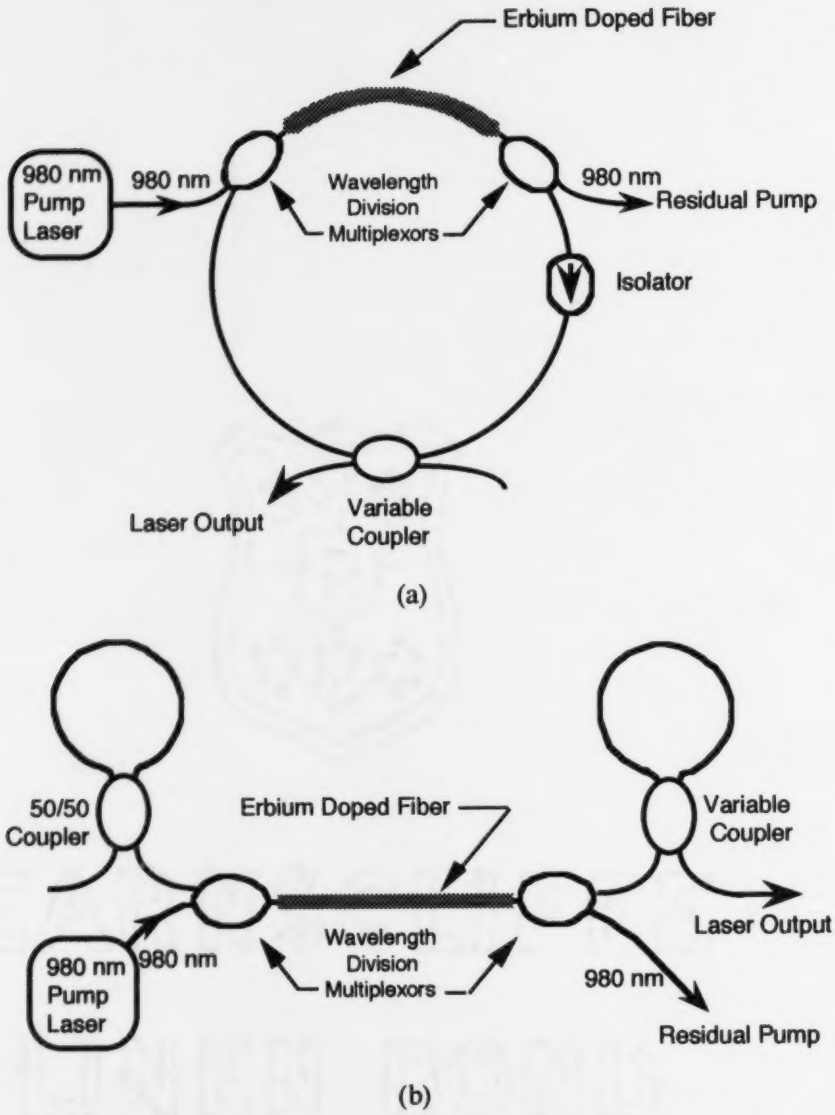

Figure 3.2 Experimental laser configurations: (a) fiber ring laser (b) fiber mirror laser

The total round trip intra-cavity losses of all components were ≈ 6 dB and 8 dB for the ring and fiber mirror configurations, respectively. As a function of output coupling mirror reflectivity, the calculated and measured lasing wavelengths of the two respective laser configurations are as shown in Fig. 3.3a and Fig. 3.3b. As can be seen from Figures 3.3a and 3.3b, at some fixed reflectivities the laser was measured to be operational at more

than one wavelength. In these cases it is not known whether the laser is rapidly *hopping* between individual wavelengths or is operating *simultaneously* at multiple wavelengths.

Although direct measurement of this is difficult, one can make some assumptions based on the structure of the laser and its gain media characteristics. In general, lasers that use amplifying media that are homogeneously broadened tend to have their longitudinal modes briefly compete after initial power up, but then one mode that requires the least gain to oscillate will quickly dominate over the others within microseconds by absorbing power from the other wavelength transition bands due to the homogeneous broadening effect.

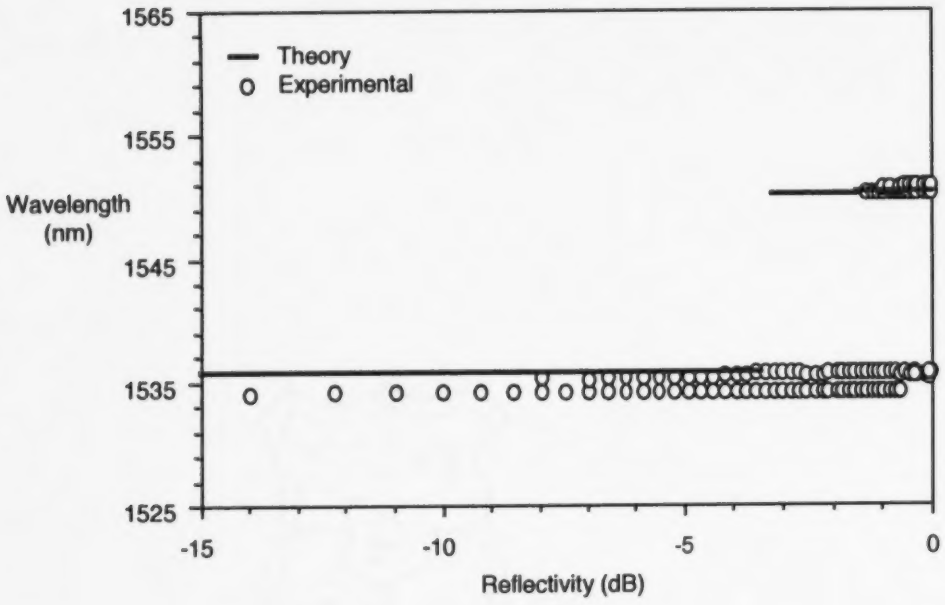

(a)

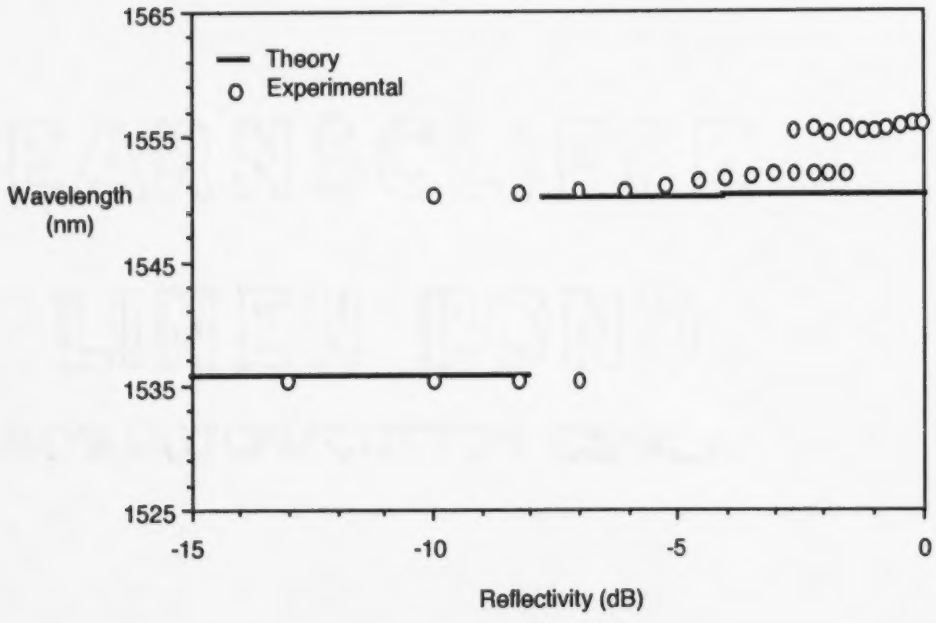

(b)

Figure 3.3 Wavelength of observed lasing peaks vs. reflectivity (a) ring configuration (b) fiber mirror configuration.

One possible exception to this is for Fabry-Perot laser resonator designs. In these resonators the light within the cavity sets up a standing wave pattern along the cavity length where there are local maximums and minimums in intensity every half wavelength. The points of local maximum tend to locally saturate out the gain media while minimum points leave the medium unsaturated. This effect, commonly referred to as *spatial* hole burning, can allow additional modes to spatially take advantage of the unsaturated gain medium points . This can result in simultaneous lasing of multiple wavelengths within a single homogeneously broadened amplifying medium.

Lasers with inhomogeneously broadened gain media tend to not share energy between their transitions so it is possible that lasing at many wavelengths can simultaneously occur as long as the round trip phase and gain conditions are met. There will be points within the gain spectrum that use wavelengths of light that do not meet the lasing conditions thereby leaving gaps of unused gain media that are essentially wasted since their energy cannot be transferred to other wavelengths bands that do meet the conditions. This effect is called *spectral* hole burning.

Given that the erbium doped fiber structure resembles a solid state laser rather than a gas laser, it is perhaps disconcerting at first to find that erbium doped fibers are described widely as being homogeneously broadened devices [30]. Solid state lasers such as Nd-YAG Lasers that have their gain media trapped within a lattice structure tend to be inhomogeneously broadened while gas lasers such as CO_2 that allow free movement are homogeneously broadened. Researchers attribute the homogeneous broadening to energy sharing between ions through phonon emissions.

Using the assumption that the laser is homogeneously broadened as reported, it is probably most likely that the laser is operating at only one wavelength at a time, and that the monochromator scans that shows two wavelengths lasing are actually showing the laser hopping between wavelengths. There has been only one paper, to the author's knowledge, that claims simultaneous operation of two laser lines within a single erbium doped fiber

gain medium [31]. However, the experiment used two different resonant ring cavities sharing the same gain media to achieve the claimed result.

One other group has published a paper that claims to have produced a wideband optical comb [32] which implies simultaneous operation, however this was not proven.

Nevertheless, given the uncertainty in the wavelength dependent absorption and emission cross sections, the agreement between the calculated and measured wavelengths is good, illustrating that the operative wavelength shifting mechanism is associated with the wavelength dependence of the emission and absorption cross sections, since there are no wavelength dependent components inside the laser cavities.

Both configurations had linearly polarized outputs, however the degree of polarization between two mutually orthogonal axes, called the ordinary and extraordinary, varied depending upon configuration. The ring configuration had a 12 dB polarization extinction ratio while the fiber mirror configuration had only a 5 dB difference.

The laser output spectrum in either configuration was relatively broad, being on the order of 1 nm as shown in Fig. 3.4.

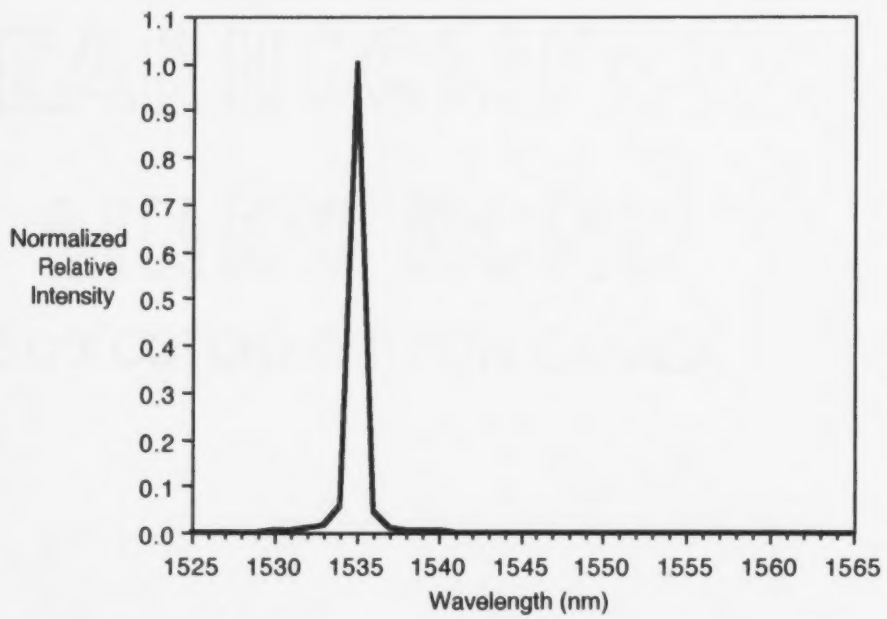

Figure 3.4 Typical spectral shape of observed laser oscillations.

The output power and residual pump power as a function of reflectivity for each configuration is shown in Fig. 3.5.

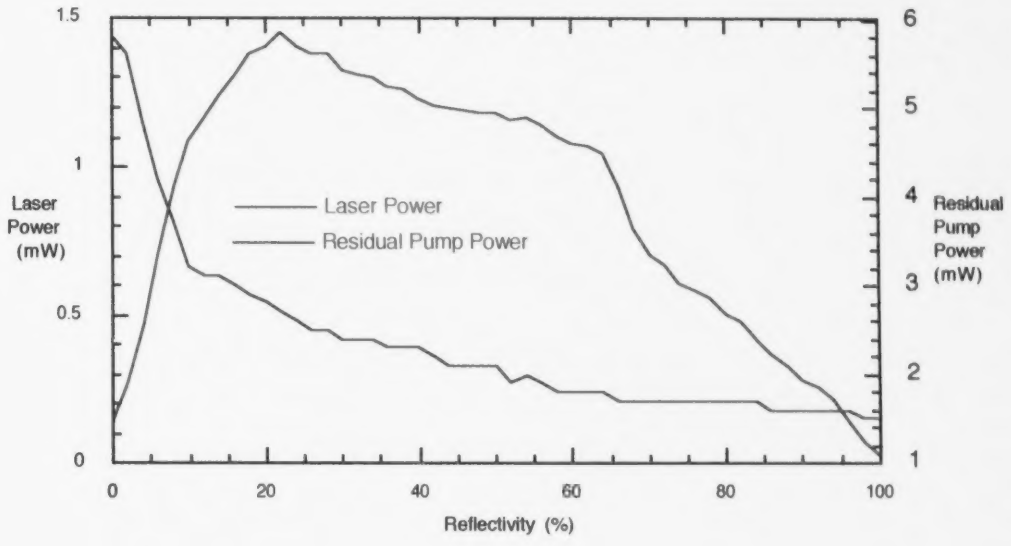

(a)

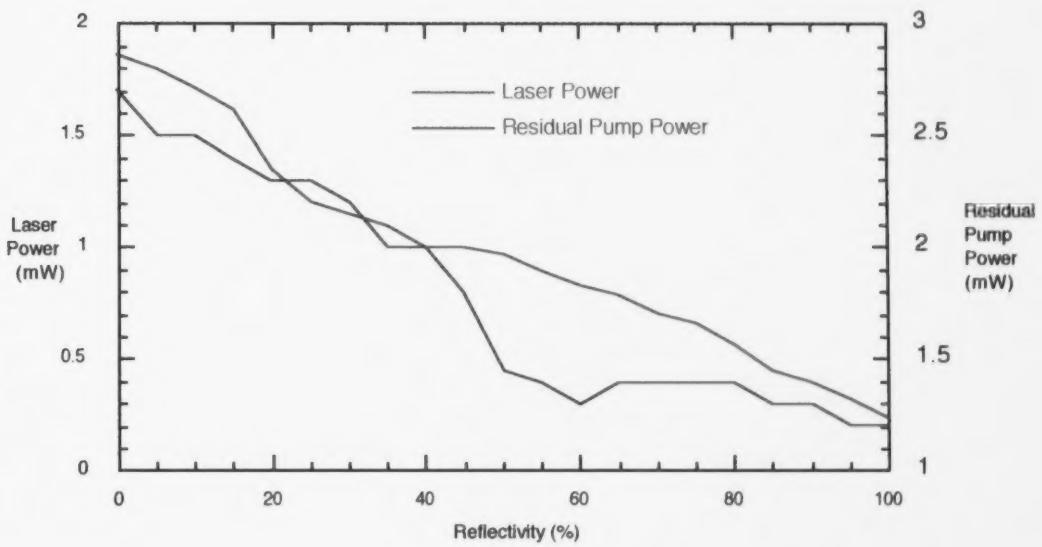

(b)

Figure 3.5 Observed laser output power and pump residual power vs. reflectivity (a) ring configuration (b) fiber mirror configuration.

It must be noted that the residual pump power measurements of Fig 3.5 are referenced to the exit of the erbium fiber. Also, according to Fig 3.5 there is still output laser power at 100% and 0% reflectivity and this is attributed to inaccuracy in the couplers. 100% and 0% are in fact some small deviation from this, enough to create lasing and some output power.

If we compare the experimental power vs. reflectivity curves of Fig. 3.5 with the corresponding theoretical curves of Fig. 2.15 and Fig. 2.16 we see that there is at best qualitative agreement between theory and experiment. This is to be expected as the measured G_o is for 1550 nm signals only and in this experiment the laser wavelength changes and G_o is substantially higher at the lower reflectivities where the operating wavelength is 1535 nm.

In Fig. 3.6 we show the laser output power as a function of input pump power for the mirror configuration with output coupling set at 20%. The input pump power is referenced to the input of the erbium fiber. Considering $L_1 = L_2 = 2$ dB, $R = 20\%$, $P_f = 5.3$ mW, $P_{th} = 8.4$ mW and $G_o = 15$ dB equation (2.9.1) predicts about a 16.4 % slope efficiency while the experimental attained 14.4% efficiency with respect to input pump power. It is noted that the pump power stated is the injected pump power and that in actual fact not all the power is absorbed as can be inferred from the residual pump power measurements shown in Fig. 3.5. This can account for some of the discrepancy between theory and experimental but nevertheless there is reasonable agreement between the two in terms of slope efficiency and threshold pump power.

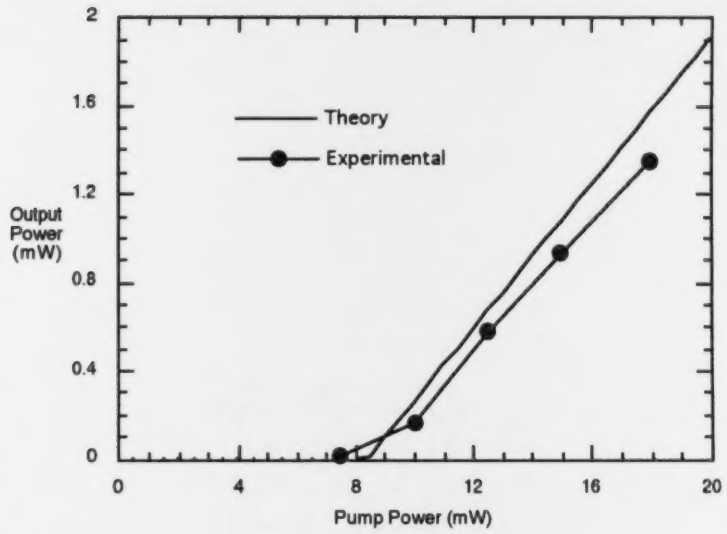

Figure 3.6 Measured output power vs. injected pump power for fiber mirror laser set at R = 20%.

4

Laser Spectral Width and Noise Properties

4.1 Mode Measurement Theory

As configured in chapter 2, the two fiber lasers operated with a spectral width on the order of one nm. Since the monochromator takes about three minutes to complete a scan from 1500 to 1600 nm, the observed results represent a time average rather than an instantaneous view of the laser's output spectrum. As a result, it is difficult to determine whether the viewed spectrum is due to many longitudinal mode lines or optical frequencies operating simultaneously, or a few lines hopping within the one nm range seen. Further information about the laser's operating behavior can be obtained through shining the laser's output on a photo diode and observing the resulting electrical spectrum on an RF spectrum analyzer. Fig. 4.1 illustrates the experimental layout.

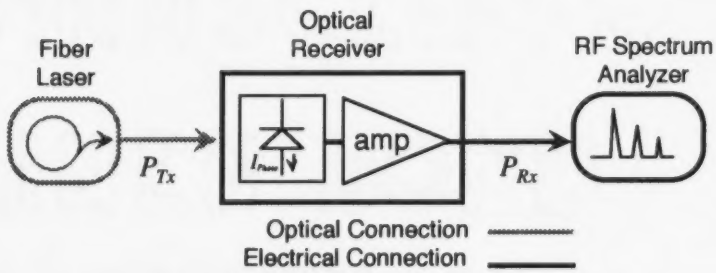

Figure 4.1 Experimental layout for measurement of laser modes

The theory behind this technique is relatively simple but will be summarized briefly in order to better understand the results that will be presented.

The laser's total transmitted (CW) optical power P_{Tx}, composed of one or more laser longitudinal modes or lines with electric fields E_i operating at frequencies f_i,

generates a photo-current I_{Photo} in the photo-detector that is proportional to the sum of the input optical electric fields squared as defined below:

$$I_{Photo} \alpha \sum_i E_i \cdot E_i^* \alpha \left\{ \sum_i E_i \cos(2\pi f_i t) \right\}^2 \tag{4.1}$$

Due to this "square law" property, the electrical signal seen at the output and as viewed in the frequency domain will be composed of carriers at the sum and difference frequencies or "beat" frequencies of the electrical fields. Fig. 4.2 shows the spectral beating effect expected versus the number of laser lines transmitted.

For the perfectly ideal single longitudinally moded 1550 nm laser emitting an oscillating electrical field corresponding to f_i = 194 THz we should see an observed output spectrum corresponding to Fig. 4.2 (a). The expected beat frequencies would theoretically occur at DC and at $2f_i$. Given that typical spectrum analyzer coverage is from about 100 Hz to several GHz, this instrument will not measure the DC component and the $2f_i$ product is too high in frequency.

As the number of modes or operating frequencies, separated by *df* increases as in Figures 4.2 (b), (c) and (d), the number of beat products also increases in number and in amplitude. For a multi-longitudinal mode operating laser, the expected frequency spacing *df* between modes is given by (2.6.1) and (2.6.2). Given that *l* is typically several tens of meters, it would be expected that beat products should occur in approximately 5 MHz increments. In reality, the highest beat frequencies observable will be limited by the frequency response limitations inherent to the photo diode, receiver amplifier and spectrum analyzer.

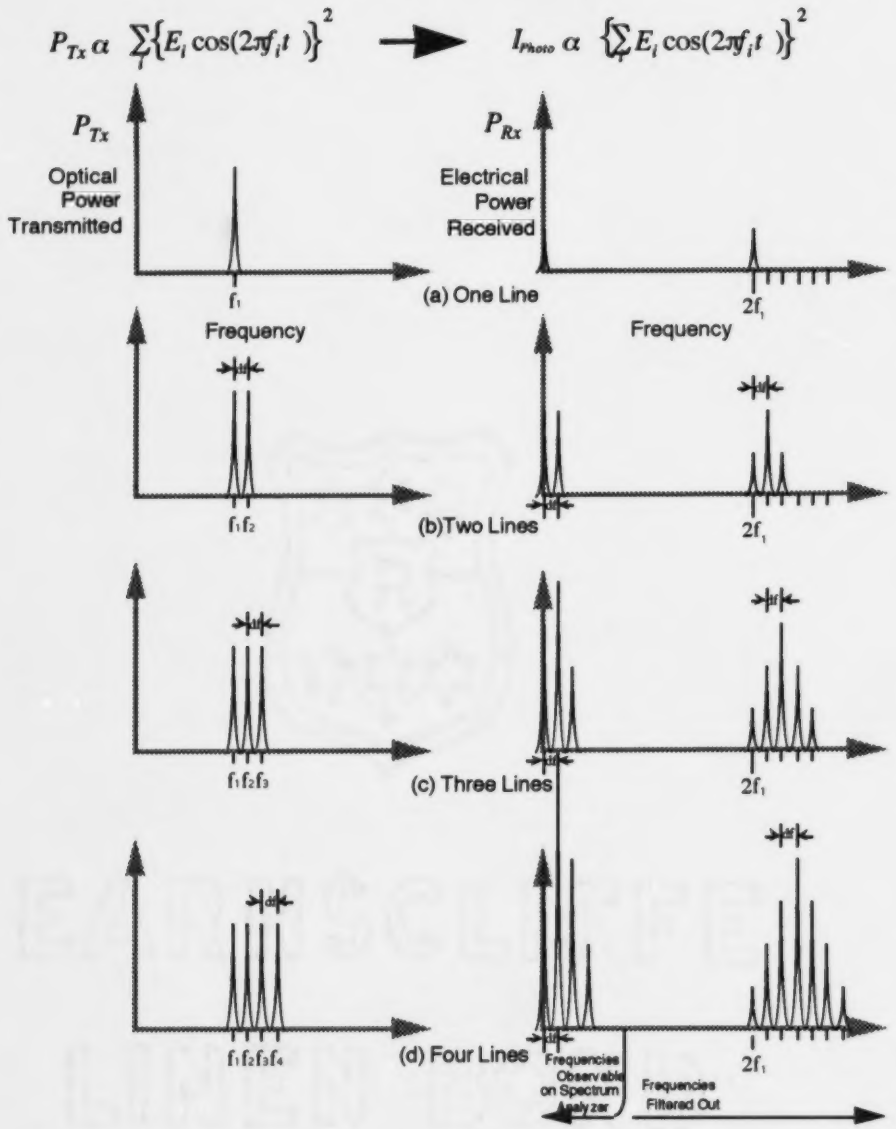

Figure 4.2 Expected spectral beating effect of laser lines in the detection process as a function of the number of operating longitudinal modes: (a) one line (b) two lines (c) three lines (4) four lines.

4.2 Measurement Equipment

The equipment used for the measurement was a Hewlett Packard 71400™ Lightwave Signal Analyzer. This device is essentially a wide bandwidth optical detector, amplifier and fundamentally mixed spectrum analyzer combination that provides a calibrated optical power reading over the 100 KHz to 22 GHz frequency range. This equipment was used to obtain further information on the number of operating modes within the 1 nm wide line width observed by the monochromator.

4.3 Laser Mode Beat Products for Basic Loop Configuration

Fig. 4.3 shows a typically observed RF spectral output in terms of effective input optical power measured within a 1 MHz resolution bandwidth for the fiber ring laser configuration. It is apparent that the laser is clearly not operating single moded as there are peaks seen at regular 6.2 MHz intervals that correspond to the frequency spacing of laser modes expected, using equation (2.6.2), for a laser with about a 33 m round trip cavity length. It must also be noted that although the peaks appear rounded at the top, triangular in shape and stopping short of the noise floor, they are in reality very narrow spikes extending down to the noise floor. Closer scans of individual spikes were seen to have a 3 dB width of less than 10 KHz. Essentially the linewidth shown in Fig. 4.3 is wider than the actual linewidth due to the chosen 1 MHz spectrum analyzer resolution bandwidth, but the peak power measured for each spike is accurate.

The shape of the recorded lines is a function of the spectrum analyzer's resolution and video bandwidth used. A narrower resolution bandwidth could have been used to increase the sharpness; however, the sweep time of the analyzer correspondingly increases thus causing the acquisition time of results to reach impractical lengths. As a result, a compromise between speed and resolution was made and should be kept in mind when viewing any spectrum analyzer results.

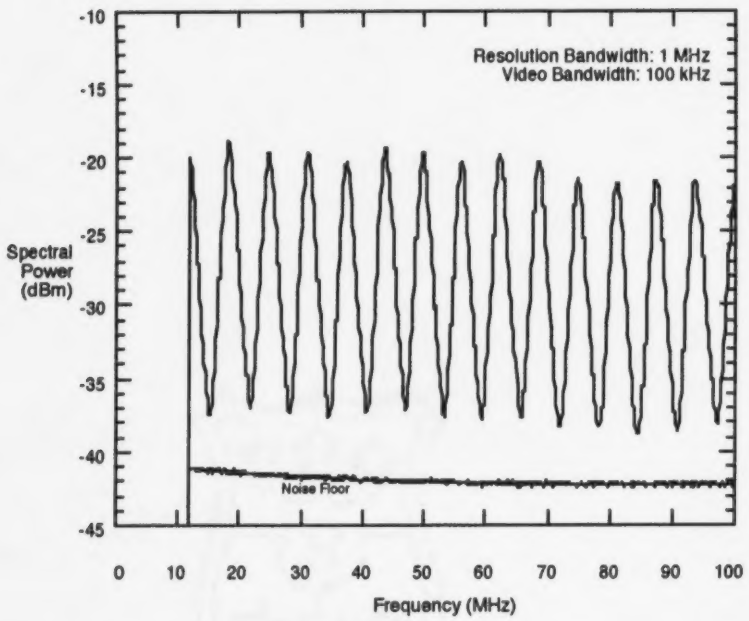

Figure 4.3 Spectral output vs. frequency for 33 m ring laser (10 to 100 MHz).

As configured the laser showed a highly multi-moded behavior with mode beat products extending well into the GHz range (Fig 4.4), indicating that the total laser spectral width was at least 10 GHz. As a potential communications source, the laser was obviously unacceptable; therefore, a new modified configuration was needed in an attempt to produce a better quality laser.

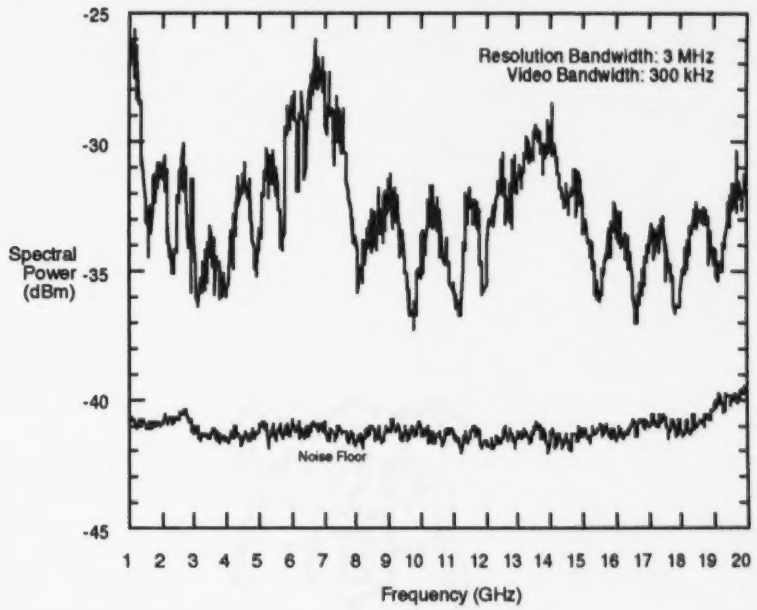

Figure 4.4 Spectral output vs. frequency for ring laser (1 to 20 GHz)

4.4 Reduction of Modes

4.4.1 Band Pass Filtering

Several papers have reported producing single mode lasers using a variety of filtering techniques. The easiest method of reducing line width was to utilize a tunable 1 nm bandpass filter available in the lab. For both the mirror and loop configuration, the laser spectral width was reduced to about 0.3 nm. To compensate for the insertion loss of the filter, a higher power 980 nm pump laser (≈ 40 mW) was used to drive the laser . Other changes included residual pump wavelength division multiplexor removal since the filter installed attenuated any residual pump. The experimental layout for the filtered mirror configuration is shown in Fig. 4.5a.

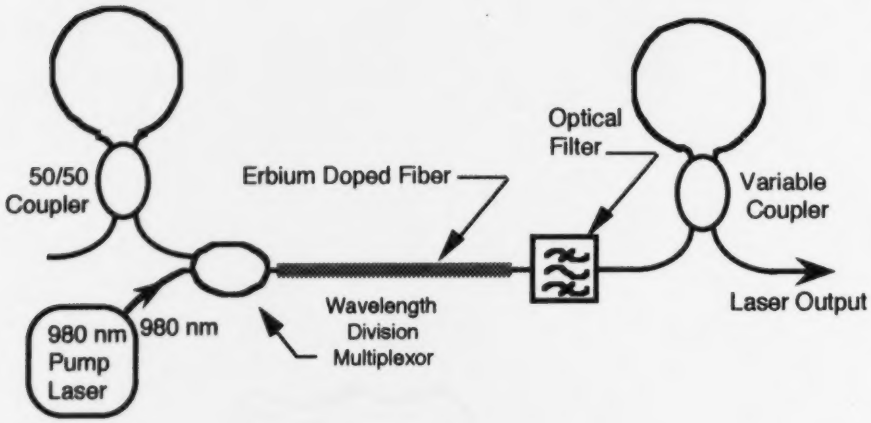

Figure 4.5a Experimental layout for filtered fiber mirror configuration with intra-cavity tunable band pass filter.

Plots of output power vs. operating wavelength obtained by adjusting the filter in the mirror configuration of Fig 4.5a are shown in Fig. 4.5b.

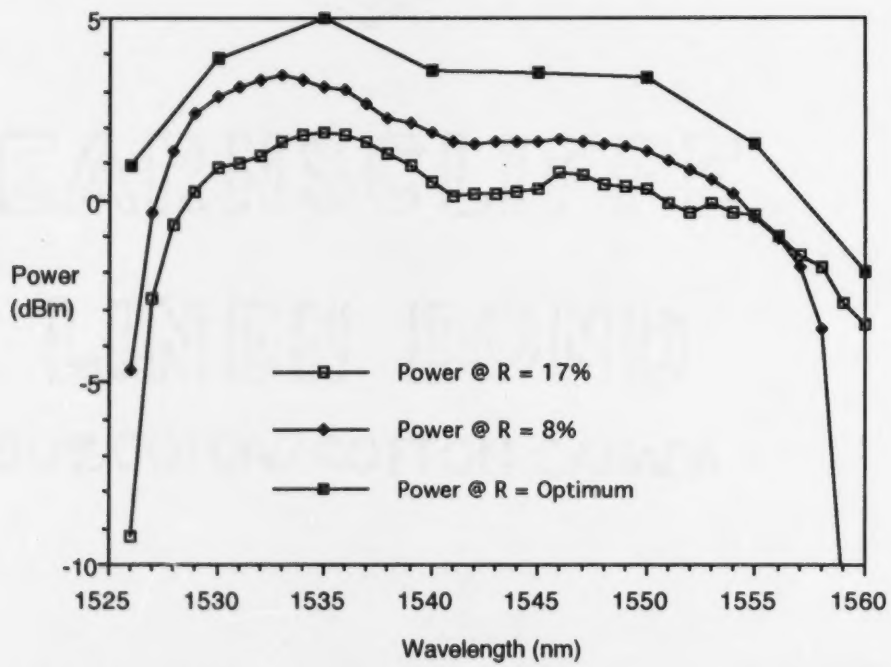

Figure 4.5b Observed peak power vs. wavelength and various reflectivities for the fiber mirror laser with intra-cavity tunable bandpass filter.

The effects of insertion loss of an internal cavity component on output power were also investigated using a variable optical attenuater within the resonator as shown in Fig. 4.6a.

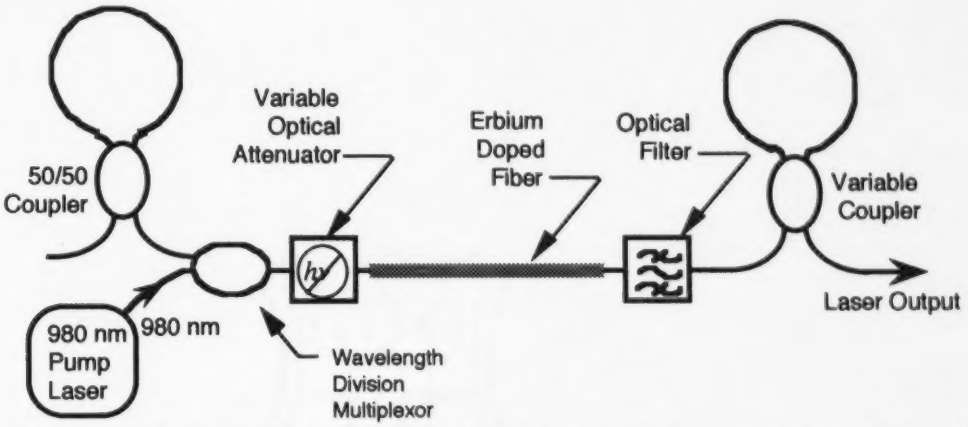

Figure 4.6a Experimental layout for fiber mirror configuration using an intra-cavity optical attenuator.

The effects of output power versus insertion loss at 1535 nm is shown in Fig. 4.6b and demonstrates the linear relationship as predicted earlier.

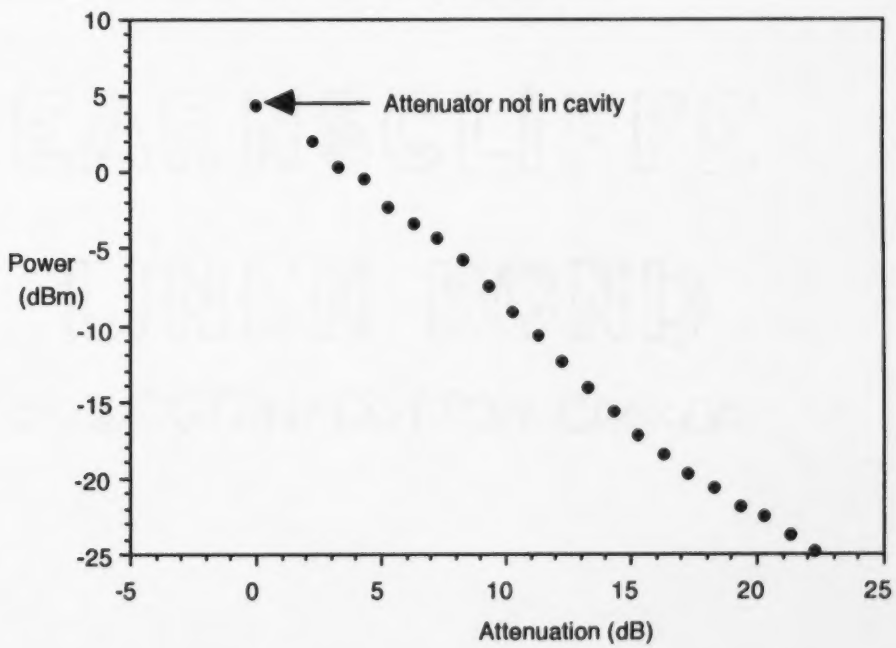

Figure 4.6b Peak output power vs. intra-cavity attenuation for the fiber mirror laser with intra-cavity tunable bandpass filter set at 1535 nm.

Although this configuration can be used as a tunable light source for other experiments [34], to produce a source more suitable for communications purposes, additional filtering techniques were needed since little reduction in mode beat products was observed for frequencies less than 10 GHz.

4.4.2 Fiber Filtering

Other possible choices of filters include the Fabry-Perot and fiber loop type. Although they produce a comb filter effect they have a much sharper filter response than a simple band pass filter [35]. Of special interest is the reported use of fiber filters since these can be readily constructed using existing couplers in the lab. The three filter configurations considered are shown in Fig. 4.7.

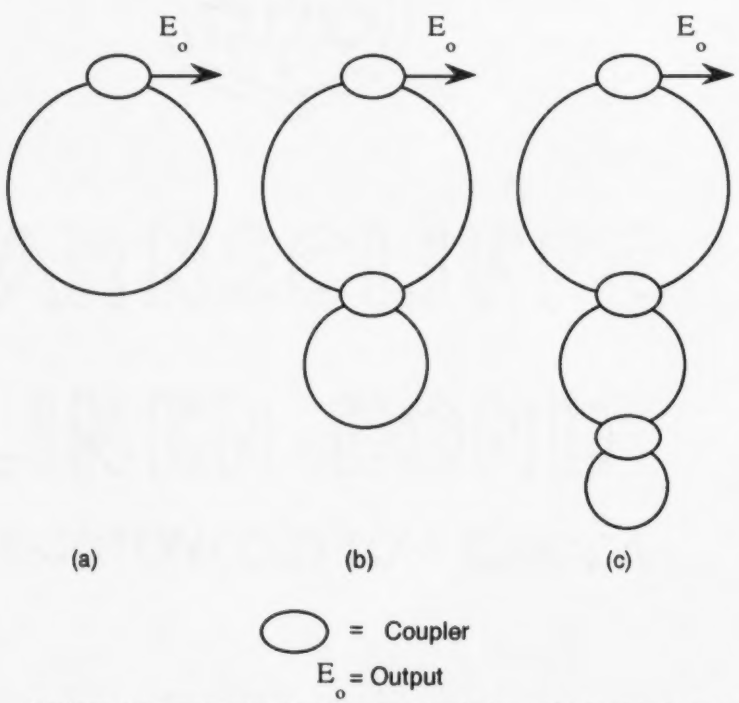

Figure 4.7 Various ring resonator designs: (a) single loop (b) double loop (c) triple loop.

Fig. 4.7(a) is obviously the configuration already tried and widely reported. Fig. 4.7(b) simply adds a second loop which has been reported, although in a slightly different

coupling arrangement, to improve spectral behavior [36]. The resonator in Fig. 4.7(c) has not been reported on, to the author's knowledge, but would be expected to add an additional level of filtering to the resonator.

4.4.2.1 Passive Loop Filter Theory- Equating of Fields

In order to model the filtering effect of a multi-loop resonator, we can first view the device as passive filter with an input and output, similar to the way the modeling of a standing wave Fabry-Perot resonator can be approached. See Fig. 4.8.

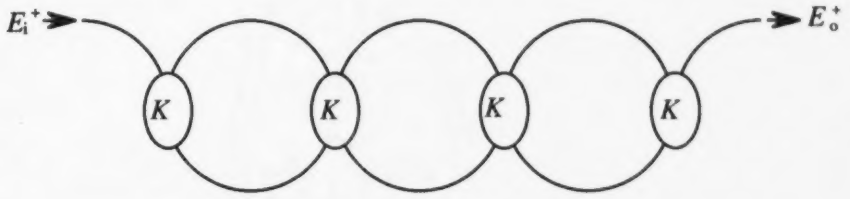

Figure 4.8 Triple ring filter layout.

Knowing the way electric fields are coupled as shown in Fig. 4.9 and accounting for phase delays due to fiber between couplers, we can determine the electric fields at each entrance and exit point of every coupler.

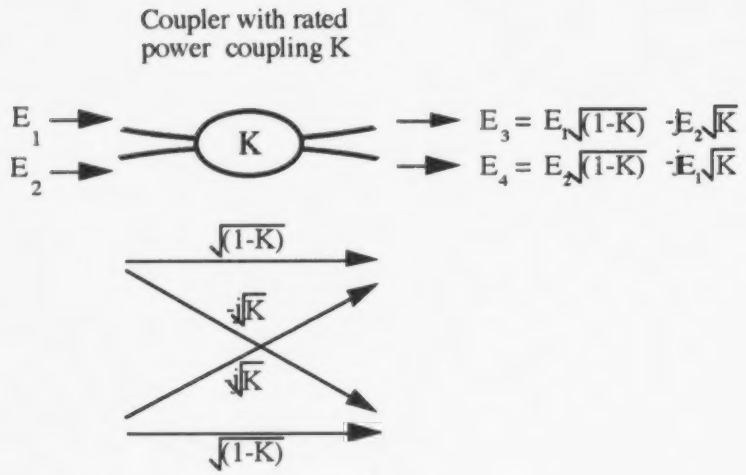

Figure 4.9 Diagram showing the coupling of electric fields across a coupler.

This technique requires solving many simultaneous equations and unknowns in order to determine the transfer function which is tedious and prone to mistakes. A much simpler approach is a matrix formalism [37] approach.

4.4.2.2 Passive Loop Filter Theory- Matrix Approach

A fiber coupler with power coupling coefficient K_i can be viewed with an input and output relationship as shown in Fig 4.10.

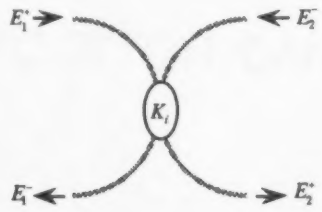

Figure 4.10 Input-output view of coupler for matrix approach.

Neglecting phase delays due to fiber lengths, the corresponding matrix transfer function [37] is:

$$\begin{bmatrix} E_1^+ \\ E_1^- \end{bmatrix} = \frac{j}{t_i} \begin{bmatrix} -1 & r_i \\ -r_i & 1 \end{bmatrix} \begin{bmatrix} E_2^+ \\ E_2^- \end{bmatrix} \qquad (4.4.2.2.1)$$

where,

$$r_i = \sqrt{(1 - K_i)} \qquad (4.4.2.2.2)$$

$$t_i = \sqrt{K_i} \qquad (4.4.2.2.3)$$

To account for phase delays in the lengths of fiber connected to the coupler we consider fiber pigtails as in Fig. 4.11.

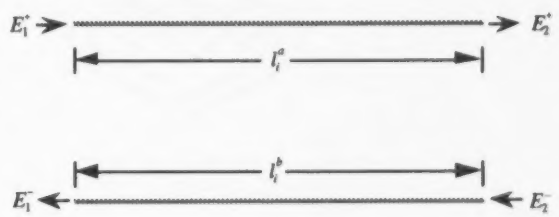

Figure 4.11 Input and output notation for sections of optical fiber when using the matrix formalism.

For two lengths of optical fiber, with lead lengths not necessarily equal, the relationship between input and output can be written as:

$$\begin{bmatrix} E_1^+ \\ E_1^- \end{bmatrix} = \begin{bmatrix} e^{-jk_i l_i^a} & 0 \\ 0 & e^{jk_i l_i^b} \end{bmatrix} \begin{bmatrix} E_2^+ \\ E_2^- \end{bmatrix} \qquad (4.4.2.2.4)$$

where,

$$k_i = \frac{2\pi n}{\lambda_s} \qquad (4.4.2.2.5)$$

A multi-cavity filter is simply an alternating concatenation of these two functions as shown in Fig. 4.12.

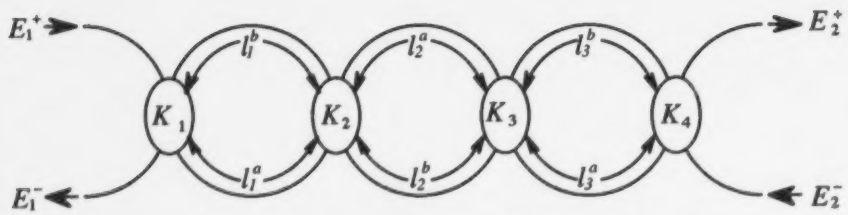

Figure 4.12 Triple ring filter layout for matrix formalism.

The relationship between input and output is essentially the individual transfer matrices multiplied together in the same order that they appear physically laid out. Multiplying out the matrices results in:

$$\begin{bmatrix} E_1^+ \\ E_1^- \end{bmatrix} = A_1B_1A_2B_2A_3B_3A_4 \begin{bmatrix} E_2^+ \\ E_2^- \end{bmatrix} = C \begin{bmatrix} E_2^+ \\ E_2^- \end{bmatrix} = \begin{bmatrix} c_{11} & c_{12} \\ c_{21} & c_{22} \end{bmatrix} \begin{bmatrix} E_2^+ \\ E_2^- \end{bmatrix} \qquad (4.4.2.2.6)$$

where,

$$A_i = \frac{j}{t_i} \begin{bmatrix} -1 & r_i \\ -r_i & 1 \end{bmatrix} \qquad (4.4.2.2.7)$$

$$B_i = \begin{bmatrix} e^{-jk_i l_i^a} & 0 \\ 0 & e^{jk_i l_i^b} \end{bmatrix} \qquad (4.4.2.2.8)$$

In considering the multi-ring structure as a filter with only one output E_o from E_2^+ and one input E_i taken from E_1^+ as shown in Fig. 4.13, we can determine the transfer function $\frac{E_o}{E_i}$ by setting $E_2^- = 0$ in (4.4.2.2.6) and solving for $\frac{E_2^+}{E_1^+}$:

$$\frac{E_o}{E_i} = \left.\frac{E_2^+}{E_1^+}\right|_{E_2^- = 0} = \frac{1}{c_{11}} \qquad (4.4.2.2.9)$$

The expected transfer function is shown in equation (4.4.2.2.10).

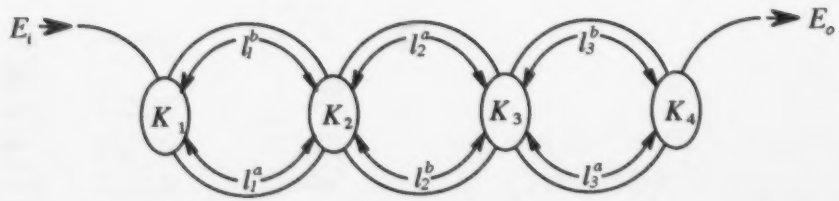

Figure 4.13 Input and output notation for filter transfer function.

$$\frac{E_o}{E_i} = \frac{t_1 t_2 t_3 t_4 e^{j(k_1 l_1^a + k_2 l_2^a + k_3 l_3^a)}}{1 - r_1 r_2 e^{j(k_1 l_1)} - r_2 r_3 e^{j(k_2 l_2)} - r_3 r_4 e^{j(k_3 l_3)} + r_1 r_3 e^{j(k_1 l_1 + k_2 l_2)} + r_2 r_4 e^{j(k_2 l_2 + k_3 l_3)} + r_1 r_2 r_3 r_4 e^{j(k_1 l_1 + k_3 l_3)} - r_1 r_4 e^{j(k_1 l_1 + k_2 l_2 + k_3 l_3)}} \quad (4.4.2.2.10)$$

$$l_i = l_i^a + l_i^b \quad (4.4.2.2.11)$$

Using this approach, the determination of the filter transfer function is much simpler to obtain than with the equating of fields technique and lends itself readily to solving via computer algebraic multiplication and reduction algorithms. It is therefore a very fast and accurate technique.

4.4.2.3 Simulation Results

Obviously for a high gain high loss laser utilizing a multi-ring resonator filter, a Rigrod type analysis would have to ensue that would account for the effects of the filter resonator's coupler losses, coupler values and fiber gain. However due to the numerically intense calculations involved and their sensitivity to conditions the multi-ring filter was viewed as a "black box" with an overall filtering effect and insertion loss.

Using equation (4.4.2.2.10), the filtering of a one, two or three loop filter can be modeled and was done so by assuming no losses or gain within the filter, no polarization rotation and 10^{-5} coupling for each coupler. Modeling in this fashion essentially predicts a filter's best case side mode suppression behavior. Using practical fiber length values readily available in the lab, one can determine whether building such a resonator is even worth attempting.

The predicted filtering effect of a single 50 m loop configuration is shown in Fig. 4.14. A two loop configuration with a second parasitic 10 m long loop, as in Fig. 4.7(b), has a filtering effect shown in Fig. 4.15. The addition of a third 1.4 m long loop as in Fig. 4.7(c) will have a filtering function as in Fig. 4.16.

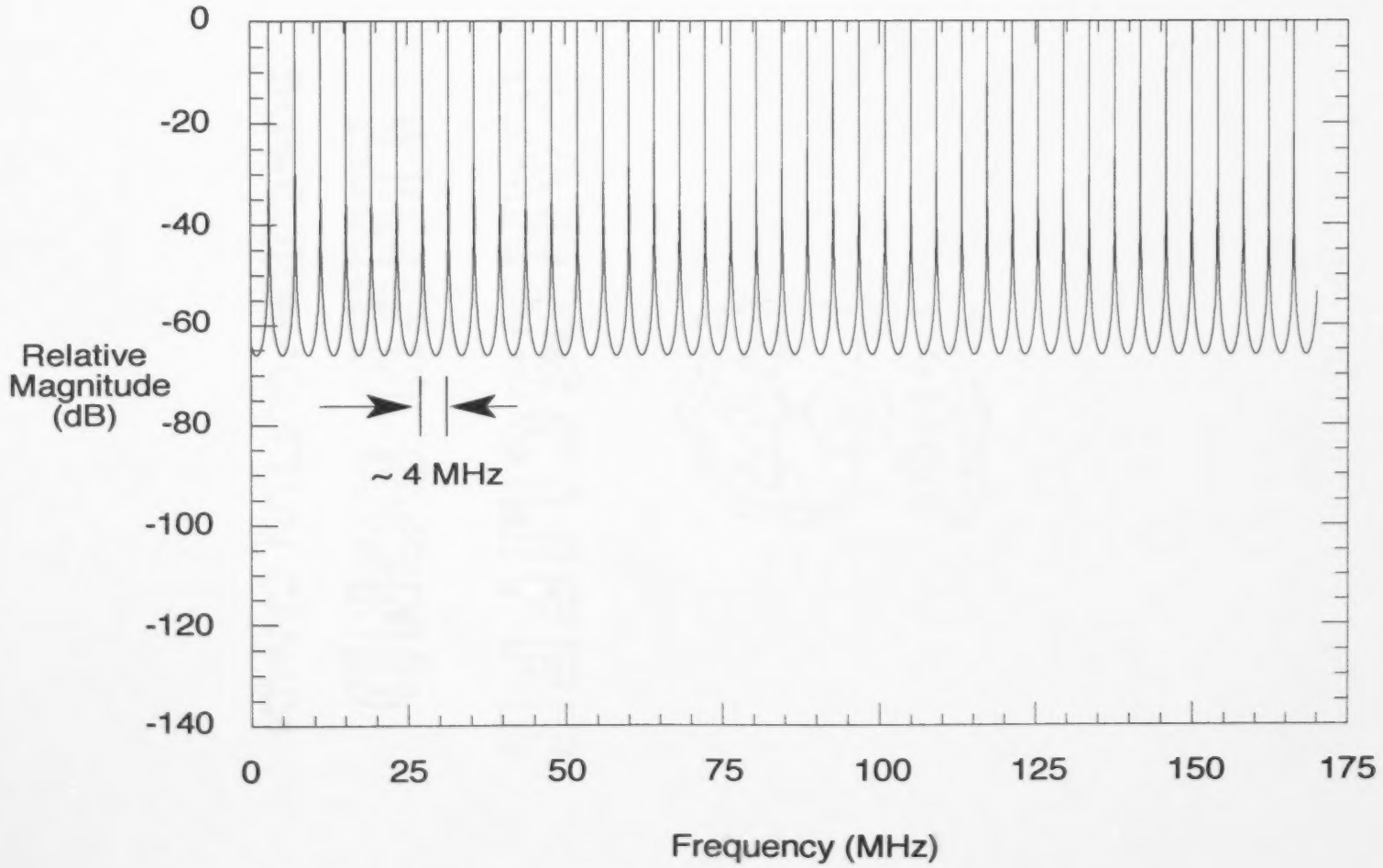

Figure 4.14 Theoretical response for a single 50m loop filter.

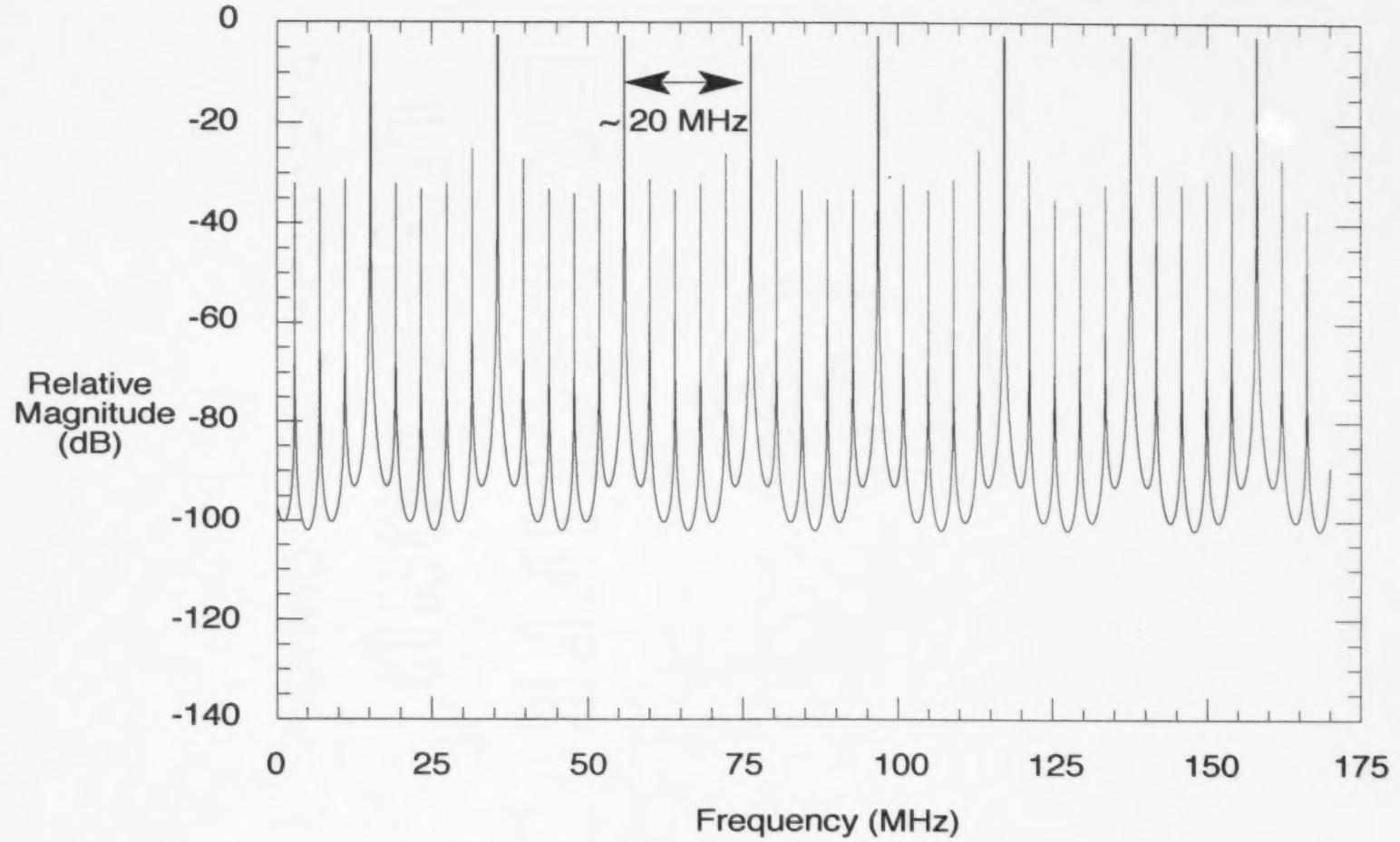

Figure 4.15 Theoretical response for a 50m/10m double loop filter.

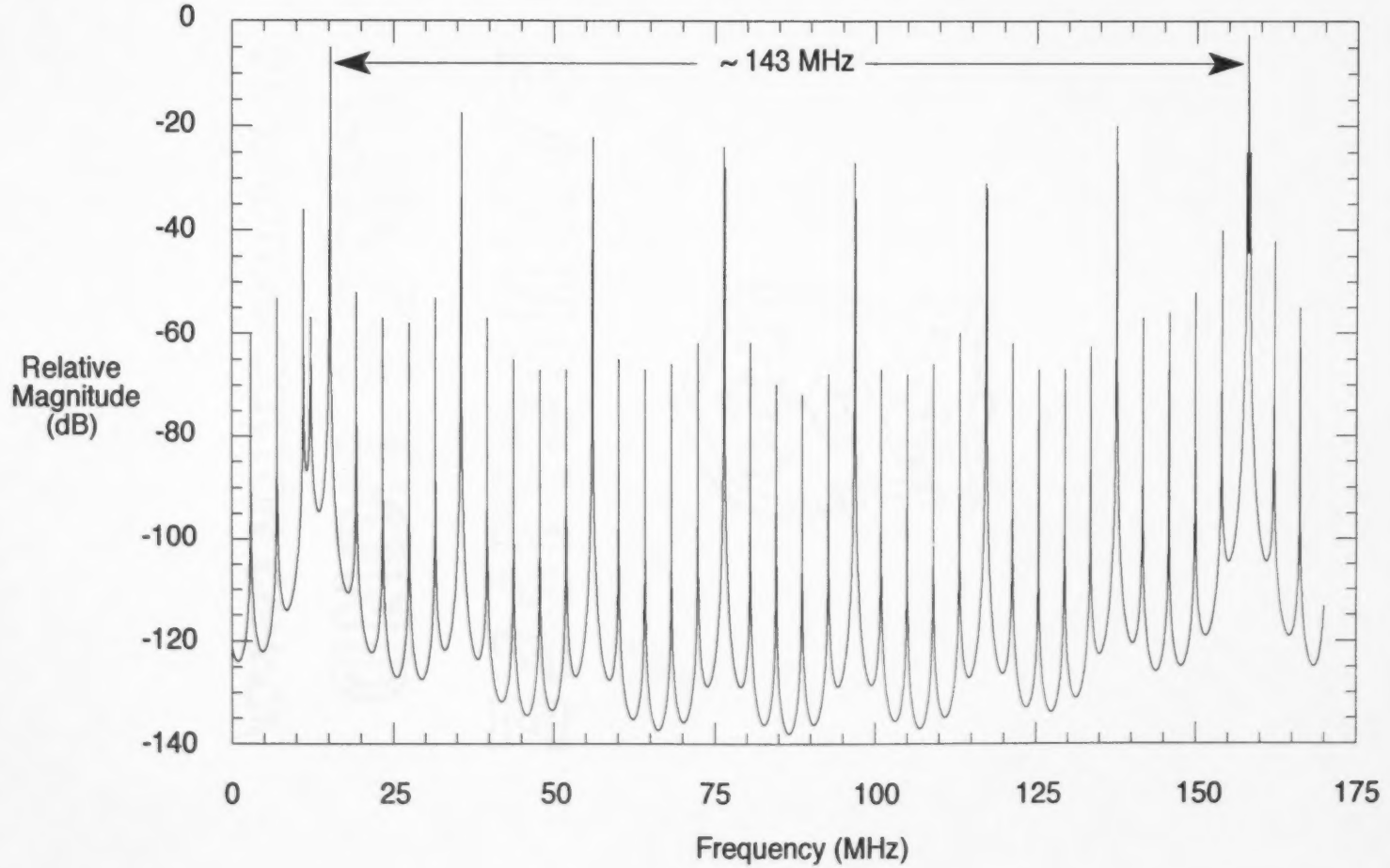

Figure 4.16 Theoretical response for a 50m/10m/1.4m triple loop filter.

It is readily seen that as more rings are added, the filtering between lines increases from 4 MHz to 20 MHz then to 143 MHz. Essentially, the largest frequency spacing observed for each configuration generally corresponds to the inverse round trip time it takes for the light to travel around the smallest of the loops (equation (2.6.2)). In theory, the wider spacing should result in progressively better filtering by filtering out more modes and thereby producing a more spectrally narrow laser.

The above simulations are for a passive cavity structure with very small coupling coefficients, other values of the coupling coefficients are much less effective in suppressing modes. In a multi-ring laser similar variations in the coupling coefficients can cause the laser to operate in multiple modes as determined by the experimental results that follow.

4.4.2.4 Experimental Results

Using equipment available in the lab a low noise laser configuration was constructed and is shown in Fig. 4.17 with variable couplers C1 and C2 set to about 80% and 50% respectively (+/- 1%).

The addition of a polarizer and rotator was deemed essential for the purposes of creating a more polarized output which would be necessary when considering external modulation of the light source using a polarization sensitive Mach-Zehnder modulator.

With all these additional components, the laser internal cavity losses have increased dramatically resulting in a significantly lower laser output power (~-7 dBm). However the polarization improved by 16 dB resulting in about a 28 dB difference between two orthogonal axes.

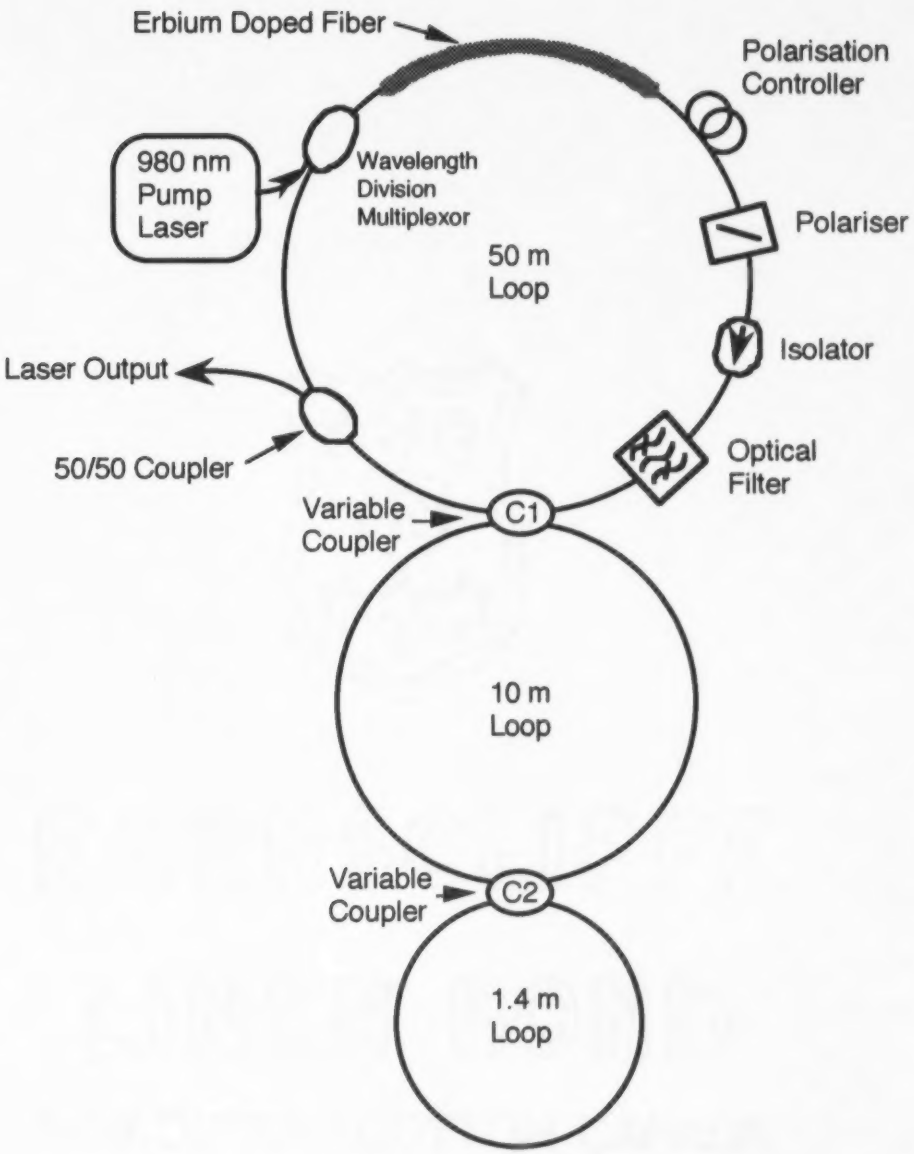

Figure 4.17 Experimental triple ring resonator configuration.

The configuration had a slope efficiency of about 0.7% with a power out versus injected pump power as shown in Fig. 4.18.

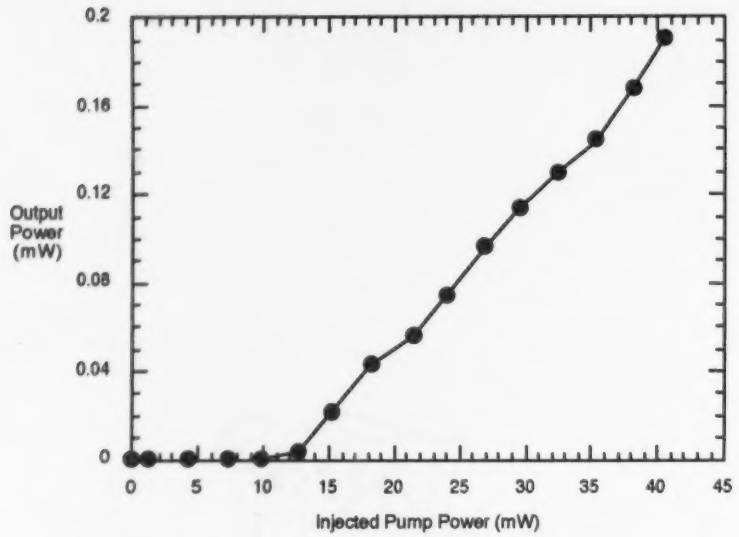

Figure 4.18 Output power versus injected pump power for the triple ring resonator configuration.

Residual pump power measurements were not possible in this configuration; however, the injected pump power was most likely not 100% absorbed. To compare with theory, we must normalize with respect to this and consider the injected threshold power to be 12 mW. The three ring filter loss was estimated through Fig. 4.16 to be at least 5 dB and was lumped in with the tunable filter, rotator, polarizer, isolator losses for a total L_2 loss of 10.8 dB. L_1 was estimated at 1 dB, R = 50% and an estimated G_o based on [18] of 30 dB. The theoretical peak power is more than experimentally obtained but this is attributed to an underestimation of the three ring filter resonator insertion loss of 5 dB and an overestimation of the fiber small signal gain. The estimated output power characteristic versus pump power has about a 1% slope efficiency and is shown in Fig. 4.19.

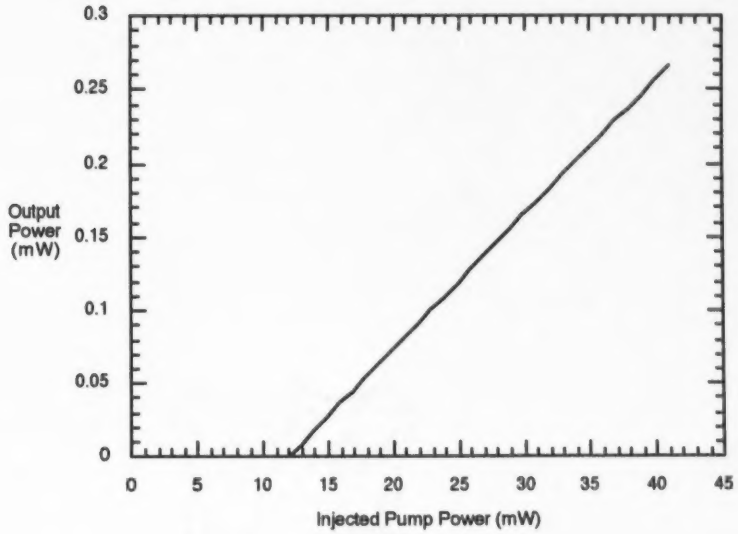

Figure 4.19 Theoretical output power versus injected pump power for the triple ring resonator configuration.

The laser was tunable from 1530 nm to 1560 nm with corresponding changes in the output power as shown in Fig. 20.

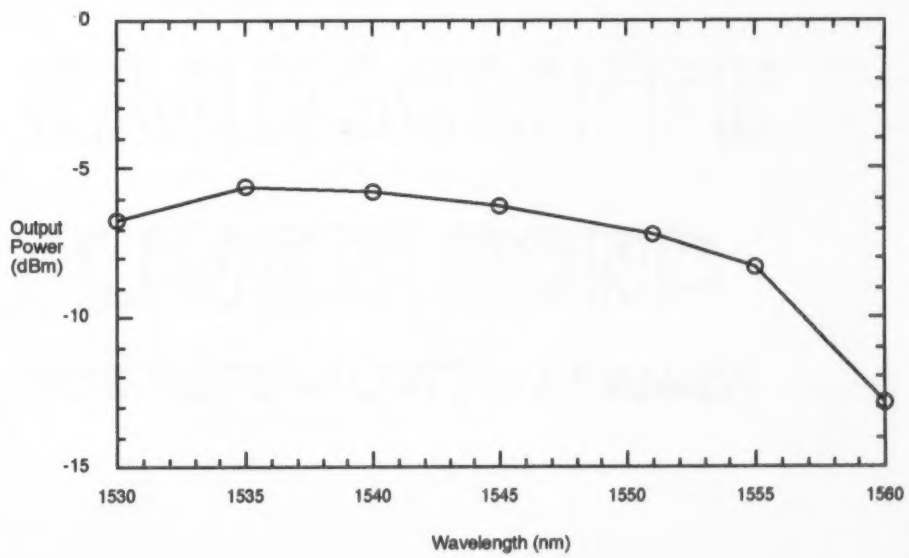

Figure 4.20 Measured laser output power versus operating wavelength for the triple ring resonator.

However, the RF spectral properties of the laser were improved dramatically over the basic single loop configuration as can be seen in Fig. 4.21, 4.22 & 4.23 where the beat products are shown over various frequency ranges. In these traces the three loop laser spectral content is suppressed by better than 32 dB (optical) with respect to the average output power considered. In comparison, for the same optical input power to the detector, mode beat products for the basic single loop configuration are only suppressed by 12 dB (optical). The triple ring resonator results in about a 20 dB improvement in effective side mode suppression.

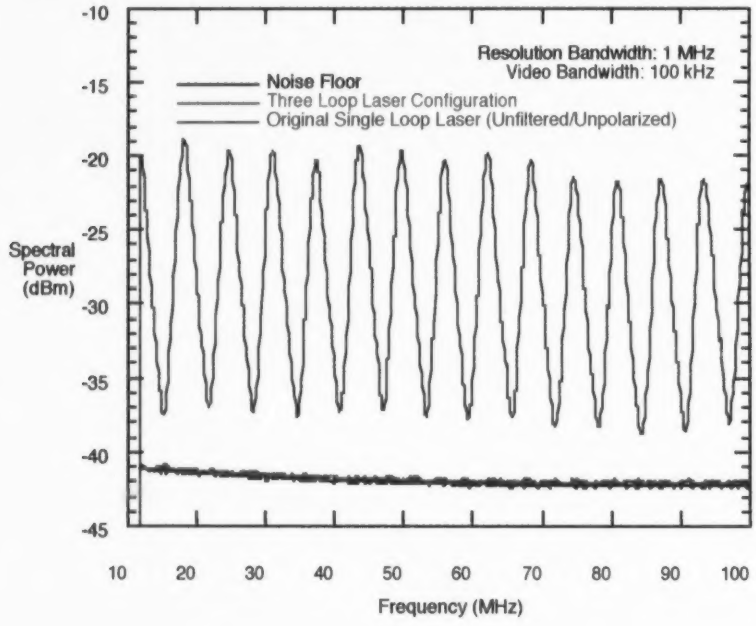

Figure 4.21 Laser spectral output vs. frequency for triple ring resonator (10 to 100 MHz).

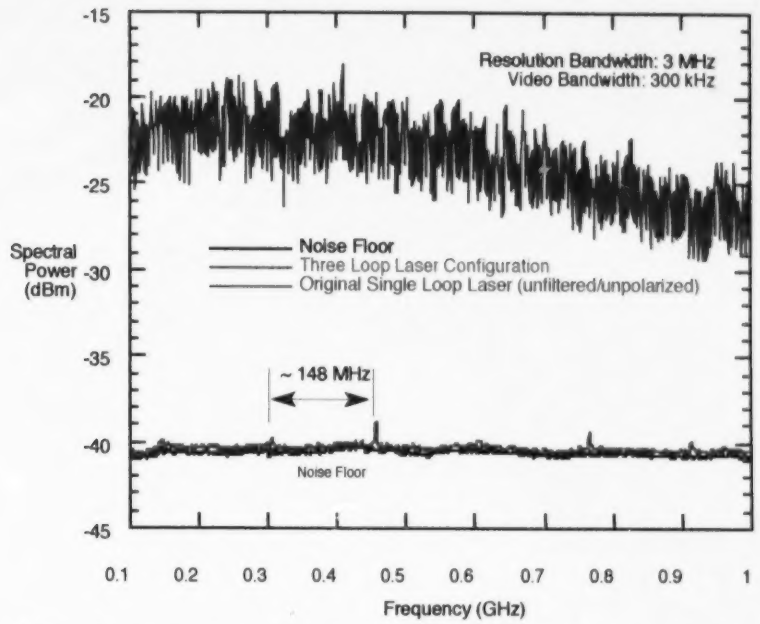

Figure 4.22 Laser spectral output vs. frequency for triple ring resonator (0.1 to 1 GHz).

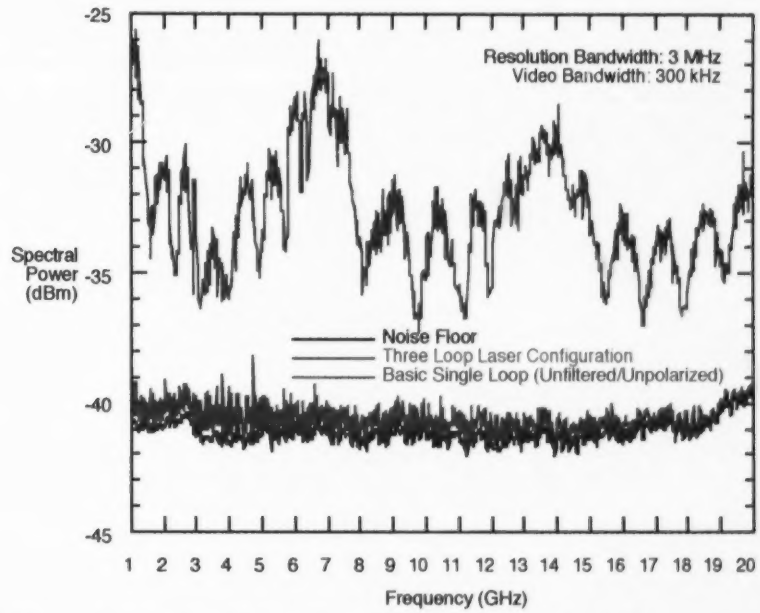

Figure 4.23 Laser spectral output vs. frequency for triple ring resonator (1 to 20 GHz).

Although the mode beat products are significantly attenuated, there are some small spikes visible. In Fig. 4.22 the peaks appear about 148 MHz apart, which would

correspond to a loop of about 1.38m long which differs from the estimated 143 MHz or 1.40 m long loop that was simulated. The 2 cm difference is less than that but is within reasonable error given the fact that the loop length was never broken and stretched out for a precise measurement. The length was instead estimated based on the loop diameter.

It is also interesting to note the effects of de-coupling C2, or setting C2 to 0% coupling, as shown in Fig. 4.24, which in essence eliminates the third loop, leaving a two loop configuration. The spacing between peaks is seen to be about 19 MHz, close to what is theoretically predicted and shown in Fig. 4.15.

The results of de-coupling coupler C1 are also shown in Fig. 4.24 and a four MHz separation is noted which is agreement with Fig. 4.14 and equation.(2.6.2).

The effects of singularly removing or de-tuning other components is also shown and demonstrates that the parasitic loops are primarily responsible for the sharp reduction in multi-mode beat products.

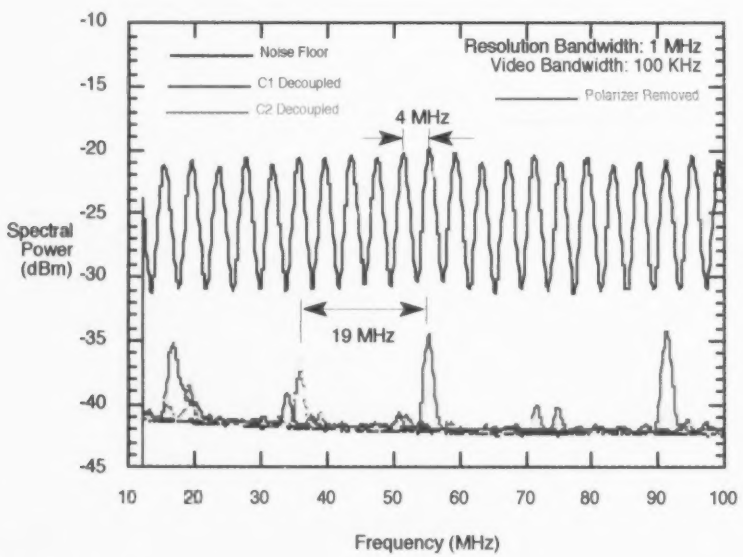

Figure 4.24 Laser spectral output vs. frequency for triple ring resonator (10 to 100 MHz) after various resonator modifications.

4.5 Relative Intensity Noise Measurement

Using the triple ring resonator configuration, the relative intensity noise (RIN) of the laser was determined using the HP Lightwave analyzer equipped with appropriate software (RIN DLP). Results are shown in Fig 4.25.

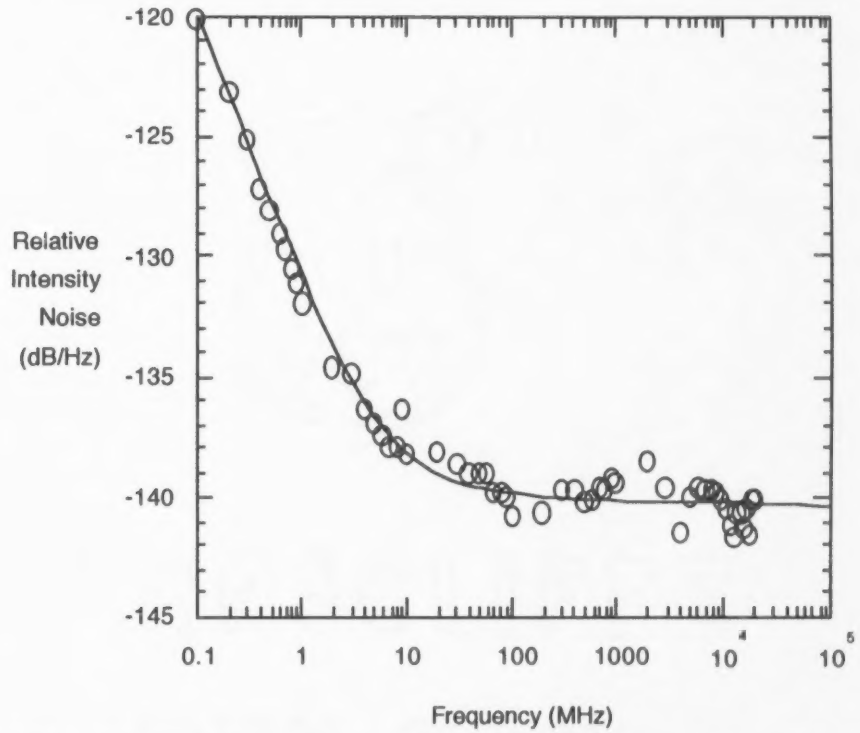

Figure 4.25 Relative intensity noise (RIN) vs. frequency for triple ring resonator configuration.

From Fig 4.17 it can be seen that the RIN is lowest at the higher frequencies where it reached about -142 dB/Hz. It should also be noted that due to the low power of the laser, the limits of calculating RIN are reduced [38] so that the actual RIN is equal to or better than actually measured. An effort to measure the RIN was made using a receiver independent technique [39] (see Appendix A); however, it too suffered limitation due to low power values. Some minor noise results have been reported by others [40],[41]

since the inception of the project, however they do not discuss noise over such a large frequency range.

The RIN was noted to be worst toward the lower frequencies which makes sense as that is where the relaxation oscillations inherent to this laser should occur.

4.6 Low Frequency Observations

Viewing the output of the three loop laser again as was done in Fig 4.1 except at a lower frequency, found the output spectra to vary with pump power as is shown in Fig. 4.26.

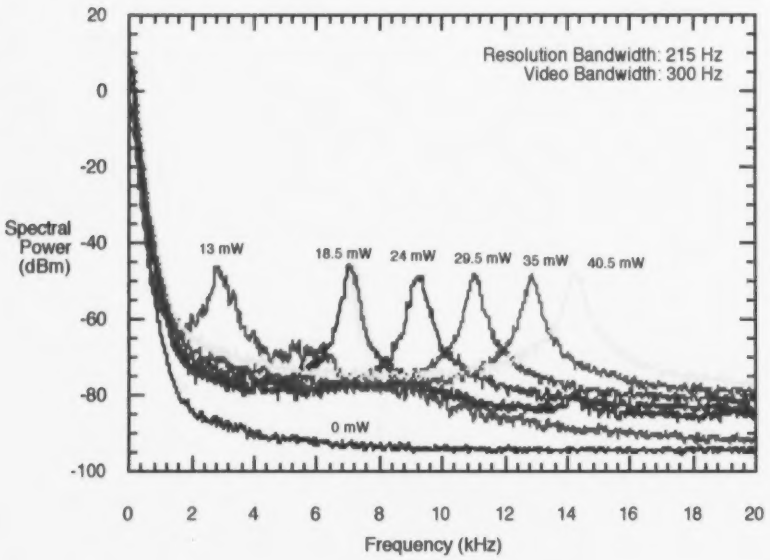

Figure 4.26 Spectral output vs. frequency for triple ring resonator at various injected pump power levels.

It is believed that these are relaxation oscillations since they are too low to be laser mode beat products and are within the relaxation oscillation range expected for the lasers under consideration.

A theoretical comparison was made using equation (2.17.1) based on a measured pump threshold value of 12 mW, upper state lifetime of 14 ms and pump powers ranging

from 13 mW to 40.5 mW. The three loop laser considered has a multi-cavity structure, therefore it is difficult to estimate the photon lifetime; however, estimating about 13 dB of internal losses, and 50% effective cavity reflectivity, the observed peaks are compared to theory assuming a number of different cavity lengths in Fig. 4.27.

The three ring multi cavity laser appears to have a photon lifetime inherent to a single cavity laser with a 4 m cavity length. Rather than viewing the laser with an effective cavity length it could be said that the laser has an effective photon lifetime of about 20 ns. Sometimes the measurement of the relaxation oscillation frequency is used as an indirect method of determining or verifying certain unknown laser parameters such as the laser photon lifetime [57].

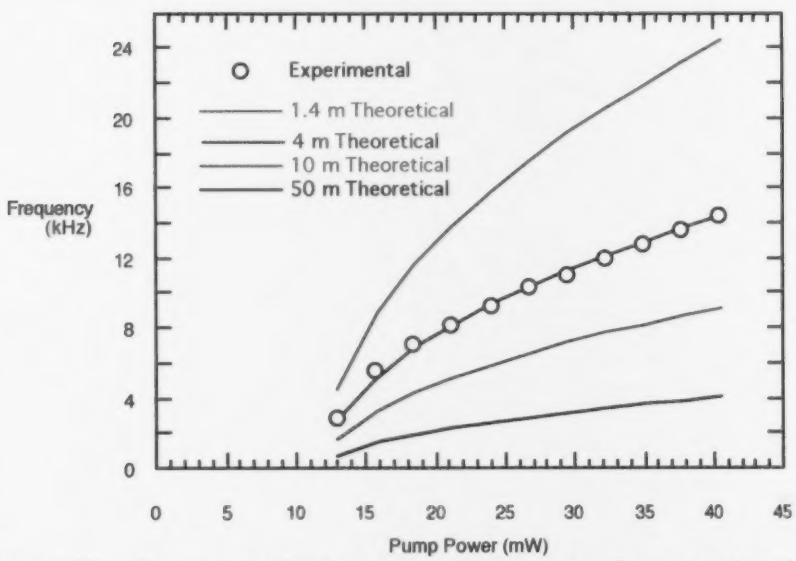

Figure 4.27 Experimentally observed oscillation center frequency for triple ring resonator vs. pump power. Theoretical calculations shown for a single ring resonator of various cavity lengths.

4.7 Linewidth

Other than the very low frequency relaxation oscillations and some small high frequency laser line beat products, the laser was essentially single longitudinally moded

with a line width measured to be less than 30 KHz. The delayed self-homodyne technique was used to measure the linewidth [43] as shown in Fig. 4.28. The resultant observed spectral 3 dB width is taken as the laser's line width and can be seen in Fig. 4.29.

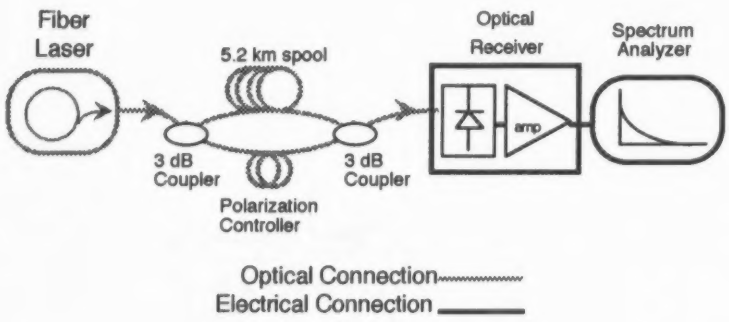

Figure 4.28 Experimental layout for measuring laser linewidth.

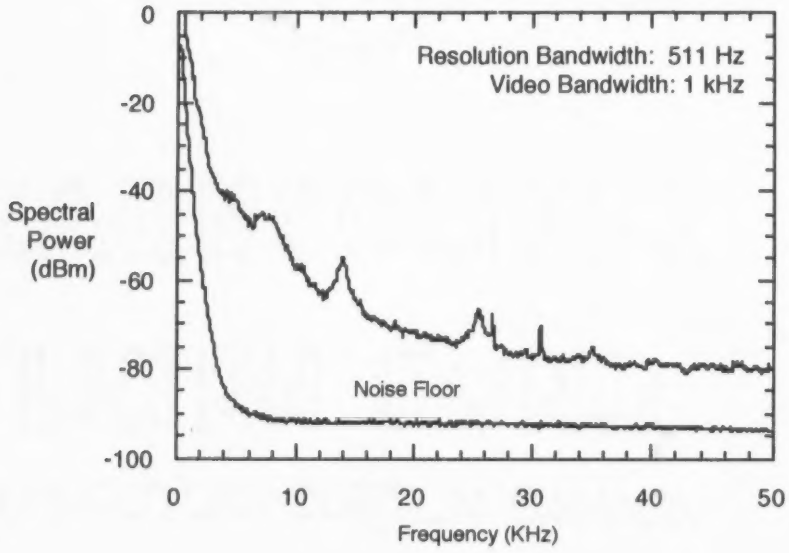

Figure 4.29 Delayed self-homodyne spectral output vs. frequency.

If the laser was inifitely narrow in linewidth, the spectral output would show a strong peak and 0 Hz and a flat output beyond. A laser with a 30 KHz linewidth would

have a Lorentzian line shape with a 3 dB roll-off at 30 KHz. From Fig 4.24 it is seen that there is a 3 dB roll-off much sooner than 30 KHz; therefore, the linewidth is probably much less than 30 KHz. However, since the fiber delay loop was limited to 5.2 km, the linewidth measurement is only statistically valid down to 30 KHz [43].

5

Transmission Using An Erbium Doped Fiber Laser Source

5.1 Introduction

The next step was to demonstrate the potential of the erbium fiber laser as a useful optical communications light source by incorporating it into a transmission experiment and modulating its light intensity. Given the slow upper state lifetime of the erbium ion, ≈14 ms, and the large round trip cavity size of the resonator, the switching time is very limited as predicted by equation (2.16.1). It is apparent that modulation of the laser light through modulation of its pumping laser would be limited to something less than a MHz for certain and is impractical for today's multi-GHz transmission systems.

Thus as a practical experiment for demonstrating the laser as a communications source, the triple ring resonator was run in continuous wave form and modulated externally using a Mach-Zehnder modulator as shown in Fig 5.1. The modulator was digitally modulated at the OC-48 rate through the control of a bit error rate test set (BERT). The received signal also went back into the BERT and was used to determine eye diagrams and bit error rates. The output of the laser was tuned to 1551 nm with ≈ -7 dBm of linearly polarized output power. The power tended to fluctuate +/- .1 dB over a period of a few seconds; however, with the low noise configuration of the laser, no significant spectral content in the RF domain past 50 KHz existed that should, at least ostensibly, pose a problem.

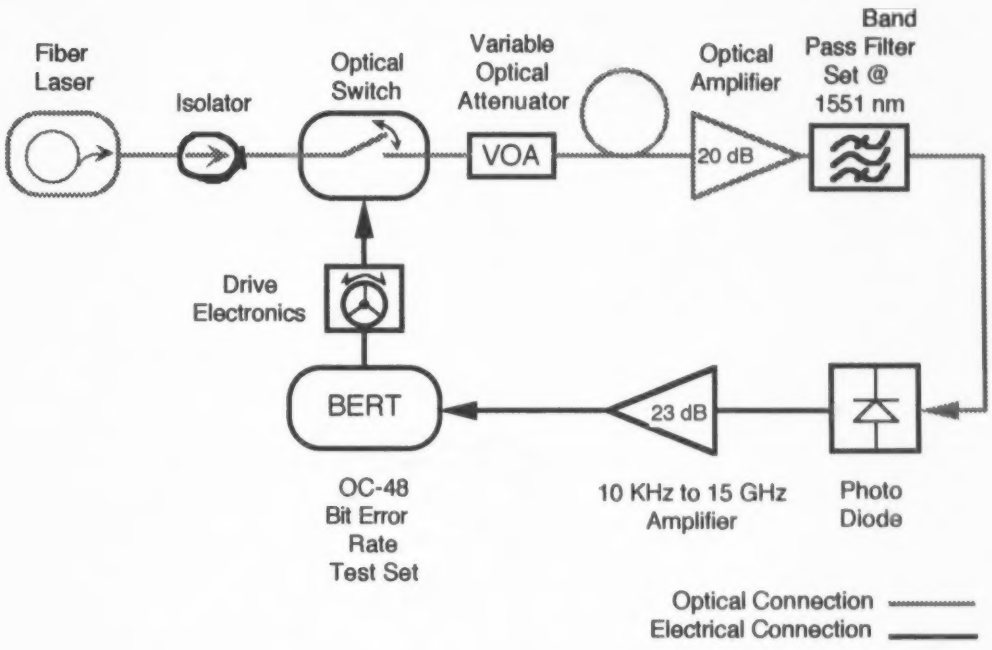

Figure 5.1 Transmission experiment layout using the erbium fiber laser.

5.2 Results

An "eye diagram" of the received digital pulses is shown in Fig 5.2. Although the individual bits can be discerned, the diagram is still not very clean and as a result, the BERT had trouble locking in on the received signal, and bit error rate measurements could not be made. The reason for this is not fully known, although the experiments that follow make some progress in determining the possible causes.

The experiment was repeated again using a Fujitsu 1551 nm DFB semiconductor laser with a 50 MHz linewidth as the source. In this case the BERT successfully locked on to received signal even with average power levels that were as much as 10 dB lower than was the case with the erbium fiber laser experiment.

The likely cause for the BERT lock-in failure is its inability to determine an average decision threshold level which it sees as constantly changing due to an unstable laser. The average laser output power drifts +/- .1 dB over a few seconds; however, this should not

present a problem since the electrical amplifier just before the BERT has a lower bandwidth limit of 10 KHz.

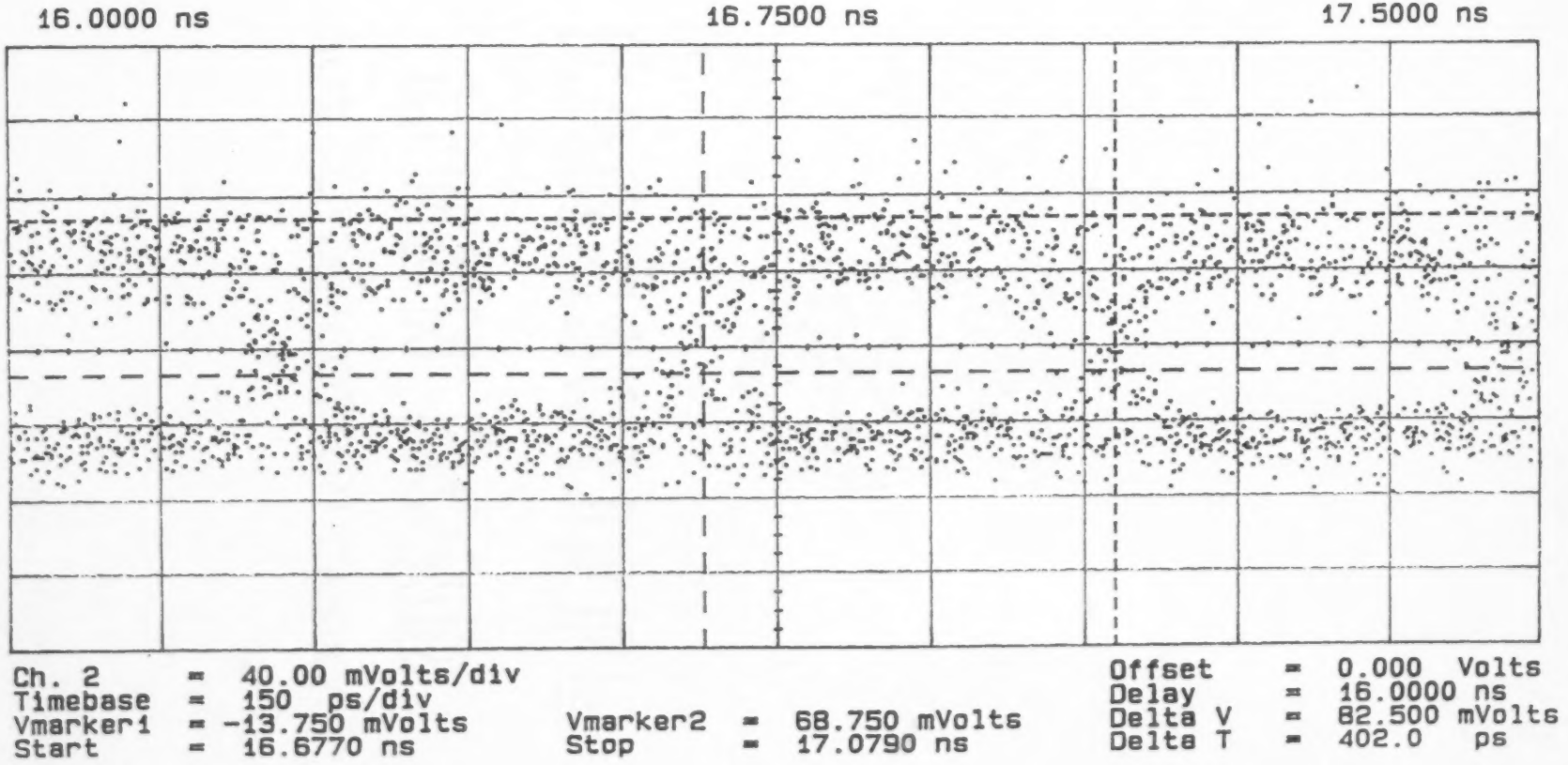

Figure 5.2 Eye diagram from transmission experiment.

5.3 Time Domain Analysis

Further insight to the lasers operation was obtained by viewing results from time domain analysis of the laser's output. The test configuration is shown in Fig 5.3.

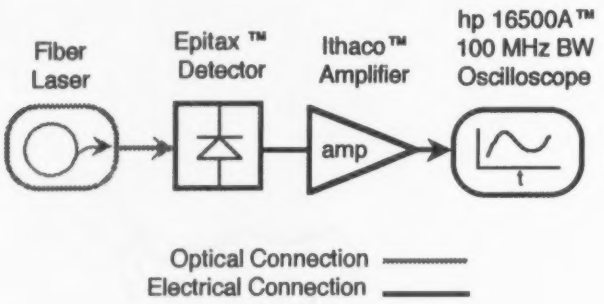

Figure 5.3 Experimental setup for time domain measurement.

Since the output of the Ithaco amplifier is DC coupled, the fiber laser's average power offsets the AC portion of the signal by about 720 mV, as seen in the digital storage scope's 10 second "snapshot", Fig. 5.4. From the results, it can be seen that the laser is fluctuating or spiking with peak modulation depths as much as ≈10%.

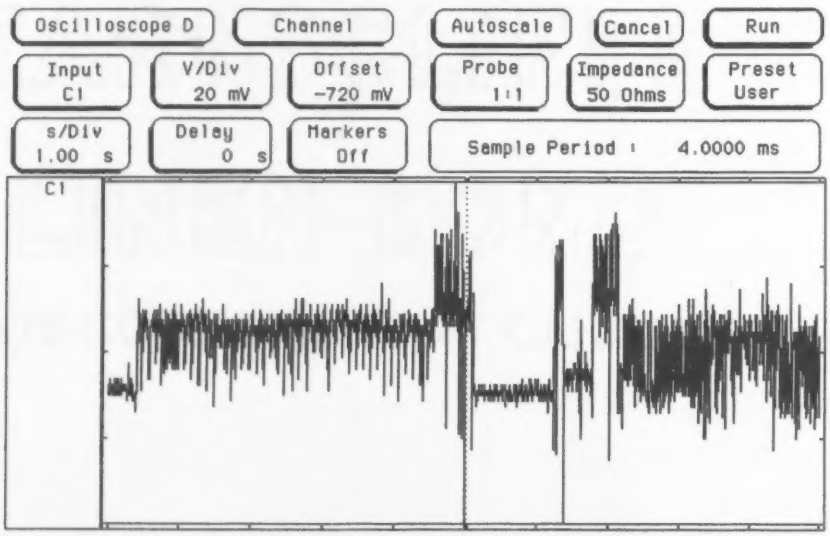

Figure 5.4 Time domain plot of laser output. (1 s/Div scale).

A closer look on a 1 ms/Div scale as displayed in Fig. 5.5 shows the spikes to actually be damped relaxation oscillations as theoretically discussed in section 2.17.

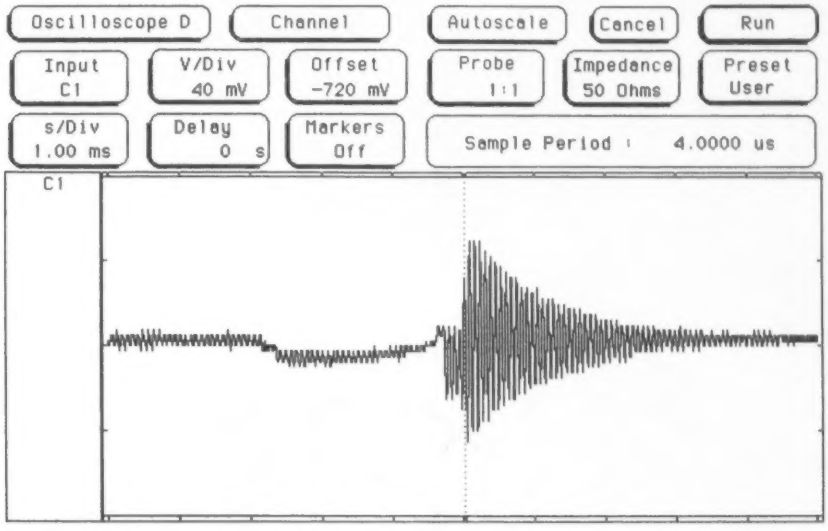

Figure 5.5 Time domain plot of laser output. (1 ms/Div scale).

Fig 5.6 is an expanded scale view of Fig. 5.5 and reveals the relaxation oscillation frequency to be on the order of about 14 KHz which coincides with the low frequency RF spectral peaking observed in Fig. 4.26.

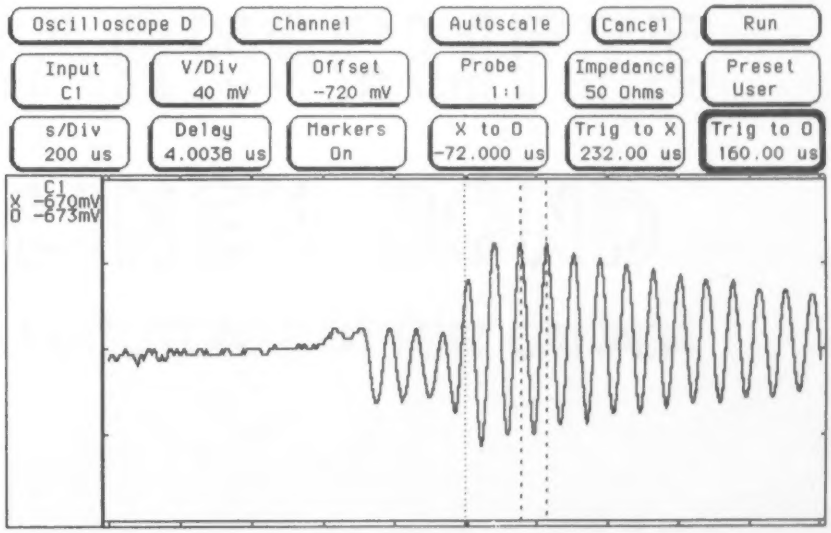

Figure 5.6 Time domain plot of laser output. (200 μs/Div scale).

The strange, and unpredictable way the laser fluctuates could be due to the fact that the laser cavity, being very long and laid out loosely over the experiment bench, could be susceptible to vibrations. The vibrations could translate into changes in the cavity length and or polarization. Any changes in these could bring about a situation where the round trip conditions for lasing are broken and the laser stops lasing. Mean while, the 980 nm pump laser continues to pump the erbium ions and when the fiber cavity moves back into alignment, the energy is released rapidly in the form of a gain switched pulse.

If a more mechanically stable fiber laser resonator layout was chosen, utilizing a floating optical table and fastening down all loose fiber ends for example, it may be possible to reduce the pulsing effect thus allowing the BERT to lock-in on a externally modulated signal. It may in fact actually have been easier to transmit analog signals such as an analog television signal, which would not require some sort of BERT instrument to lock-in on the received signal.

Others have recently reported similar unexplained pulsing behavior [41] as well as strange passive soliton pulsing effects at high pump power levels where high laser cavity light intensities start to induce non linear intra-cavity transmission effects [44]. There may be fundamentally limiting effects in addition to the simple mechanical limitations mentioned in operation of this test laser.

Thus, further work on the laser is needed, however given project time limitations, research on the laser was drawn to a close, and numerous conclusions have been drawn on the work done thus far .

6

Conclusions

6.1 Summary

The erbium doped fiber laser work completed here has accomplished goals or made headway in three areas.

First the wavelength tuning effect due to output coupling changes was determined in two resonator configurations. The tuning appeared to be more of a wavelength shifting effect over three wavelength bands 1535 nm, 1550 nm and 1555 nm in agreement with theory.

The fiber mirror configuration appeared to be the best layout as a wide band tunable light source with powers reaching as much as +5 dBm over the filter range from 1526 nm to 1555 nm with a spectral width of about 0.3 nm.

The fiber ring laser configured in a novel triple ring resonator structure was found to be a better layout for low noise, narrow linewidth operation. A linewidth lower than 30 kHz and relative intensity noise measurement as low as -142 dB/Hz were observed; these values were limited only by equipment resolution.

As a source for communications purposes, the three loop laser appears to have an instability problem which causes difficulty in reception thus leaving it inappropriate for transmission testing at this time.

6.2 Future Research

Based on the work done thus far, suggestions with regards to possible future erbium fiber laser research can be made:

- Any further work on stabilizing the laser should also be done with resonator components and bench space designated specifically for the purpose of that research. Although it may have been cost effective to share equipment, repeatedly

having to disassemble and re-assemble the resonator for sharing components and lab space proved often an inefficient use of time. About 50% of the lab time was often spent trying to get back to what was had earlier since the laser's output was found to change dramatically and require a lot of component "tweaking".

- The power level of the laser should also be increased through a combination of higher gain, and lowering of the resonator internal losses. This would also allow for a more accurate measurement of the laser's true RIN as it is suspected to be very low. The receiver independent RIN calculating technique could prove this as it has been shown to be capable of calculating RIN levels as low as -170 dB/Hz on YAG lasers [39].
- To further widen the spacing between longitudinal modes, smaller loop lengths may also be considered where possible.

If future research on the laser was continued, and it incorporated the above suggestions, it is believed by the author that a stable low noise tunable erbium fiber laser could be developed.

References

[1] Wyatt, R., "High-Power Broadly Tunable Erbium-Doped Silica Fibre Laser", Electronics Letters, Vol. 25, No 22, pp. 1498-1499, October, 1989.

[2] Barnes, W.L., Reekie, L., and Payne, D.N., "Highly Efficient Er3+ Doped Fibre Lasers Pumped at 980 nm", IOOC paper 20A3-3, 1989.

[3] Iwatsuki, K., Takada, A., Hagimoto, K., Saruwatari, M., and Kimura, Y., "Er3+-Doped Fiber-Ring-Laser with less than 10 KHz Linewidth", Post Deadline Paper PD5-1, OFC 1989.

[4] Morkel, P.R., Cowle, G., and Payne, D.N., "Traveling-Wave Erbium Fiber Ring Laser With 60 KHz Linewidth", Electronics Letters, Vol. 26, No 10, pp. 632-634, 1990.

[5] Payne, D.N. and Reekie, L. , "Rare Earth Doped Fiber Lasers and Amplifiers", European Conference on Optical Communications, pp. 87-94, 1987.

[6] Chen, C.Y., Choy, M.M., Andrejco, M.J., Saifi, M.A., Lin, C., "A Widely Tunable Erbium-Doped Fiber Laser Pumped at 532 nm", IEEE Photonics Technology Letters, Vol. 2, No 1, March 1, pp. 18-20, 1990.

[7] Benterud, K., "Encoding and Optical Time Division Multiplexing High Speed Digital Signals Using Optical Switches", M.Sc. , 1994.

[8] Saleh, A.A.M., "Fundamental Limit on Number of Channels in Subcarrier-Multiplexed Lightwave CATV System", Electronics Letters, Vol. 25, No 12, pp. 776-777, June 8, 1989.

[9] Saleh, A.A.M., "Ultimate TV Channel Capacity of Subcarrier-Multiplexed Lightwave CATV Systems", Optical Fiber Communications Conference, Paper THG2, 1990.

[10] Olshansky, R., Lanzisera, V.A., and Hill, P.M. , "Subcarrier Multiplexed Lightwave Systems for Broad Band Distribution", IEEE Journal of Lightwave Technology, Vol. 7, No 9, pp. 1329-1342, 1989.

[11] Way, W.I., "Subcarrier Multiplexed Lightwave System Design Considerations For Subscriber Loop Applications", IEEE Journal of Lightwave Technology, Vol. 7, No 11, pp. 1806-1818, 1989.

[12] Darcie, T.E. and Bodeep, G.E., "Lightwave Multi-channel Analog AM Video Distribution Systems", International Communications Conference, Paper 32.4.1, 1989.

[13] Darcie, T.E. and Bodeep, G.E., "Lightwave Subcarrier CATV Transmission Systems", IEEE Transactions on Microwave Theory and Techniques, Vol. 38, No 5, pp. 524-533, 1990.

[14] Darcie, T.E., "Lightwave Analog Video Transmission Techniques", Optical Fiber Communications Conference, Paper WH1, 1990.

[15] Darcie, T.E., Lipson, J., Roxlo, C.B., and McGrath, C.J., "Fiber Optic Device Technology for Broadband Analog Video Systems", IEEE Lightwave Communications Systems Magazine, Vol. 1, No 1, pp. 46-52, 1990.

[16] Conradi, J., Maciejko, R., and Kim, H.B., "Effect of Laser Noise on Analogue Fiber Optic Systems", Electronics Letters, Vol. 16, pp. 230-231, 1980.

[17] Reekie, L., Mears, R.J., Poole, S.B., Payne, D.N., "Tunable Single-Mode Fiber Lasers", Journal of Lightwave Technology, Vol. LT-4, No 7, July, pp. 956-960, 1986.

[18] Freeman, J.E., "Theory, Design and Characterization of Erbium-Doped Fiber Amplifiers", University of Alberta MSc Thesis, Fall 1991.

[19] Yariv, A. , "Optical Electronics", Third Edition, CBS College Publishing, p 150, 1985.

[20] O'Cochlain, C. R., and Mears, R. J.: "Broadband Tunable Single Frequency Diode-Pumped Erbium Doped Fibre Laser", Electronics Letters, Vol. 28, No 2, pp. 124-126, 1992.

[21] Ball, G. A., and Morey, W. W.: "Continuously tunable single-mode erbium fibre laser", Optics Letters, Vol. 17, No 6, pp. 420-422, 1992.

[22] Namkyoo, P., Dawson, J. , and Vahala, K.J.: "All fiber, low threshold, widely tunable single frequency, erbium-doped fiber ring laser with a tandem fiber Fabry-Perot filter", Applied Physics Letters, Vol. 59, No 19, pp. 2369-2371, 1991.

[23] Smith, D. A., Maeda, M.W., Johnson, J. J., Patel, J. S., Saifi, M. A., and Von Lehman, A.: "Acoustically tuned erbium-doped fiber ring laser", Optics Letters, Vol. 16, No 4, pp. 387-389, 1991.

[24] Scrivener, P.L., Tarbox, E. J., and Maton, P. D.: "Narrow linewidth tunable operation of Er^{3+}-doped single-mode fibre laser", Electronics Letters, Vol. 25, No 8, pp. 549-550, 1989.

[25] Chaoyu, Y., Jiangde, P., and Bingkun, Z.: "Tunable Nd^{3+}-doped fibre ring laser", Electronics Letters, Vol. 25, No 2, pp. 101-102, 1989.

[26] Millar, C. A., Miller, I. D., Mortimore, D. B., Ainslie, B. J., and Urquhart, P.: "Fibre laser with adjustable fibre reflector for wavelength tuning and variable output coupling", IEE Proceedings, Vol. 135, No 4, pp. 303-309, 1988.

[27] Millar, C. A., Miller, I. D., and Mortimore, D. B.: "Tunable fiber laser", Conference on Lasers and Electro-optics (CLEO), Baltimore, paper WD2, 1987.

[28] Nielsen, A. O., Povlsen, J.H., Bjarklev, A., Lumholt, D., Rasmussen, T.P., and Rottwitt, K.: "Fast method for accurate prediction of Fibre Laser Oscillation Wavelength", Electronics Letters, Vol. 27, No 18, pp. 1644-1645, 1991.

[29] Giles, R., and Desurvire, E.,: "Modeling erbium-doped fiber amplifiers", Journal of Lightwave Technology, Vol. 9, No 2, pp. 271-283, 1991.

[30] Ball, G.A., and Glenn, W.H., "Design of a Single-Mode Linear-Cavity Erbium Fiber Laser Utilizing Bragg Reflectors", Journal of Lightwave Technology, Vol. 10, No 10, October, pp. 1338-1343, 1992.

[31] Okamura, H., Iwatsuki, K., "Simultaneous oscillation of Wavelength-Tunable, single mode lasers using an Er-doped Fibre Amplifier.", Electronics Letters, Vol. 28, No 5, February 27, pp. 461-463, 1992.

[32] Schmuck, H., and Pfeiffer, Th., "Fibre-Pigtailed Fabry-Perot Filter Used as Tuning Element and for Comb Generation in an Erbium Doped Fibre Ring Laser", IOOC paper TuB3-3, 1991.

[33] Verdeyen, J.T., "Laser Electronics", second edition, Prentice Hall, p 183, 1989.

[34] Freeman, J., Chung, C.J., Conradi, J., "Gain Compression Due to Bi-directional Signaling in Erbium-Doped-Fiber Amplifiers", OFC, Paper ThF3, 1993.

[35] Stokes, L.F., Chodorow, M., Shaw, H.J., "All-Single-Mode Fiber Resonator", Optics Letters, Vol. 7, No 6, pp. 288-290, June, 1982

[36] Yue, C., Reng, J., and Zhou, B. , "Fiber Ring Lasers", ICICE Transaction, Vol. E 74, No 9, pp. 2929-2934 September 1991.

[37] Capmany, J., Muriel, M.A., "A New Transfer Matrix Formalism for the Analysis of Fiber Ring Resonators: Compound Coupled Structures for FDMA Demultiplexing", Journal of Lightwave Technology, Vol. 8, No 12, p 1904-1919, December, 1990.

[38] Hewlett-Packard Inc., "Lightwave Signal Analyzers Measure Relative Intensity Noise", product note #71400-1, 1991.

[39] Childs, R.B., O'Byrne, V.A., "Receiver Parameter Independent Technique for Measurement of Laser Relative Intensity Noise", CLEO, Paper CWD7, 1990.

[40] Park, N., Sanders, S., Dawson, J.W., Vahala, K.J., "Measurement of Intensity Noise in a Single Frequency Erbium-Doped Fiber Ring Laser and Calibration Relative to the Standard Quantum Limit", CLEO, Paper CWE5, 1992.

[41] Tong, F., Liu, K., Bhathena, F., Miller, C.M., "Single Frequency Tunable Fiber Laser for USO in Optical Communications", CLEO, Paper CThI61, 1992.

[42] Siegman, A.E., "Lasers", University Science Books, p. 482, 1986.

[43] Kikuchi, K., Okoshi, T., "High Resolution Measurement of the Spectrum of Semiconductor Lasers;", Japan Annual Review On Electronics, Comp., Telecomm., Opt. Devices and Fibres, Amsterdam, Netherlands, pp. 51-59, 1982.

[44] Richardson, D.J., Laming, R.I., Payne, D.N., Matsas, V.J., Phillips, M.W., "Pulse Repetition Rates in Passive Self Starting, Femtosecond Soloton Fibre Laser", Electronics Letters, Vol. 27, No 16, August 1, pp. 1451-1453, 1991.

[45] Koehler, B.G., Bowers, J.E., "In-Line Single-Mode Fiber Polarization Controllers at 1.55, 1.3 and 0.63 μm", Applied Optics, Vol. 24, No 3, February 1, pp. 353, 1985.

[46] Hentschel, C., "Fiber Optics Handbook", Third Edition, Hewlett Packard, p. 189, 1989.

[47] McCumber, D.E., "Intensity Fluctuations in the Output of cw Laser Oscillators. I.", Physical Review, Vol. 141, No 1, pp. 306-322, January, 1966.

[48] Verdeyen, J.T., "Laser Electronics", second edition, Prentice Hall, p. 192, 1989.

[49] Verdeyen, J.T., "Laser Electronics", second edition, Prentice Hall, p. 195, 1989.

[50] Verdeyen, J.T., "Laser Electronics", second edition, Prentice Hall, p. 127, 1989.

[51] Verdeyen, J.T., "Laser Electronics", second edition, Prentice Hall, p. 188, 1989.

[52] Verdeyen, J.T., "Laser Electronics", second edition, Prentice Hall, p. 166-169, 1989.

[53] Yariv, A. , "Optical Electronics", Third Edition, CBS College Publishing, p 162, 1985.

[54] Yariv, A. , "Optical Electronics", Third Edition, CBS College Publishing, p 156, 1985.

[55] Siegman, A.E., "Lasers", University Science Books, p. 485, 1986.

[56] Verdeyen, J.T., "Laser Electronics", second edition, Prentice Hall, p. 235-236, 1989.

[57] Siegman, A.E., "Lasers", University Science Books, p. 964, 1986.

[58] Verdeyen, J.T., "Laser Electronics", second edition, Prentice Hall, p. 133, 1989.

[59] Miller, C.M., "Intensity Modulation and Noise Characterization of High-Speed Semiconductor Lasers", IEEE LTS, pp. 44-53, May, 1991.

[60] Siegman, A.E., "Lasers", University Science Books, p. 521, 1986.

[61] Rosadiuk, T., Conradi, J., "Output Coupling Induced Wavelength Shifts in Erbium-Doped Fiber Lasers", IEEE Photonics Technology Letters, Vol. 5, No 7, pp. 758-760, July 1993.

Appendix A

Relative Intensity Noise Calculations Using LabVIEW™

A.1 Introduction

The receiver independent technique used to calculate the relative intensity noise of a light source is a very simple technique based on reference [39]. If we consider a light source with average power P_{opt} and relative intensity noise RIN, shinning onto an optical receiver with photo detector responsivity $\Re$, transimpedance R, and gain G, the electrical output noise power P_{rx} measured within an electrical bandwidth B, can be expressed as:

$$P_{rx} = (i_n^2 + 2qI + I^2 RIN)RGB \tag{A.1.1}$$

where I is the average photo current, or DC photo current generated through the detector, i_n is the effective noise current inherent to the receiver and q is the charge of a electron. Assuming that accurate knowledge of the thermal noise, shot noise, and transimpedance gain are known then the RIN value is obtained by measuring the total power received P_{rx} then subtracting off the thermal and shot noise terms. However by taking simple derivatives, the RIN can also be isolated as follows:

$$RIN = \left\{ \frac{\left[\frac{d^2 P_{rx}}{dI^2} \right]}{\left[\frac{dP_{rx}}{dI} \Big|_{I=0} \right]} \right\} q \tag{A.1.2}$$

In this calculation only the power received versus the photo current must be determined and specific information about the receiver's noise or gain within the measured bandwidth is not necessary.

Figure A.1 shows the functional block diagram of how P_{rx} vs. I curves are generated experimentally through adjusting a variable optical attenuater.

The actual experimental layout used is shown in Fig. A.2. Since a photo current monitor point was not readily available, the photo current was determined indirectly through multiplying the power incident on the detector by the known detector responsivity. Power incident on the detector was found by sampling 10% of the JDS™ VOA light as measured on an hp 8515™ optical power meter, and applying a calibration factor of about -10.3 dB. The optical detector and receiver used was an analog device made by the Ipitek™ company. It is made and sold with the intention of being a CATV quality receiver and was thus found to be very linear over the 10 to 550 MHz frequency range and input powers up to +7 dBm. The 50Ω input spectrum analyzer shown was used as a combination electrical filter/power meter and required a transformer to properly impedance match with the 75Ω output of the Ipitek™ receiver. The Ipitek™ detector had a responsivity of .85 A/W at 1550 nm, and the receiver had a noise current of 5 pA/√Hz, and a power gain of about 25 dB which was necessary to lower the overall measurement noise figure and put weak signals above the spectrum analyzer noise floor. Although other receivers can be used, the Ipitek™'s low noise, high gain, responsivity, and power linearity represented the best receiver available for measurements taken in the 10 to 550 MHz range.

All the instrumentation equipment was linked via the general interface buss (GPIB) and controlled by a Macintosh computer equipped with a GPIB interface card and LabVIEW™ control software which enabled automation of the calculation process. The process consisted of incrementing the VOA over a range of values, and measuring the effective detector photo current and received power on the spectrum analyzer at each point. From this data, a P_{rx} vs. I curve can be generated where P_{rx} varies parabolically with respect to I as in equation (A.1.1). Using a least squares analysis to curve fit the data, the coefficients of the (A.1.1) equation can be found which can then be used to determine the

first and second order derivatives necessary for calculating the RIN according to equation (A.1.2). Section A.2 details the actual LabVIEW™ virtual instrument (VI) created to control the calculation process.

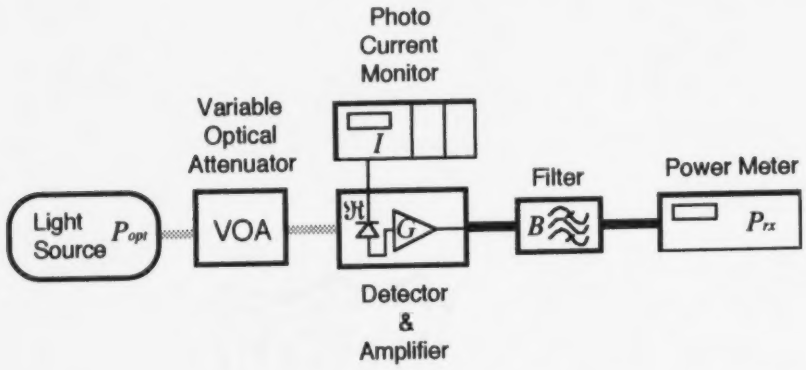

Figure A.1 Block diagram illustrating the general technique for calculating relative intensity noise (RIN).

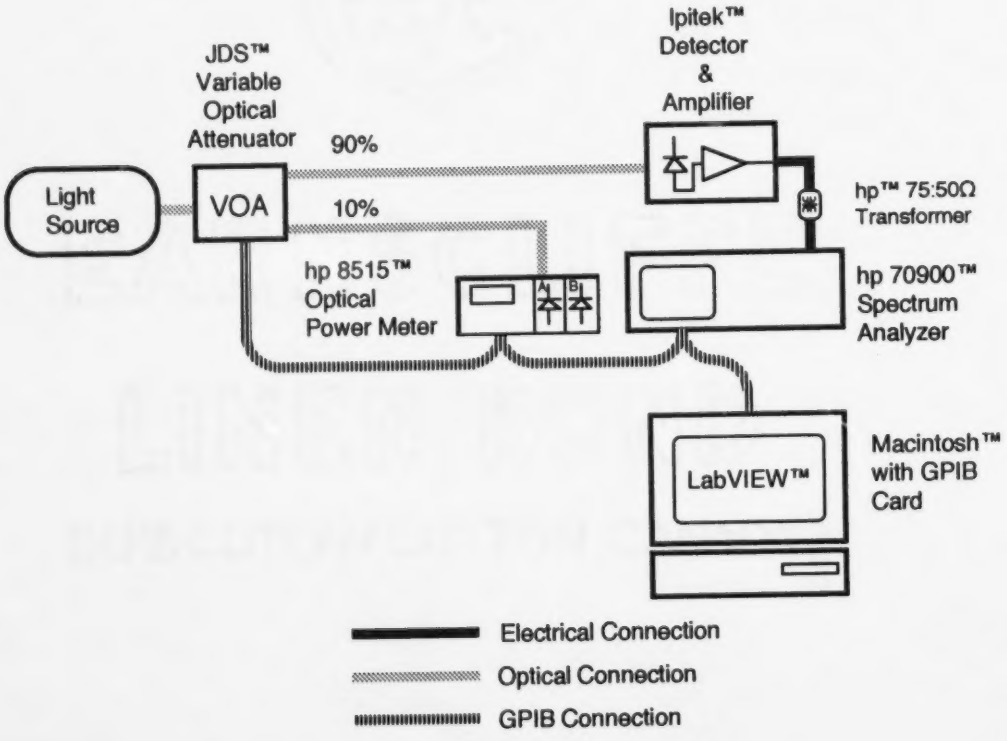

Figure A.2 Experimental setup used for calculating relative intensity noise (RIN).

A.2 VI for LabVIEW™ Controlled RIN Measurements

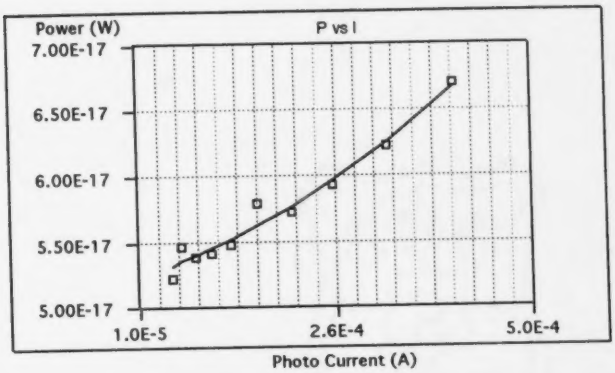

Results

Interpolated

P @ I = 0	0.00E0
d^2P/di^2	8.20E-11
d P/dI @ I = 0	1.99E-14
Rin (dB)	-152

Parameters

Total Iterations	10
Current Iteration	10
Start Attenuation	10
Stop Attenuation	0
delta Attenuation	-1.0
Current JDS Attenuation	0.00

Ch A Time Constant (ms)	200
Ch A Calibration Factor (dB)	-10.6
Detector Responsivity R (A/W)	0.85
Time Delay Between HP Readings (s)	2
Waiting time for S.A. to Settle (s)	30

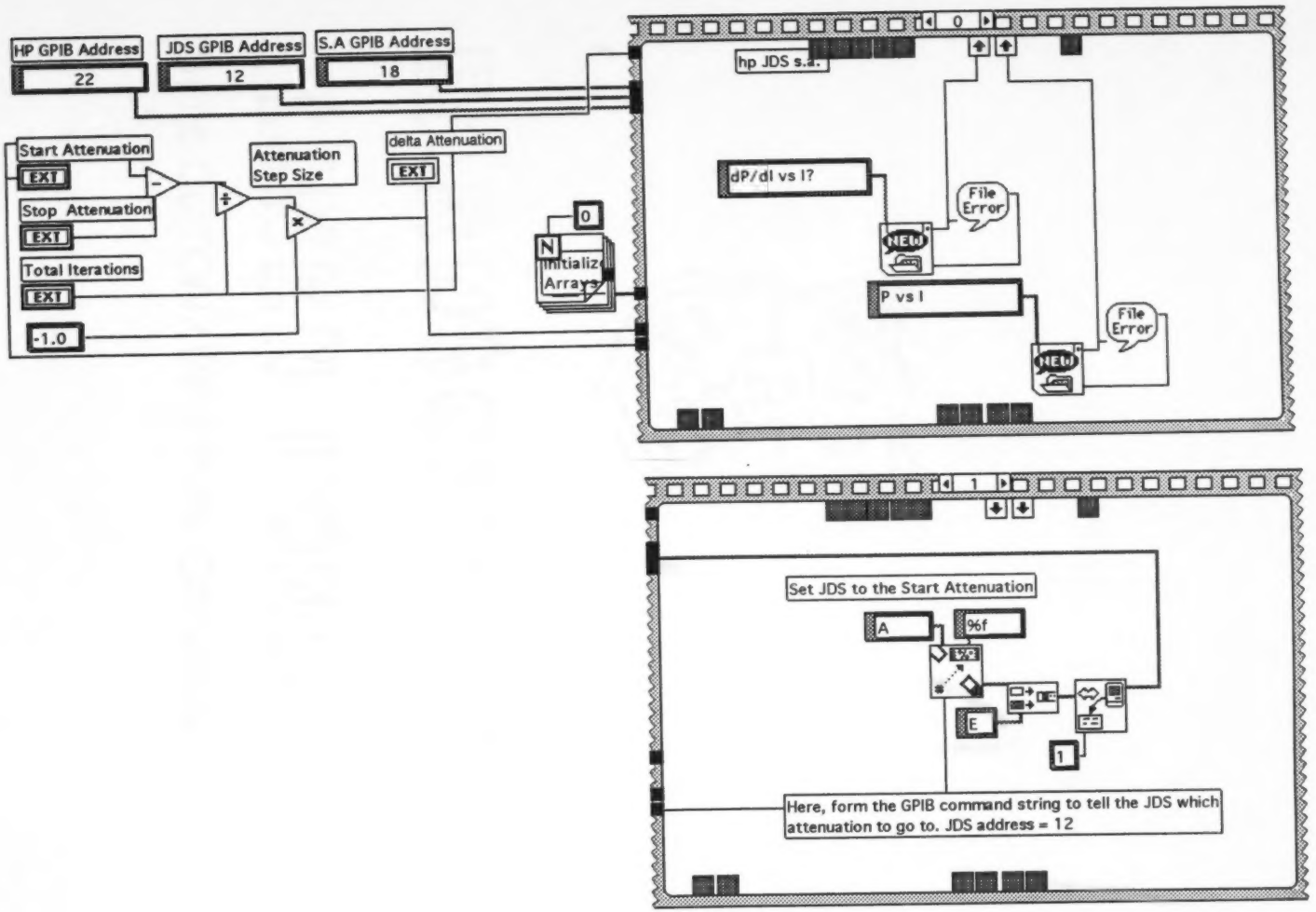
HP GPIB Address
22
JDS GPIB Address
12
S.A GPIB Address
18
Start Attenuation
EXT
Stop Attenuation
EXT
Total Iterations
EXT
-1.0
Attenuation Step Size
delta Attenuation
EXT
0
Initializ Arrays
0
hp JDS s.a.
dP/dI vs I?
File Error
NEW
P vs I
File Error
NEW
1
Set JDS to the Start Attenuation
A
%f
E
1
Here, form the GPIB command string to tell the JDS which attenuation to go to. JDS address = 12

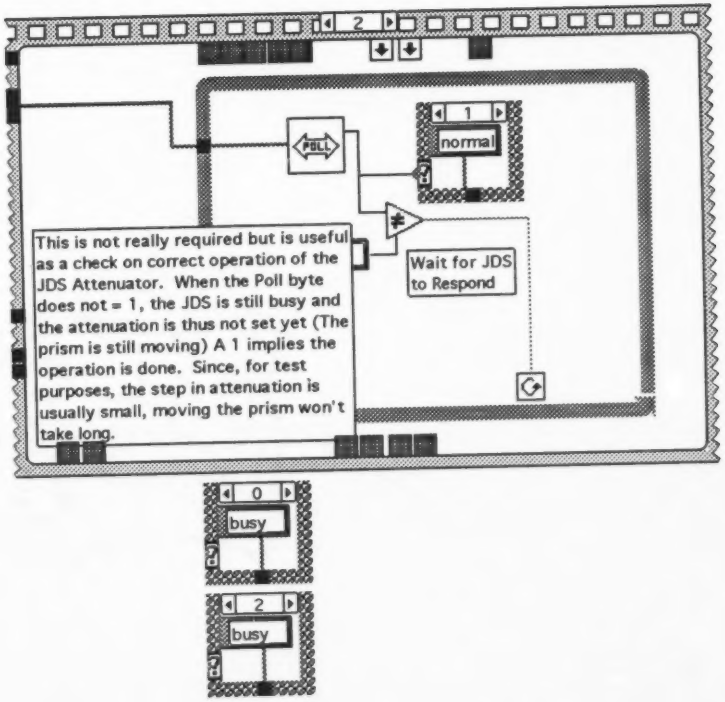
2
1
normal
POLL
This is not really required but is useful as a check on correct operation of the JDS Attenuator. When the Poll byte does not = 1, the JDS is still busy and the attenuation is thus not set yet (The prism is still moving) A 1 implies the operation is done. Since, for test purposes, the step in attenuation is usually small, moving the prism won't take long.
Wait for JDS to Respond
0
busy
2
busy

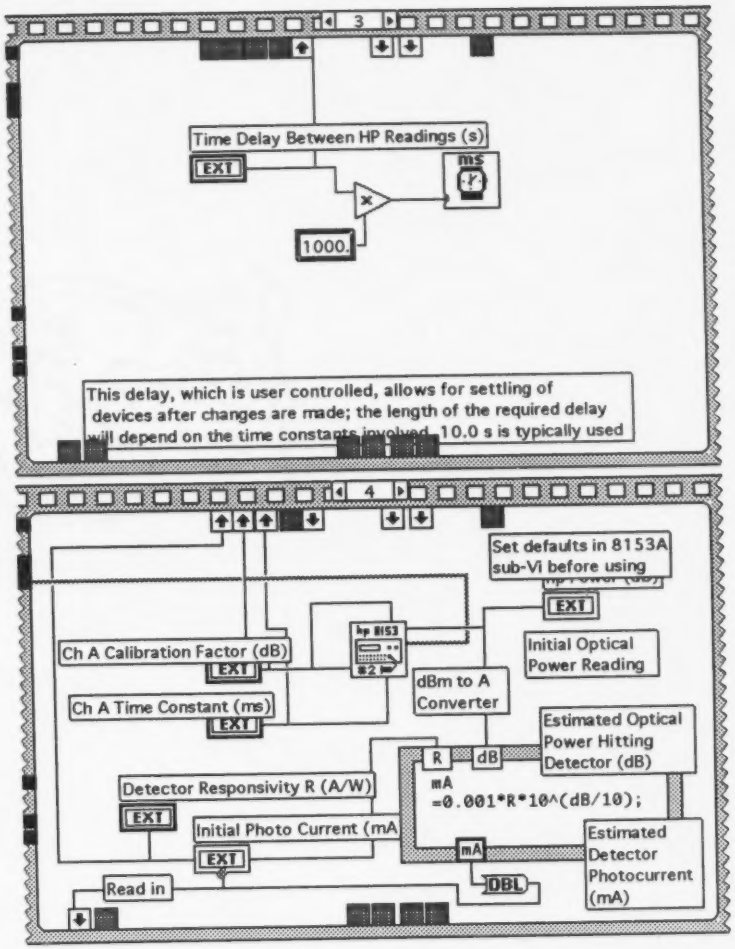
3
Time Delay Between HP Readings (s)
EXT
ms
x
1000.
This delay, which is user controlled, allows for settling of
devices after changes are made; the length of the required delay
will depend on the time constants involved. 10.0 s is typically used
4
Set defaults in 8153A
sub-Vi before using
EXT
Ch A Calibration Factor (dB)
EXT
hp 8153
#2
Initial Optical
Power Reading
dBm to A
Converter
Ch A Time Constant (ms)
EXT
Estimated Optical
Power Hitting
Detector (dB)
R
dB
mA
=0.001*R*10^(dB/10);
Detector Responsivity R (A/W)
EXT
Initial Photo Current (mA
EXT
mA
Estimated
Detector
Photocurrent
(mA)
DBL
Read in

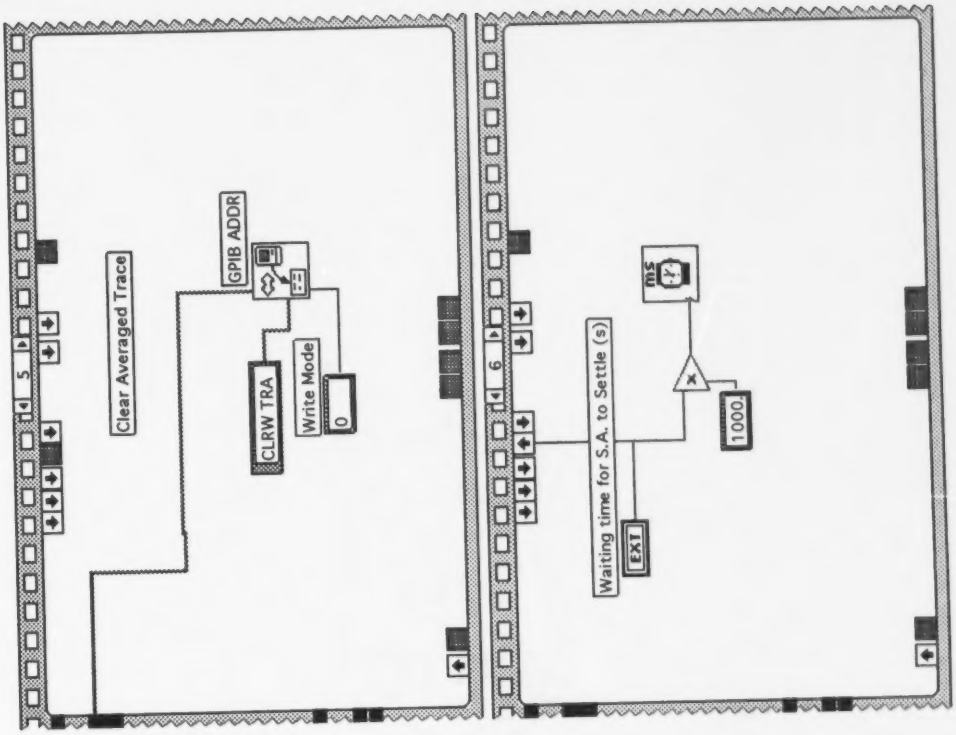
5
Clear Averaged Trace
GPIB ADDR
CLRW TRA
Write Mode
0
6
Waiting time for S.A. to Settle (s)
EXIT
ms
1000

Ask spectrum analyzer to send its measured power value at the current marker position shown on the screen.
GPIB ADDR
Read Value At Marker Command
MKA?
Write Mode
0
7
8
ms
1000

Read in first data point from spectrum analyzer as requested in last frame.
First S.A. Power Read In
GPIB Address
Byte Count
15
Read Mode
0
Convert dB to mW
A. Power Read In (mW)
EXT
mW=0.001*10^(dB/10);
Current Iteration
N
i

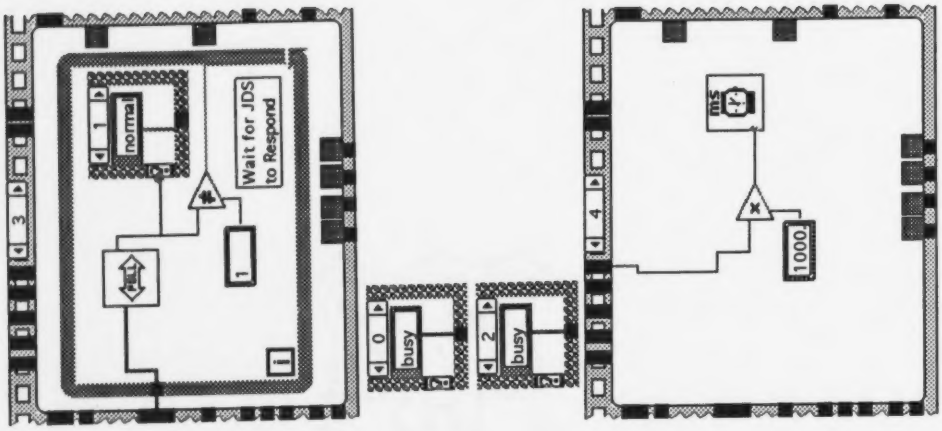
Wait for JDS to Respond
normal
busy
busy
1000

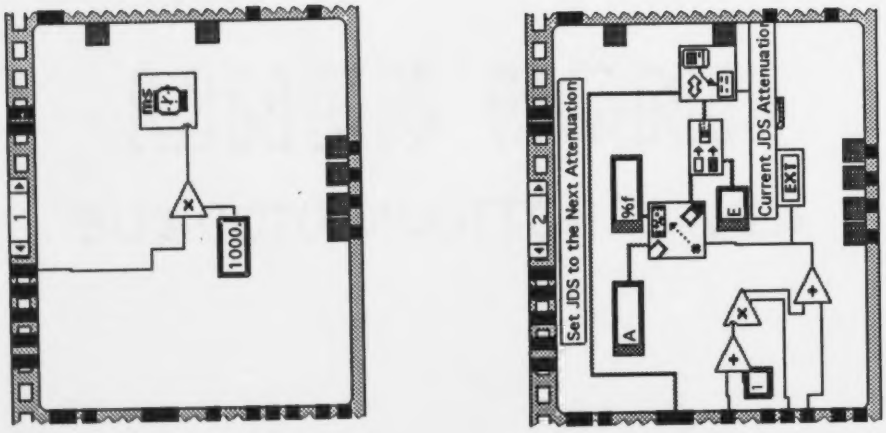
Set JDS to the Next Attenuation
Current JDS Attenuation
%f
A
E
EXT
1000

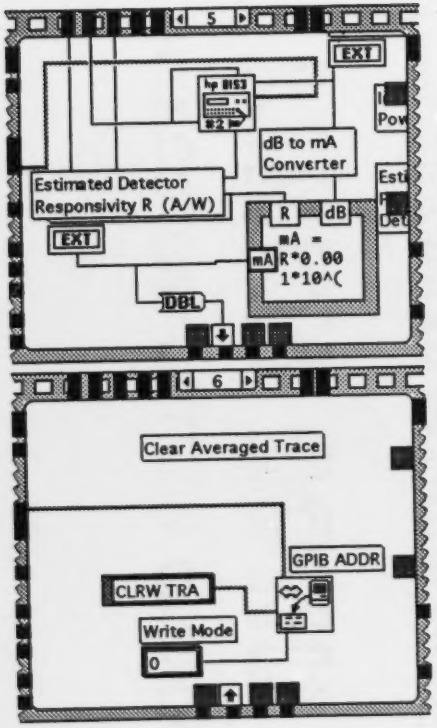
5
EXT
dB to mA
Converter
Estimated Detector
Responsivity R (A/W)
EXT
R
dB
mA =
R*0.00
1*10^(
DBL
6
Clear Averaged Trace
GPIB ADDR
CLRW TRA
Write Mode
0

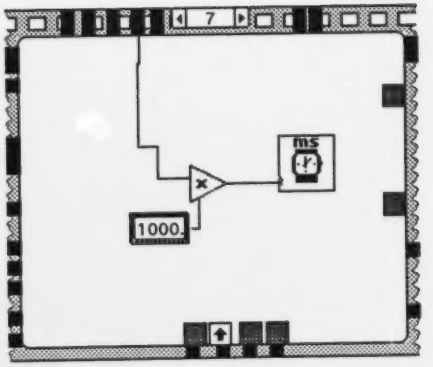
7
ms
1000.

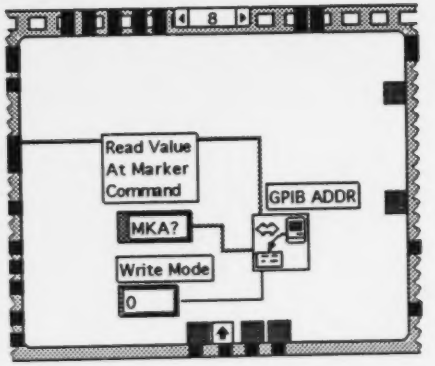
8
Read Value
At Marker
Command
GPIB ADDR
MKA?
Write Mode
0

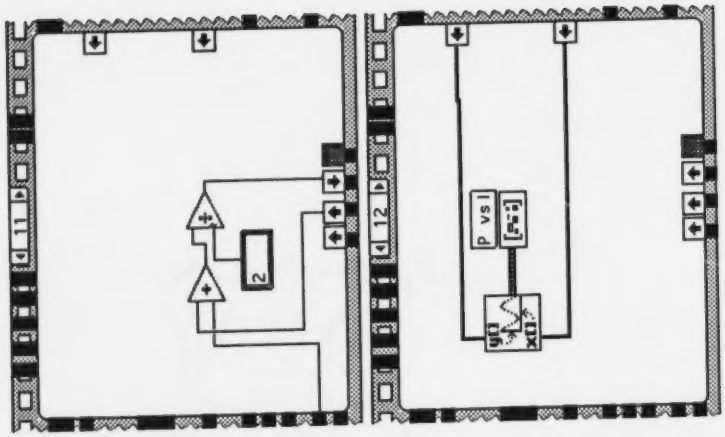
11
2
12
P vs I

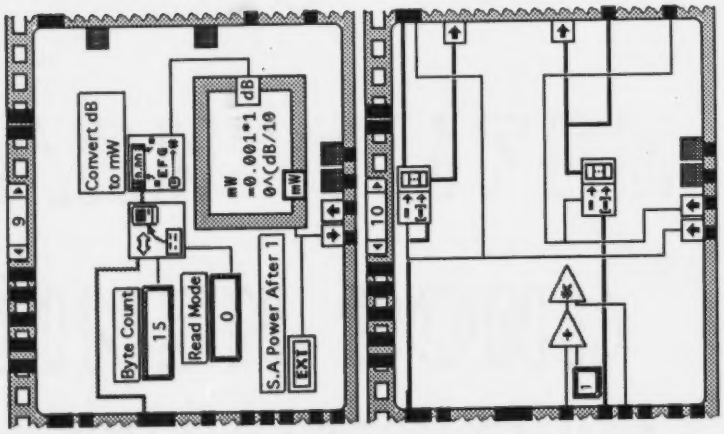
9
Convert dB
to mW
dB
mW
-0.001*1
0^(dB/10
mW
Byte Count
15
Read Mode
0
S.A Power After 1
EXIT
10
1

15
11
Slope of dP/dI
Y Intercept dP/dI
Calculated RIN
Calculated RIN (dB
EXT
mean
Mean
q=df/d*cn;
q2=10*log(q)
df
d
cn
q
q2
1.6E-19

13
d / dx
x2
Δy
Δx
y2
y1
x1
EXT

14

Rin (dB
EXT
dP/dI
EXT
q=2*df/d*cn;
q2=10*log(q);
q
q2
df
d
cn
dP/dI = 0
EXT
1.6E-19
P@I = 0
EXT
12
13
Best Fit Only
best fit
dP/dI and Best Linear
y vs x (not real time)

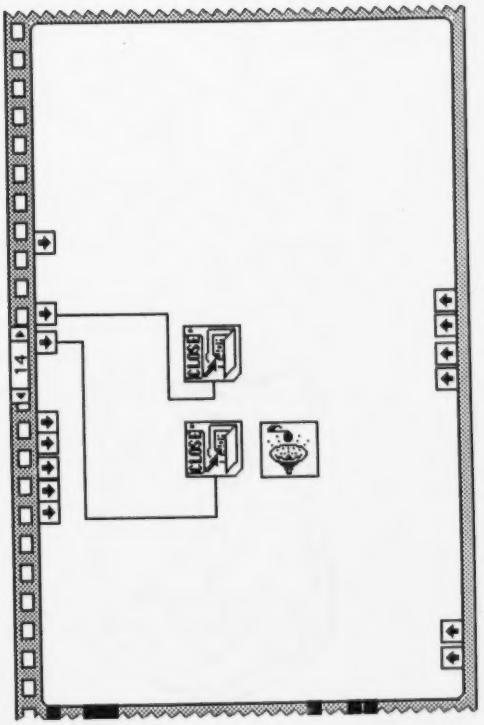
14
CLOSE
CLOSE

Appendix B

Screen Capture Using LabVIEW™

B.1 Introduction

The spectrum analyzer screen capture was done through a LabVIEW™ controlled GPIB interface with a hp™ 70000 series spectrum analyzer. It was found to be very useful and thus the LabVIEW™ program or Virtual Instrument (VI) has been included on the next few pages as reference for those interested.

HP 70000 (Fast) Cleaned Up
Tuesday, September 21, 1993 7:07 PM

Front Panel

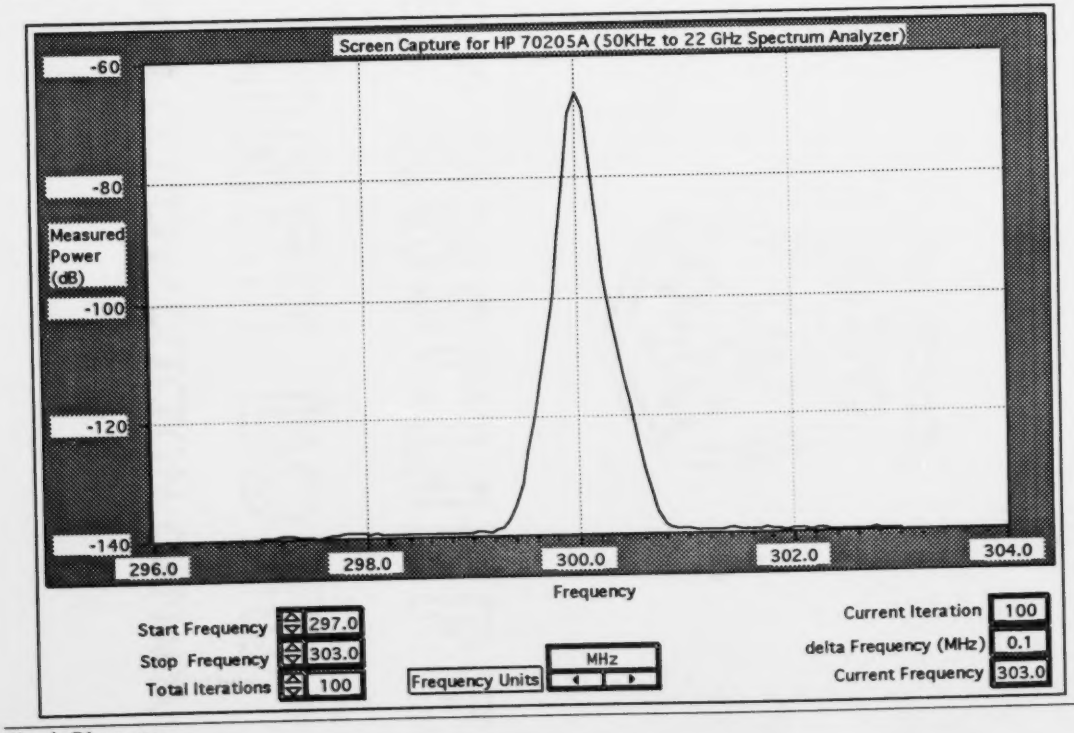

Block Diagram

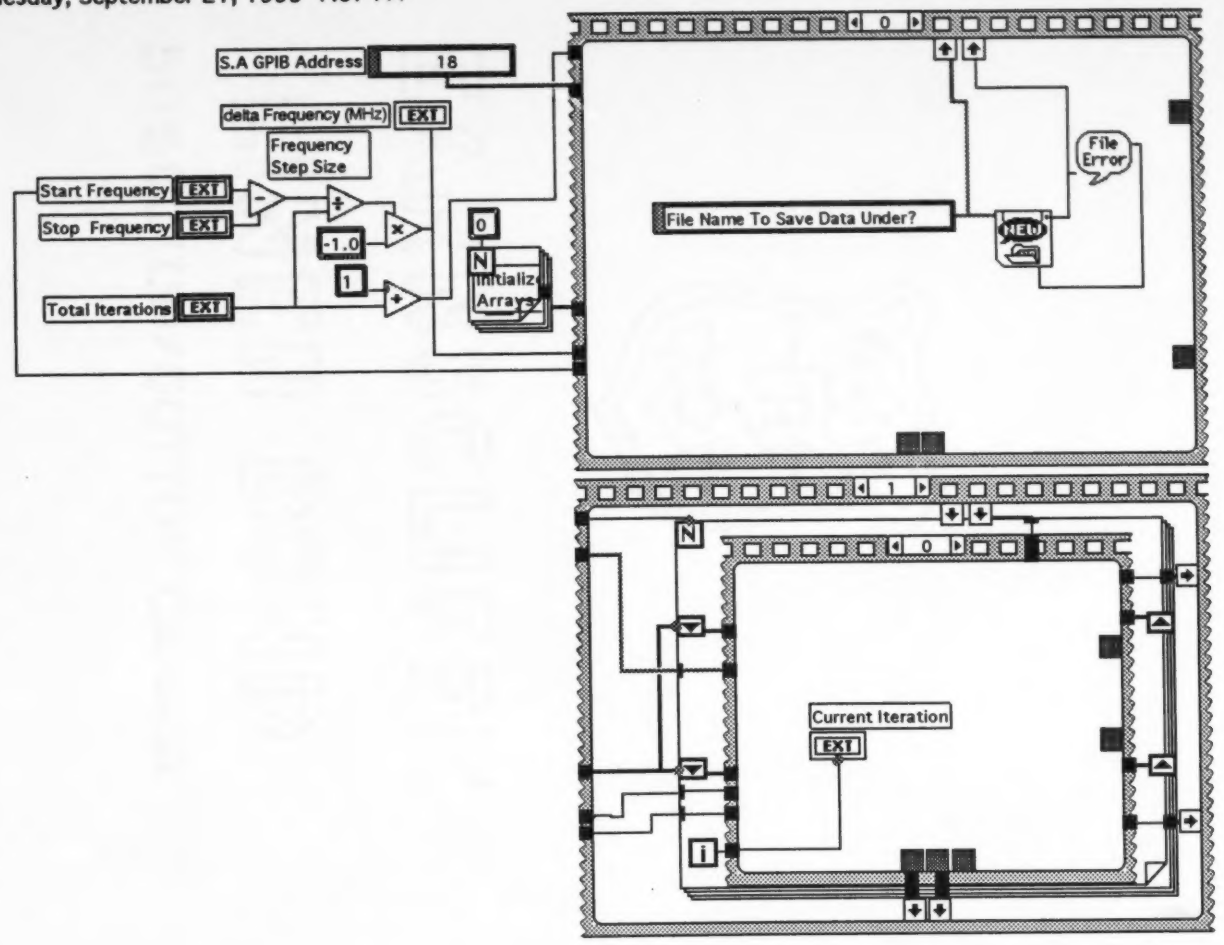
S.A GPIB Address
18
delta Frequency (MHz)
EXT
Frequency Step Size
Start Frequency
EXT
Stop Frequency
EXT
-1.0
1
Total Iterations
EXT
0
N
Initializ Arrays
0
File Name To Save Data Under?
File Error
1
N
0
Current Iteration
EXT
i

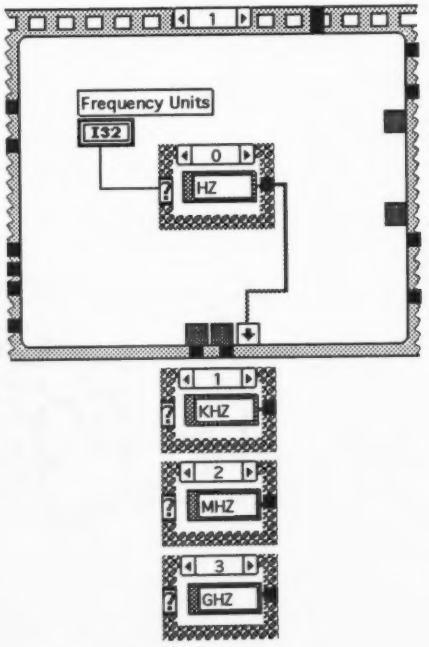
1
Frequency Units
I32
0
HZ
1
KHZ
2
MHZ
3
GHZ

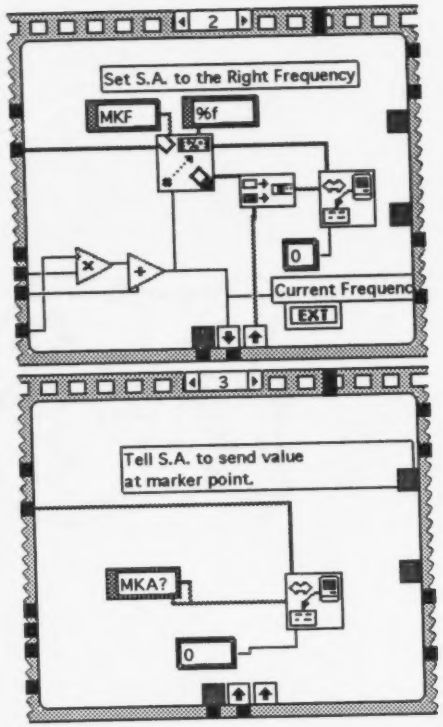
2
Set S.A. to the Right Frequency
MKF
%f
0
Current Frequenc
EXT
3
Tell S.A. to send value
at marker point.
MKA?
0

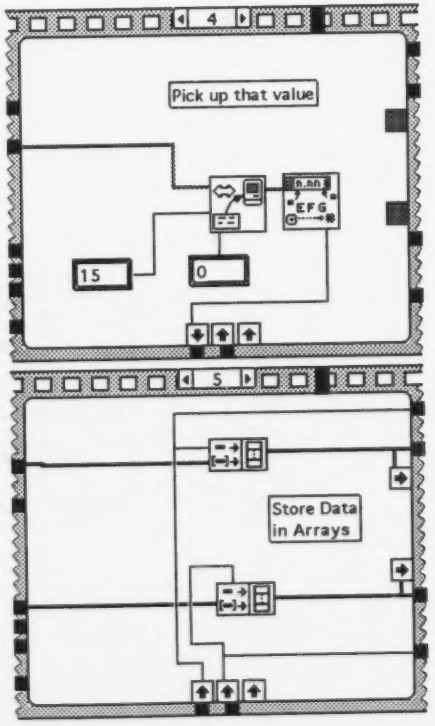
4
Pick up that value
CFG
15
0
5
Store Data
in Arrays

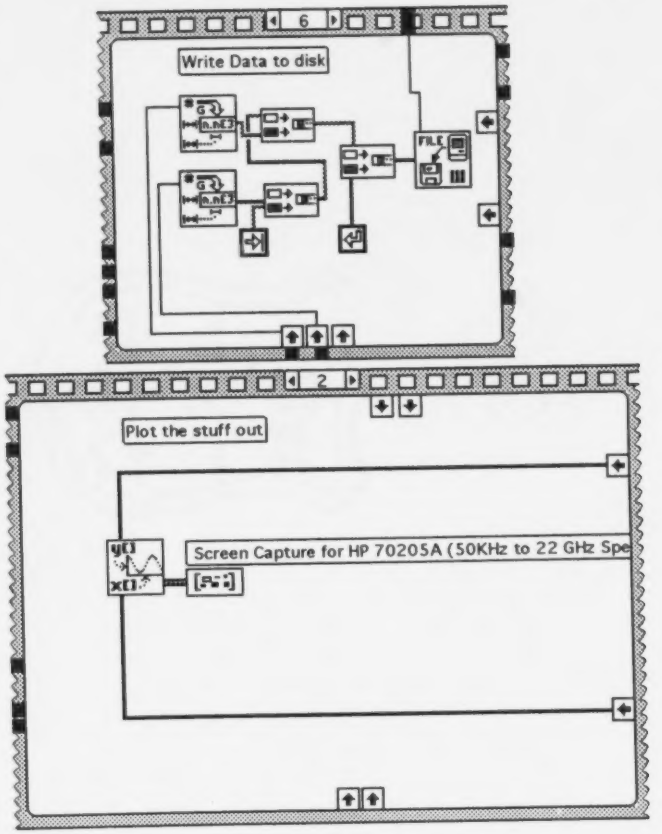
6
Write Data to disk
2
Plot the stuff out
Screen Capture for HP 70205A (50KHz to 22 GHz Spe

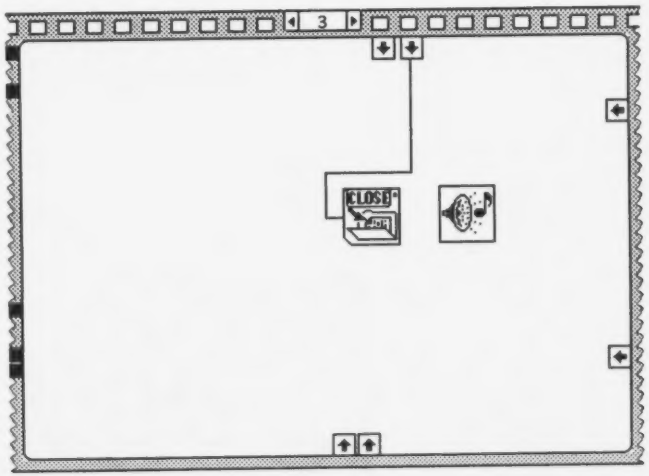
3
CLOSE

Appendix C

Polarization Rotator

C.1 Overview

The necessary control of the optical fiber light polarization was accomplished through a simple mechanical polarization controller. Given that several were needed in the lab for this and other projects and that they are an easily made mechanical device of which the theory is well known [45], several were designed and built for about 1/4 the cost of commercially sold units. The rotators worked well, therefore mechanical drawings and operating description have been included for those interested in the device.

C.2 Operating Notes

The mechanical drawings on the following pages show the various parts and design of the polarization controller. Looking at the assembly diagram, it can be seen that the device centers around two rotators which are held in place by three rotator supports bolted to a base plate. It is intended that a fiber optic cable, less than .9 mm in diameter, carrying ~1550 nm light be fed in the left support, wrap around the left rotator, feed through the middle support, wrap around the right rotator and exit out the right support. The fiber is held in place within the rotator grooves by the rotator cover plates. It is also advisable to insert a piece of foam around the fiber at the input and exit sides of the assembly to hold the fiber centered, thus keeping it from slipping into either rotator clamp slot and risk crimping or shearing the fiber.

It is intended that one rotator be wrapped *twice* to produce a quarter wave device and the other *three* times to create a half wave device. The quarter wave rotator converts linearly polarized light to circularly/elliptically polarized light, or vice versa. The half wave rotator rotates linearly polarized light to any other linearly polarized angle desired, or vice

versa. It is usually necessary to sequentially adjust each rotator back and forth several times to achieve the desired output polarization properties .

Once the optimum polarization is created, the rotators can be locked in place by tightening the socket head cap screw on the slotted side of each rotator support- the bottom screw as seen on the assembly diagram. Use a 3/32" Allen wrench with a T-handle for best results; a standard L-handle wrench will eventually strip the bolt socket head after repeated tightening and loosening.

This is just a brief description of the polarization controller. A more complete description can be found in reference [45] which discusses the theory in depth, and was used as the main information source for the design.

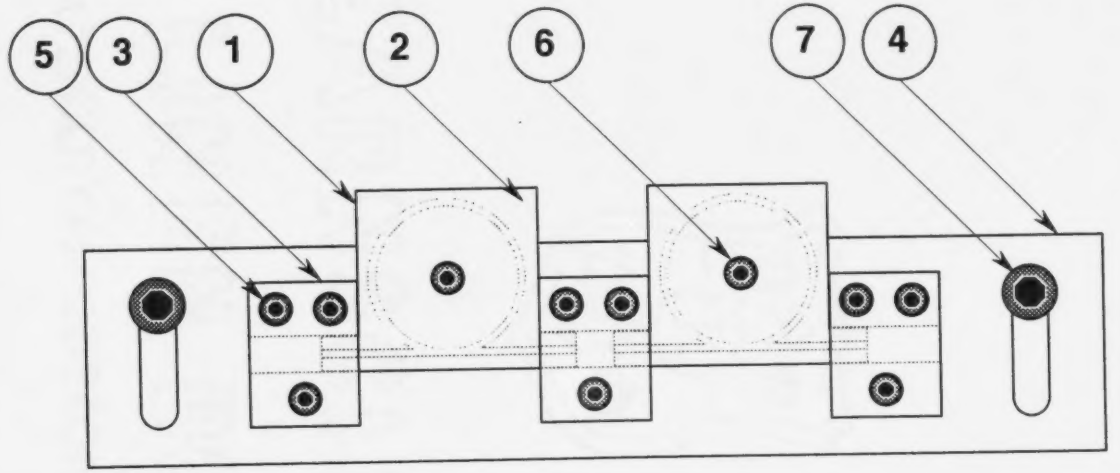

Title: Polarisation Controller Assembly

Shown mounted to optical table with .25-20 UNC cap screws - part 7

Piece	Quantity	Description	Material	Finish
1	2	Rotator	6061-T6 Aluminum	Black Anodized
2	2	Rotator Cover Plate	6061-T6 Aluminum	Black Anodized
3	3	Rotator Support	6061-T6 Aluminum	Black Anodized
4	1	Base Plate	6061-T6 Aluminum	Black Anodized
5	9	.5 inch 4-40 Socket Head Cap Screw	Steel	
6	2	.125 inch 4-40 Socket Head Cap Screw	Steel	
7	2	.5 inch .25-20 Socket Head Cap Screw	Steel	

Company: TRLabs
Telecommunications Research Laboratories

DO NOT SCALE
Dimensions In Inches
Tolerance = +/- 0.002
Chamfer all edges .03125
Mill smooth all surfaces 32 Micro Inches

Page: 1 of 5 | Drawn By: TR
Rev: 1 | Checked By:
Date: 09.16.92 | Approved By:

1 Rotator

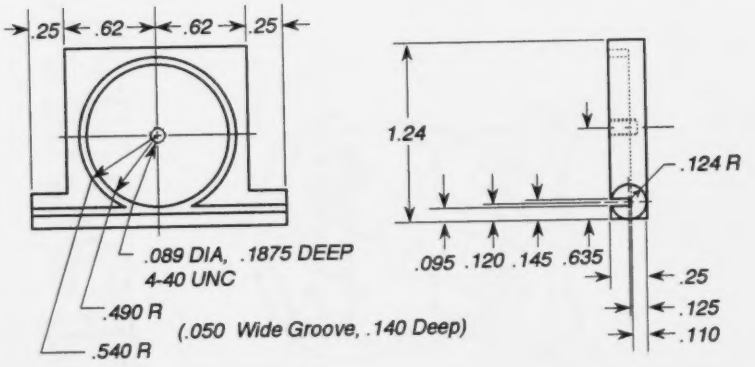

Title: Rotator

Piece	Quantity	Description	Material	Finish
1	2	Rotator	5061-T6 Aluminum	Black Anodized

Company: TRLabs
Telecommunications Research Laboratories

DO NOT SCALE
Dimensions In Inches
Tolerance = +/- 0.001
Chamfer all edges .03125
Mill smooth all surfaces 32 Micro Inches

Page: 2 of 5	Drawn By: TR
Rev: 1	Checked By:
Date: 09.16.92	Approved By:

2 Rotator Cover Plate

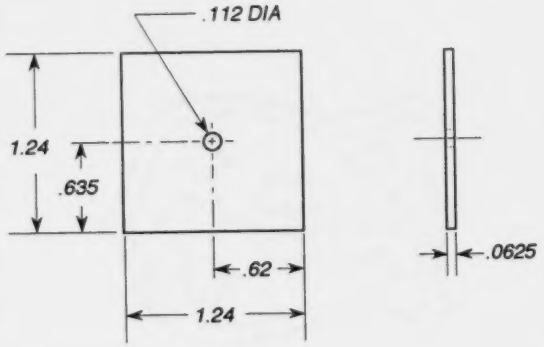

Company: TRLabs
Telecommunications Research Laboratories

Title: Rotator Cover Plate

Piece	Number Req.	Description	Material	Finish
2	2	Rotator Cover Plate	6061-T6 Aluminum	Black Anodized

DO NOT SCALE
Dimensions In Inches
Tolerance = +/- 0.002
Chamfer all edges .03125
Mill smooth all surfaces 32 Micro Inches

Page: 3 of 5	Drawn By: TR
Rev: 1	Checked By:
Date: 09.16.92	Approved By:

3 Rotator Support

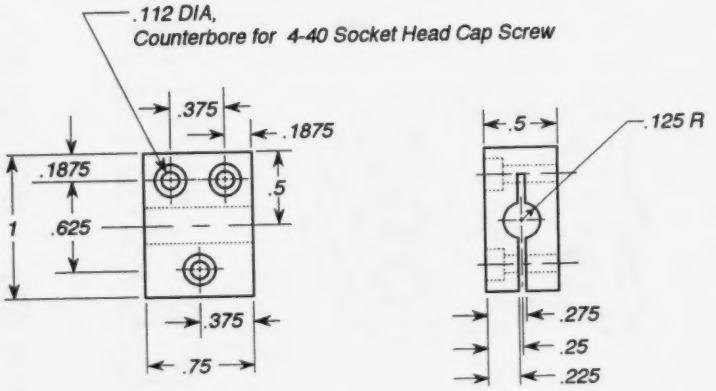

Company: TRLabs — Telecommunications Research Laboratories

Title: Rotator Clamp

Piece	Quantity	Description	Material	Finish
3	3	Rotator Support	6061-T6 Aluminum	Black Anodized

DO NOT SCALE
Dimensions In Inches
Tolerance = +/- 0.002
Chamfer all edges .03125
Mill smooth all surfaces 32 Micro Inches

Page: 4 of 5	Drawn By: TR
Rev: 1	Checked By:
Date: 09.16.92	Approved By:

4 Base Plate

Note: To Be Cut .375 Thick

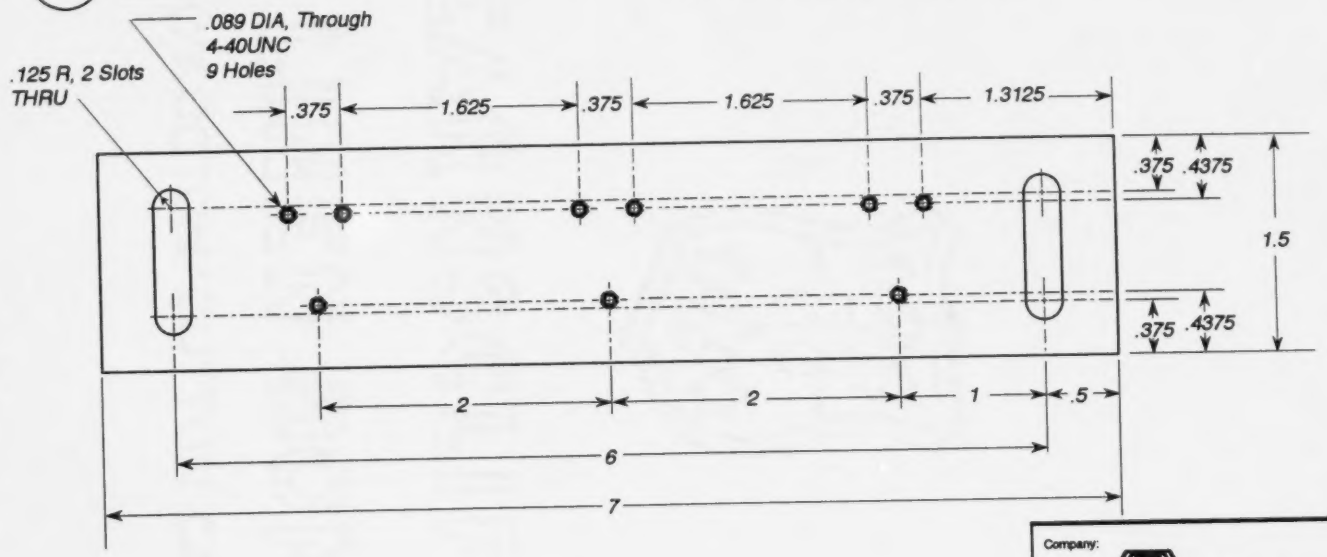

Company: TRLabs
Telecommunications Research Laboratories

Title: Base Plate

Piece	Quantity	Description	Material	Finish
1	1	Base Plate	6061-T6 Aluminum	Black Anodized

DO NOT SCALE
Dimensions In Inches
Tolerance = +/- 0.002
Chamfer all edges .03125
Mill smooth all surfaces 32 Micro Inches

Page: 5 of 5	Drawn By: TR
Rev: 1	Checked By:
Date: 09.16.92	Approved By:

Appendix D

Directional Coupler Operation

D.1 Coupler Theory

The fiber optic directional coupler is a simple device that transfers optical power from one fiber to another [46] as shown in Fig. D.1.

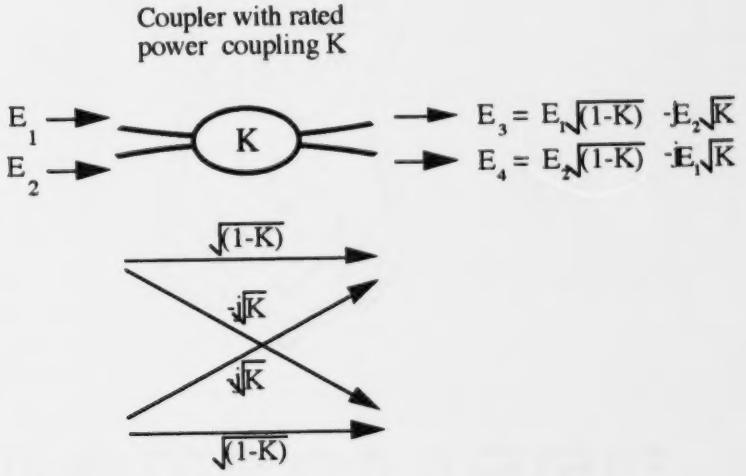

Figure D.1 Diagram showing the coupling of electric fields across a coupler.

D.2 Fiber Mirror Theory

Making use of the coupling phase shift property, a fiber "mirror" can be constructed by connecting the two output ports as shown in Fig D.2.

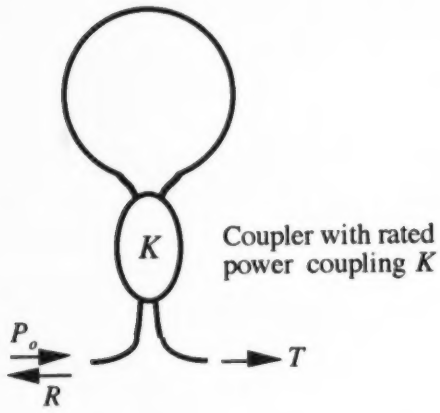

Figure D.2 Coupler configured in a fiber mirror configuration with power reflectivity R and power transmission T.

Assuming a fractional power coupling of K and an incident power traveling into the fiber of P_o, the reflected power R is given by:

$$R = 4K(1-K)P_o \tag{D.2.1}$$

and the transmitted power T is given by:

$$T = [1-4K(1-K)]P_o \tag{D.2.2}$$